

ตัวรับรู้ไอออนโลหะแบบเรืองแสงจากอนุพันธ์เอไมด์ของ 8-อะมิโนควิโนลีน



บทคัดย่อและแฟ้มข้อมูลฉบับเต็มของวิทยานิพนธ์ตั้งแต่ปีการศึกษา 2554 ที่ให้บริการในคลังปัญญาจุฬาฯ (CUIR)  
เป็นแฟ้มข้อมูลของนิสิตเจ้าของวิทยานิพนธ์ ที่ส่งผ่านทางบัณฑิตวิทยาลัย

The abstract and full text of theses from the academic year 2011 in Chulalongkorn University Intellectual Repository (CUIR)  
are the thesis authors' files submitted through the University Graduate School.

วิทยานิพนธ์นี้เป็นส่วนหนึ่งของการศึกษาตามหลักสูตรปริญญาวิทยาศาสตรมหาบัณฑิต  
สาขาวิชาเคมี ภาควิชาเคมี  
คณะวิทยาศาสตร์ จุฬาลงกรณ์มหาวิทยาลัย  
ปีการศึกษา 2558  
ลิขสิทธิ์ของจุฬาลงกรณ์มหาวิทยาลัย

METAL ION FLUORESCENT SENSOR FROM AMIDE DERIVATIVES OF 8-AMINOQUINOLINE

Miss Atchareeporn Smata



A Thesis Submitted in Partial Fulfillment of the Requirements  
for the Degree of Master of Science Program in Chemistry

Department of Chemistry

Faculty of Science

Chulalongkorn University

Academic Year 2015

Copyright of Chulalongkorn University

Thesis Title	METAL ION FLUORESCENT SENSOR FROM AMIDE DERIVATIVES OF 8-AMINOQUINOLINE
By	Miss Atchareeporn Smata
Field of Study	Chemistry
Thesis Advisor	Professor Mongkol Sukwattanasinitt, Ph.D.

---

Accepted by the Faculty of Science, Chulalongkorn University in Partial  
Fulfillment of the Requirements for the Master's Degree

.....Dean of the Faculty of Science  
(Associate Professor Polkit Sangvanich, Ph.D.)

THESIS COMMITTEE

.....Chairman  
(Associate Professor Vudhichai Parasuk, Ph.D.)

.....Thesis Advisor  
(Professor Mongkol Sukwattanasinitt, Ph.D.)

.....Examiner  
(Associate Professor Paitoon Rashatasakhon, Ph.D.)

.....External Examiner  
(Gamolwan Tumcharern, Ph.D.)

อัจฉริย์พร สมัตถะ : ตัวรับรู้ไอออนโลหะแบบเรืองแสงจากอนุพันธ์เอไมด์ของ 8-อะมิโนควิโนลีน (METAL ION FLUORESCENT SENSOR FROM AMIDE DERIVATIVES OF 8-AMINOQUINOLINE) อ.ที่ปรึกษาวิทยานิพนธ์หลัก: ศ. ดร.มงคล สุขวัฒน์นาศินิทธิ, 67 หน้า.

การออกแบบและสังเคราะห์ตัวรับรู้เรืองแสงสำหรับไอออนโลหะ เป็นเรื่องที่น่าสนใจเนื่องจาก ตัวรับรู้เหล่านี้มีความไวสูง และมีความจำเพาะสูง ทั้งยังมีความสามารถช่วยให้เห็นภาพเรืองแสง เพื่อใช้ในการตรวจวิเคราะห์ ในทางชีวภาพ และในสิ่งแวดล้อม ในงานวิจัยนี้อนุพันธ์เอไมด์ของ 8-อะมิโนควิโนลีน และกรดอะมิโน 3 ชนิด ได้แก่ โกลซีน เบต้า-อะลานีน และไกลซิลไกลซีน ถูกใช้เป็นตัวรับรู้เรืองแสงแบบเพิ่มสัญญาณสำหรับไอออนโลหะ เพื่อศึกษาผลการเลือกจำเพาะกับไอออนโลหะ โดยในสารละลายบัฟเฟอร์ทริสไฮโดรคลอไรด์ พบว่ามีเพียงแต่ อนุพันธ์ของ 8-อะมิโนควิโนลีนที่ต่อด้วยสายไกลซีน (1) เท่านั้นที่มีสัญญาณการเรืองแสงที่เพิ่มขึ้นกับไอออนของสังกะสี ( $Zn^{2+}$ ) โดยมีการเรืองแสงที่เพิ่มขึ้น 24 เท่า คำนวณมาจากค่าสัมประสิทธิ์การเรืองแสง การเพิ่มขึ้นของสัญญาณการเรืองแสงเป็นผลมาจากการเข้าจับที่แข็งแรงกับ  $Zn^{2+}$  ( $K = 8.03 \times 10^5$ ) ที่สนับสนุนมาจากการหลุดออกหรือสูญเสียโปรตอนของเอไมด์ของสาร 1 ซึ่งยืนยันด้วยผลจากวิธีการทางสเปกโทรสโกปี ได้แก่  $^1H$  NMR, MS การเปลี่ยนไปของสัญญาณการดูดกลืน (absorption) และการปลดปล่อย (emission) ในขณะที่ตัวกลางที่เป็นเอทานอล และ กระดาษกรองนั้น สาร 1 สามารถเพิ่มสัญญาณการเรืองแสงได้ทั้งกับ  $Zn^{2+}$  และ ไอออนของแคดเมียม ( $Cd^{2+}$ ) โดย  $Zn^{2+}$  ( $K = 1.20 \times 10^6$ ) และ  $Cd^{2+}$  ( $K = 4.61 \times 10^5$ ) ทำให้สามารถตรวจ  $Zn^{2+}$  และ  $Cd^{2+}$  ได้พร้อมกันด้วยเทคนิคโครมาโตกราฟีอย่างง่าย สาร 1 สามารถเกิดภาพการเรืองแสง ซึ่งใช้ในการบอกว่ามี  $Zn^{2+}$  หรือ  $Cd^{2+}$  ในเซลล์พืชจากความแตกต่างในการเตรียมตัวอย่างในตัวกลาง น้ำ และเอทานอล งานวิจัยในวิทยานิพนธ์ฉบับนี้พบว่าโครงสร้างที่กะทัดรัดของ สาร 1 มีความสามารถในการเป็นตัวรับรู้เรืองแสงที่ยอดเยียมกับ  $Zn^{2+}$  และ  $Cd^{2+}$  และ สามารถใช้เป็นแกนกลางที่สำคัญของโครงสร้างที่ใช้พัฒนาประสิทธิภาพในการเป็นตัวรับรู้เรืองแสงสำหรับตรวจวัดไอออนของโลหะตัวอื่นต่อไป

ภาควิชา เคมี

ลายมือชื่อนิสิต .....

สาขาวิชา เคมี

ลายมือชื่อ อ.ที่ปรึกษาหลัก .....

ปีการศึกษา 2558

# # 5572173623 : MAJOR CHEMISTRY

KEYWORDS: FLUORESCENCE / FLUORESCENCE SENSOR / AMINOQUINOLINE / ZINC ION / CADMIUM ION / PAPER CHROMATOGRAPHY / TURN-ON / PLANT IMAGING

ATCHAREEPORN SMATA: METAL ION FLUORESCENT SENSOR FROM AMIDE DERIVATIVES OF 8-AMINOQUINOLINE. ADVISOR: PROF. MONGKOL SUKWATTANASINITT, Ph.D., 67 pp.

The design and synthesis of fluorescent sensors for metal ions are interesting due to their high sensitivity, high selectivity and imaging capability desirable for analysis of biological and environmental systems. Herein, amide derivatives of 8-aminoquinoline with three types of amino acid pendants, i.e. glycine,  $\beta$ -alanine and glycylglycine, are evaluated as turn-on fluorescent sensors for metal ions to explore their effects on metal ion binding selectivity. In Tris-HCl aqueous buffer solution, only the derivative of 8-aminoquinoline containing glycine (1) exhibits selective fluorescence enhancement, a remarkable 24-fold increase of the fluorescence quantum yield, with  $Zn^{2+}$ . The fluorescence enhancement is a result of the strong binding with  $Zn^{2+}$  ( $K = 8.03 \times 10^5$ ) which is promoted by the deprotonation of the amide proton as confirmed by  $^1H$  NMR, MS, absorption and emission spectroscopy. In ethanol and on filter paper, 1 exhibited dual fluorescence turn on signals and stronger binding to  $Zn^{2+}$  ( $K = 1.20 \times 10^6$ ) and  $Cd^{2+}$  ( $K = 4.61 \times 10^5$ ) that allows simultaneous detection of both metal ions using a simple paper chromatographic technique. Sensor 1 also allows fluorescence imaging to locate either  $Zn^{2+}$  or  $Cd^{2+}$  in plant tissue depending on either water or ethanol treatments. The results demonstrate that the simple structure of 1 is very effective for turn-on fluorescent sensors for  $Zn^{2+}$  and  $Cd^{2+}$  and it may be used as a core structure for further development of other effective metal sensing ligands.

Department: Chemistry

Student's Signature .....

Field of Study: Chemistry

Advisor's Signature .....

Academic Year: 2015

## ACKNOWLEDGEMENTS

I wish to express my deep gratitude to my advisor, Professor Dr. Mongkol Sukwattanasinitt for his generous assistance, invaluable guidance and encouragement throughout the course of this research.

I would like to gratefully acknowledge the committees, Associate Professor Dr. Paitoon Rashatasakhon, Associate Professor Dr. Vudhichai Parasuk and Dr. Gamolwan Tumcharern for their kindness, valuable suggestion and recommendations. I would like to thank Assistant Professor Dr. Anawat Ajawachom, Assistant Professor Dr. Sumrit Wacharasindhu and Dr. Sakulsuk Unarunotai for their attention and suggestion during our group meeting.

My appreciation is also given to many people in our research group; Ms. Warathip Siripornnoppakhun, Mr. Akachai Khumsri, Ms. Nattaporn Kimpitak, Mr. Watcharin Ngampeungpis and Ms. Kanokthorn Boonkitpatarakul for their helps, suggestions and guidance. I would like to thank Waroton Paisuwan, Nattapong Srimuang, Chakrit Yimsukanan, Jadetapong Klahan, Jutawat Hojitsirsayanont, Apiwat Promchat and Manutsorn Pipatsuttipong for their help during the course of my graduate research. Moreover, I gratefully thank to everyone in MAPS group for a great friendships, spirit, smile, good wish and their helps in everything.

I would like to thank Nanotechnology Center (NANOTEC), NSTDA, Ministry of Science and Technology, Thailand, through its program of Center of Excellence Network and Ratchadaphiseksomphot Endowment Fund (Chulalongkorn University) grant number RES560530126-AM for financial supported.

Finally, I would like to express my thankfulness to my beloved parents and my special one who always stand by my side during both of my pleasant and hard time.

## CONTENTS

	Page
THAI ABSTRACT .....	iv
ENGLISH ABSTRACT .....	v
ACKNOWLEDGEMENTS .....	vi
CONTENTS .....	vii
LIST OF FIGURES .....	X
LIST OF TABLES .....	xv
LIST OF SCHEME.....	xv
LIST OF ABBREVIATIONS .....	xvi
CHAPTER I INTRODUCTION.....	1
1.1 Fluorescence .....	1
1.2 Fluorescence sensors.....	3
1.2.1 Sensing modes.....	3
1.2.2 Sensing mechanisms.....	4
1.2.2.1 Photoinduced electron transfer (PET) .....	5
1.2.2.2 Internal charge transfer (ICT).....	6
1.2.2.3 Förster resonance energy transfer (FRET).....	7
1.2.2.4 Excited state intramolecular proton transfer ESIPT .....	8
1.3 Quinoline-Based Fluorescence Sensors .....	9
1.4 Objectives of this research.....	14
CHAPTER II EXPERIMENT .....	15
2.1 Reagents and materials .....	15
2.2 Analytical instruments .....	15

2.3 Synthesis of fluorophores .....	16
2.3.1 Synthesis of compound 4: <i>tert</i> -butyl-2-oxo-2-[(quinolin-8-yl)amino]ethyl carbamate .....	16
2.3.2 Synthesis of compound 5: <i>tert</i> -butyl-3-oxo-3-[(quinolin-8-yl)amino]propyl carbamate .....	16
2.3.3 Synthesis of compound 6: <i>tert</i> -butyl-2-oxo-2-(2-oxo-2-[(quinolin-8-yl)amino] ethylamino)ethylcarbamate.....	17
2.3.3.1 Preparation of Boc-Glycylglycine .....	17
2.3.4 Synthesis of compound 1: 2-amino- <i>N</i> -(quinolin-8-yl)acetamide .....	18
2.3.5 Synthesis of compound 2: 3-amino- <i>N</i> -(quinolin-8-yl)propanamide.....	19
2.3.6 Synthesis of compound 3: 2-amino- <i>N</i> -2-oxo-2-[(quinolin-8-yl)amino]ethyl acetamide.....	19
2.4 Photophysical property study .....	20
2.4.1 UV-Visible spectroscopy.....	20
2.4.1.1. Molar Absorption Coefficients ( $\epsilon$ ).....	20
2.4.2 Fluorescence spectroscopy.....	20
2.4.3 Fluorophore quantum yields .....	20
2.5 Fluorescent sensor study .....	21
2.5.1 Selectivity study.....	21
2.5.2 Fluorescence titration.....	22
2.5.3 The association constant ( $K_a$ ).....	22
2.5.4 Competition with other metal ions .....	22
2.5.5 Limit of detection for turn-on sensing.....	22
2.6 NMR titration.....	23



	Page
2.7 Fluorescence images of Zn <sup>2+</sup> and Cd <sup>2+</sup> in plant samples .....	23
2.8 Naked eye detection of Zn <sup>2+</sup> and Cd <sup>2+</sup> on paper-based sensors .....	24
CHAPTER III RESULTS AND DISCUSSION .....	25
3.1 Synthesis and characterization of 1, 2 and 3 .....	25
3.2. Photophysical properties of 1-3 .....	26
3.3 Metal ions sensing study .....	28
3.4 Metal binding properties of 1 .....	32
CHAPTER IV CONCLUSION .....	47
REFERENCES .....	48
APPENDIX .....	54
VITA .....	67



## LIST OF FIGURES

<b>Figure 1.1</b> Jablonski energy diagram, wavy lines mark non-radiative transitions.....	2
<b>Figure 1.2</b> Modes of fluorescence responses. ....	4
<b>Figure 1.3</b> Schematic simplification of PET process. ....	5
<b>Figure 1.4</b> Potential energy surfaces of the ground state ( $S_0$ ) is excited to $S_1$ then relaxed to LE, and ICT state.....	6
<b>Figure 1.5</b> Förster resonance energy transfer (FRET). ....	7
<b>Figure 1.6</b> Principal photophysics of ESIPT illustrated with 2-(20-hydroxyphenyl)-benzoxazole (HBO).....	8
<b>Figure 1.7</b> Derivatives of 8-aminoquinoline with an aryl sulfonamide. ....	9
<b>Figure 1.8</b> Proposed of <b>AQZ-Zn<sup>2+</sup></b> complexation resulting in fluorescence enhancement.....	10
<b>Figure 1.9</b> Proposed two complexes observed by <sup>1</sup> H NMR spectroscopy at different <b>ACAQ:Zn<sup>2+</sup></b> ratios .....	10
<b>Figure 1.10</b> Proposed binding of <b>QTEPA-modified MCM-41</b> and Zn <sup>2+</sup> .....	11
<b>Figure 1.11</b> (a) Structure of AQZ derivatives and (b) normalize selectivity graph of AQZ family with various metal ions. ....	11
<b>Figure 1.12</b> Proposed binding between <b>NQA</b> and Zn <sup>2+</sup> resulting in fluorescence enhancement.....	12
<b>Figure 1.13</b> Proposed complexation of Zn <sup>2+</sup> and Cd <sup>2+</sup> with <b>R-1</b> and cysteine.....	13
<b>Figure 1.15</b> Probable host-guest binding between <b>TAQ</b> and Zn <sup>2+</sup> .....	13
<b>Figure 1.16</b> Target molecules <b>1, 2, 3</b> .....	14
<b>Figure 2.1</b> the calibration curve for turn-on sensing. ....	23
<b>Figure 3.1</b> <sup>1</sup> H NMR spectra of compound <b>1-3</b> .....	26

- Figure 3.2** Normalized absorption (solid line) and emission (dash line) spectra of the fluorophores **1**, **2** and **3** in Tris-HCl aqueous buffer solution pH7.4 containing 1% methanol, v/v. The  $\lambda_{\text{max}}$  of each fluorophore was used as the excitation wavelength in the corresponding emission spectrum..... 27
- Figure 3.3** Fluorescence enhancement ratios of ligands (10  $\mu\text{M}$ ) in (a) Tris-HCl aqueous buffer pH 7.4 solution containing methanol (1% v/v) upon addition of various metal ions (100  $\mu\text{M}$ );  $\lambda_{\text{ex}} = 300 \text{ nm}$  ( $\lambda_{\text{em}} = 502, 510$  and  $502$  for **1**, **2** and **3**, respectively) (b) ethanol;  $\lambda_{\text{ex}} = 310 \text{ nm}$  ( $\lambda_{\text{em}} = 502, 510$  and  $502$  for **1**, **2** and **3**, respectively)..... 29
- Figure 3.4** Fluorescence spectra of ligands (10  $\mu\text{M}$ ) in Tris-HCl aqueous buffer pH 7.4 solution containing methanol (1% v/v) upon addition of various metal ions (100  $\mu\text{M}$ );  $\lambda_{\text{ex}} = 300 \text{ nm}$ ..... 30
- Figure 3.5** Fluorescence spectra of ligands (10  $\mu\text{M}$ ) in ethanol upon addition of various metal ions (100  $\mu\text{M}$ );  $\lambda_{\text{ex}} = 310 \text{ nm}$ ..... 31
- Figure 3.6** (a) UV-vis absorption spectra of **1** (100  $\mu\text{M}$ ) upon the addition of varied concentrations of  $\text{Zn}^{2+}$  and (b) fluorescence spectra of **1** (10  $\mu\text{M}$ ) before and after addition of  $\text{Zn}^{2+}$  (100  $\mu\text{M}$ ) ( $\lambda_{\text{ex}} = 300 \text{ nm}$ ) in Tris-HCl aqueous buffer pH 7.4 solution containing methanol (1% v/v). ..... 32
- Figure 3.7** Proposed mechanism of complex between **1** and a metal ion..... 33
- Figure 3.8** Fluorescence intensity ( $\lambda_{\text{ex}} = 300 \text{ nm}$ ;  $\lambda_{\text{em}} = 504 \text{ nm}$ ) of **1** (10  $\mu\text{M}$ ) at various pHs in Tris-HCl aqueous buffer pH 7.4 solution containing methanol (1% v/v) in the absence and presence of  $\text{Zn}^{2+}$  and  $\text{Cd}^{2+}$  (10 equivalent)..... 34
- Figure 3.9** Job plots of UV-vis absorption (at 344 nm) and emission (at 504 nm) titration between compound **1** and  $\text{Zn}^{2+}$  in Tris-HCl aqueous buffer pH 7.4 solution containing methanol (1% v/v) ( $[\text{1}] + [\text{Zn}^{2+}] = 10 \mu\text{M}$ ), (■ = absorption, ▲ = emission)..... 35
- Figure 3.10** Benesi-Hildebrand plot for determination of  $K_a$  of **1** with  $\text{Zn}^{2+}$  and  $\text{Cd}^{2+}$  in aqueous and ethanol solutions..... 36

- Figure 3.11** Positive-ion electrospray mass spectrum of **1** (10 $\mu$ M) upon addition of 0.5 equivalent of Zn<sup>2+</sup> in methanol..... 37
- Figure 3.12** Positive-ion electrospray mass spectrum of **1** (10 $\mu$ M) upon addition of 1.0 equivalent of Zn<sup>2+</sup> in methanol..... 37
- Figure 3.13** COSY correlation spectra of compound **1** in (CD<sub>3</sub>)<sub>2</sub>SO..... 38
- Figure 3.14** COSY correlation spectra of compound **1** in the presence of 0.25 equivalent of Zn<sup>2+</sup> in (CD<sub>3</sub>)<sub>2</sub>SO..... 39
- Figure 3.15** COSY correlation spectra of compound **1** in the presence of 1.5 equivalent of Zn<sup>2+</sup> in (CD<sub>3</sub>)<sub>2</sub>SO..... 39
- Figure 3.16** (a) Proposed structures of complexes between Zn<sup>2+</sup> and **1** optimized by CHARMM and (b) partial <sup>1</sup>H NMR spectra (400 MHz) of **1** (0.15 M) in (CD<sub>3</sub>)<sub>2</sub>SO in the presence of various equivalents of Zn<sup>2+</sup> ..... 40
- Figure 3.17** Fluorescence responses of **1** (10  $\mu$ M) to the addition of solution of Zn<sup>2+</sup> (10 equivalent) mixed with various metal ions (10 equivalent) in Tris-HCl aqueous buffer pH 7.4 solution containing methanol (1% v/v); ( $\lambda_{\text{ex}}$  = 300 nm and  $\lambda_{\text{em}}$  = 504 nm)..... 41
- Figure 3.18** Fluorescence spectra ( $\lambda_{\text{ex}}$  = 300 nm) of **1** (10  $\mu$ M) in Tris-HCl aqueous buffer pH 7.4 solution containing methanol (1% v/v) in the presence of Zn<sup>2+</sup> at various concentrations. .... 42
- Figure 3.19** Fluorescence intensity ratio as a function of Zn<sup>2+</sup> concentration; inset: linear calibration line for quantitative determination of Zn<sup>2+</sup> concentration..... 43
- Figure 3.20** Fluorescence images of Chinese cabbage (*Brassica rapa*.) sprout tissue samples treated with Zn<sup>2+</sup> (100  $\mu$ M) and Cd<sup>2+</sup> (100 $\mu$ M), (a) washed with Milli-Q water and (b) washed with ethanol, before and after addition of **1** (100  $\mu$ M, 10  $\mu$ L)..... 44
- Figure 3.21** Photographic image of metal ion (0.1 mM) detection by **1** (1 mM) on wax patterned filter paper tested by simple drop and dry. The sample was illuminated by black light (wavelength 365  $\pm$  50 nm)..... 45

<b>Figure 3.22</b> Photographic image for dual detection of Zn <sup>2+</sup> and Cd <sup>2+</sup> (1 nmol) by <b>1</b> (1 mM) using paper chromatography for separation after elution with CH <sub>3</sub> NH <sub>2</sub> 4% (v/v). The sample was irradiated by black light (wavelength 365 ± 50 nm).....	46
<b>Figure A.1</b> <sup>1</sup> H-NMR (400 MHz) of Boc-glycylglycine in (CD <sub>3</sub> ) <sub>2</sub> SO.....	54
<b>Figure A.2</b> <sup>1</sup> H-NMR (400 MHz) of <b>4</b> in CDCl <sub>3</sub> .....	55
<b>Figure A.3</b> MS (ESI) of <b>4</b> in Methanol.....	55
<b>Figure A.4</b> <sup>1</sup> H-NMR (400 MHz) of <b>5</b> in CDCl <sub>3</sub> .....	56
<b>Figure A.5</b> MS (ESI) of <b>5</b> in Methanol.....	56
<b>Figure A.6</b> <sup>1</sup> H-NMR (400 MHz) of <b>6</b> in CDCl <sub>3</sub> .....	57
<b>Figure A.7</b> MS (ESI) of <b>6</b> in Methanol.....	57
<b>Figure A.8</b> <sup>1</sup> H-NMR (400 MHz) of <b>1</b> in CD <sub>3</sub> OD.....	58
<b>Figure A.9</b> <sup>1</sup> H-NMR (400 MHz) of <b>1</b> in (CD <sub>3</sub> ) <sub>2</sub> SO.....	58
<b>Figure A.10</b> <sup>13</sup> C-NMR (100 MHz) of <b>1</b> in CD <sub>3</sub> OD.....	59
<b>Figure A.11</b> MS (ESI) of <b>1</b> in Methanol.....	59
<b>Figure A.12</b> IR(ATR) of <b>1</b> .....	60
<b>Figure A.13</b> <sup>1</sup> H-NMR (400 MHz) of <b>2</b> in CD <sub>3</sub> OD.....	61
<b>Figure A.14</b> <sup>13</sup> C-NMR (100 MHz) of <b>2</b> in CD <sub>3</sub> OD.....	61
<b>Figure A.15</b> MS (ESI) of <b>2</b> in Methanol.....	62
<b>Figure A.16</b> IR(ATR) of <b>2</b> .....	62
<b>Figure A.17</b> <sup>1</sup> H-NMR (400 MHz) of <b>3</b> in CD <sub>3</sub> OD.....	63
<b>Figure A.18</b> <sup>13</sup> C-NMR (100 MHz) of <b>3</b> in CD <sub>3</sub> OD.....	63
<b>Figure A.19</b> MS (ESI) of <b>3</b> in Methanol.....	64
<b>Figure A.20</b> IR(ATR) of <b>3</b> .....	64

## LIST OF TABLES

<b>Table 3.1</b> Photophysical data of <b>1</b> , <b>2</b> and <b>3</b> in Tris-HCl aqueous buffer pH 7.4 solution containing methanol (1% v/v).....	27
<b>Table 3.2</b> Association constants of <b>1</b> with $Zn^{2+}$ and $Cd^{2+}$ in aqueous and ethanol solutions.....	35
<b>Table A.1</b> The $Zn^{2+}$ sensors based on 8-aminoquinoline derivatives reported to date .....	66



## LIST OF SCHEME

**Scheme 3.1** Synthesis of 8-aminoquinoline ligands modified with amino acids..... 25

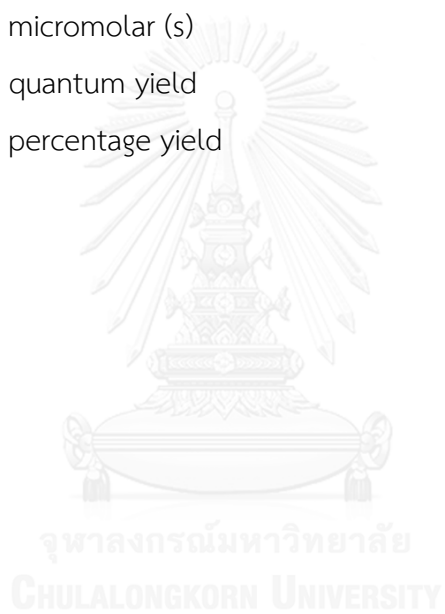


## LIST OF ABBREVIATIONS

e.g.	for example
s.	second (s)
nm	nanometer
nM	nanomolar
$\mu$ M	micromolar
v/v	volume/volume
$^1\text{H}$ NMR	proton nuclear magnetic resonance
$^{13}\text{C}$ NMR	carbon-13 nuclear magnetic resonance
MS	Mass spectrometry
ESI	electrospray ionization
FT-IR	Fourier transforms infrared spectroscopy
$m/z$	mass per charge
$K_a$	Association constant
mg	milligram (s)
mL	milliliter (s)
mmol	millimole (s)
M.W.	molecular weight
M	molar
d	doublet (NMR)
dd	doublet of doublet (NMR)
g	gram (s)
Hz	Hertz
h	hour (s)
IR	<i>infrared</i>
$J$	coupling constant
MHz	megaHerz
m	multiplet (NMR)
s	singlet (NMR)



t	tripet (NMR)
br	broad (NMR)
rt	room temperature
O/N	over night
TLC	thin layer chromatography
UV	ultraviolet
$\delta$	chemical shift
$^{\circ}\text{C}$	degree Celsius
$\mu\text{L}$	microliter (s)
$\mu\text{M}$	micromolar (s)
$\Phi$	quantum yield
% yield	percentage yield



# CHAPTER I

## INTRODUCTION

### 1.1 Fluorescence

One form of a quantum mechanical process (photoluminescence) is the term of fluorescence occurring between the ground and excited states of a molecule that can be basically described by the Jablonski energy diagram (Figure 1.1). The molecule (usually an aromatic compound or highly conjugated molecule) is in ground electronic state ( $S_0$ ) which is a singlet state at normal condition. Upon the absorption of light with appropriate energy, an electron, usually one of the valence electrons, of the molecule is excited to a higher energy level and the molecule assumes excited electronic states (e.g.  $S_1$  or  $S_2$  excited state). Absorption of light occurs extremely fast, approximately a femtosecond that the time necessary for the electron to travel within the molecule. The electronic transition occurs without geometry change which is normally called vertical transition. This can be explained from the Franck-Condon principle that a nucleus is much heavier than an electron. Thus, the motions of nuclear are much slower than the motions of electron. However, if the geometry in excited state is not the same from the ground state, the initial electronic excitation occurs geometrically relaxed to the most stable vibrational state of  $S_1$  via vibration and rotation without light emitting. This non-radiative decay is also very fast, between  $10^{-14}$  and  $10^{-10}$  s. If the initial excited state is higher than  $S_1$ , the molecule may relax to the most stable vibrational state of  $S_1$  via the coupling of geometrical and electronic relaxation which is termed as internal conversion. Then, the most stable vibrational state of  $S_1$  may return to  $S_0$  by two possible radiative pathways. First, the excited molecules may reduce its energy by emitting a photon which is termed fluorescence. The time required for this process typically in nano-second scale which is slower than most geometrical relaxation and competitive with some other nonradiative pathways. With part of the energy already lost via nonradiative geometrical relaxation and internal conversion, fluorescence spectrum is observed at longer wavelength than the corresponding absorption

spectrum. The energy of a fluorescent photon is thus always less than that of the exciting photon. The difference in wavelengths of the maximum emission and maximum absorption is called Stokes shift;  $\Delta\lambda = \lambda_{em} - \lambda_{ab} > 0$ . The molecules with many possible geometry changes will have larger Stokes shift. However, in rigid molecules for which  $S_1$  and  $S_0$  have very similar geometries, and the solvation, the Stokes shift will be small. Another pathway that a molecule may take in the dissipation of energy is called intersystem crossing (ISC). The electron changes spin multiplicity from an excited singlet state to an excited triplet state ( $T_1$ ). Usually, the transitions between  $S_1$  to  $T_1$  in common organic molecule are forbidden by the spin conservation rule. However, the ISC is allowed with spin-orbit coupling which is usually observed for a molecule containing heavy atoms like bromine or iodine. After the ISC process, radiative relaxation from  $T_1$  back to  $S_0$  is known as phosphorescence. This is the slowest process in the Jablonski diagram, several orders of magnitude slower than fluorescence, typically in the scale of ms to several minutes. It can continue to glow even after the excitation source is turned off.

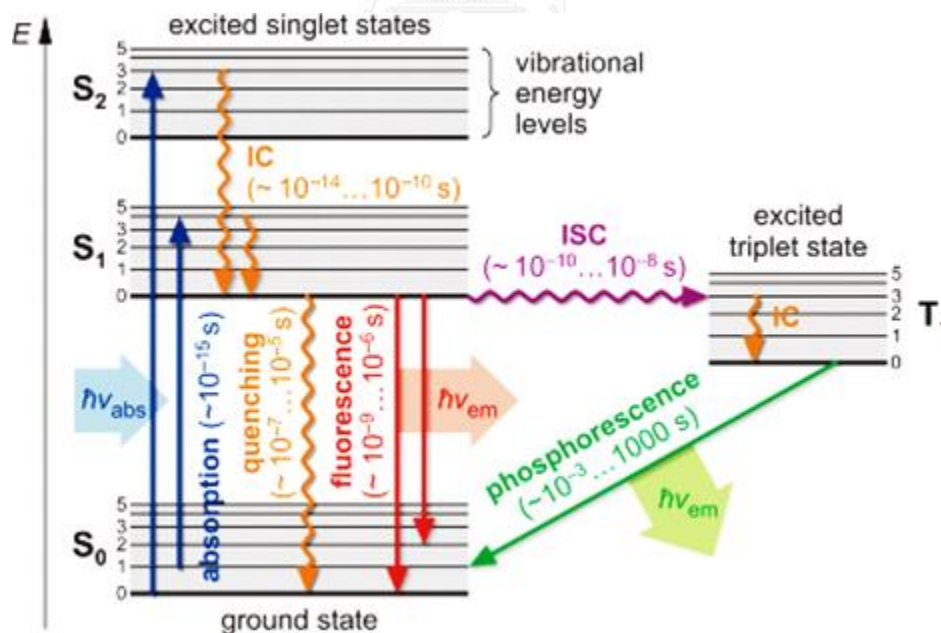


**Figure 1.1** Jablonski energy diagram, wavy lines mark non-radiative transitions. (IC = internal conversion, ISC=intersystem crossing) [1].

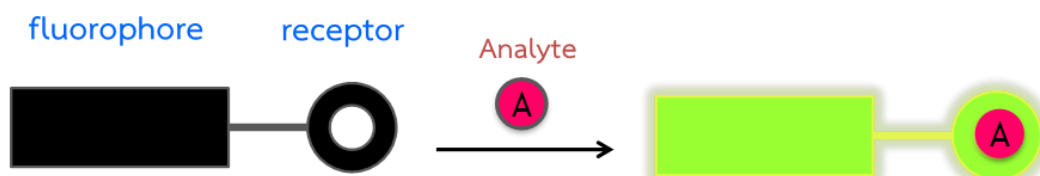
## 1.2 Fluorescence sensors

Recently, fluorescent sensors have been developed for easy to use, short response time and no sample destruction. They were designed for detection of several analytes. Fluorescent technique has several special features such as high sensitivity and high selectivity with ability to allow visual detection and optical imaging.

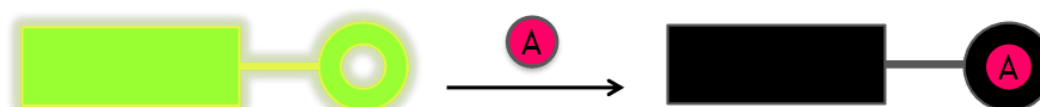
### 1.2.1 Sensing modes

Mainly, fluorescent chemosensor contains two main components: one is a selective binding site (receptor) another is the signal source (fluorophore) which provides the means of signaling this binding, whether by fluorescence turn-on, turn-off and wavelength shift. Fluorescent turn-on mode is fluorescent sensor that gives enhanced fluorescence signal upon interaction with an analyte (Figure 1.2a). In contrast, turn-off mode must have fluorophore unit which is high emission intensity and low emission intensity upon interaction with an analyte (Figure 1.2b). For the wavelength shift mode, the sensing molecule may change its electronic structure or at least its geometry upon the interaction with analyte that leads to a new fluorescence signal at different wavelength (Figure 1.2c). The ideal sensors should not be affected by environmental interference (signal-selectivity), such as photochemical reactions, concentration and matrixes (pH, polarity, temperature, etc.).

## (a) Turn-on mode (Enhancement)



## (b) Turn-off mode (Quenching)



## (c) Wavelength shift

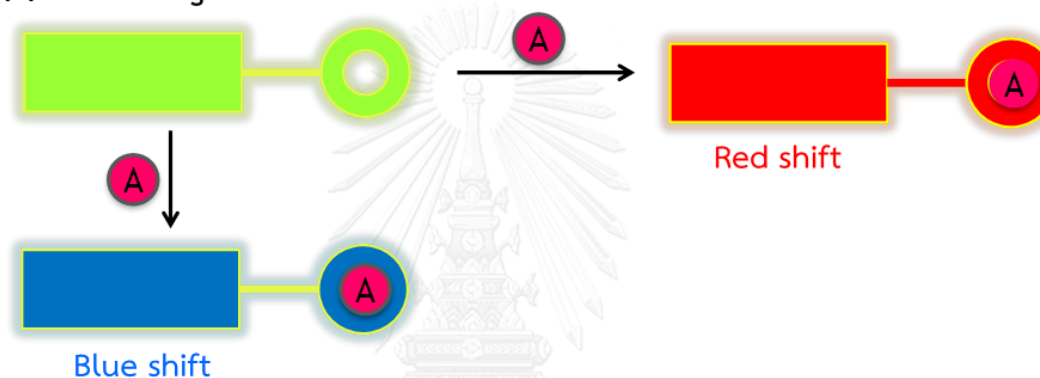


Figure 1.2 Modes of fluorescence responses.

### 1.2.2 Sensing mechanisms

The sensing compounds in this thesis have been designed based on PET and ICT.

The changes of fluorescence signals of the fluorescent sensors upon the interaction with analytes have been described by theories involving the following photophysical processes: photoinduced electron transfer (PET) [2-7], intramolecular charge transfer (ICT) [3-6], Förster resonance energy transfer (FRET) [8, 9] and excited-state intramolecular proton transfer (ESIPT) [10, 11]. A chemo sensor may transduce the chemical interaction event into fluorescent signals based on one or more of these processes. A design of sensing system having more than one processes working synergistically to enhance the fluorescence responses are challenging and required good understanding of the system.

### 1.2.2.1 Photoinduced electron transfer (PET)

PET process occurs when receptor or analyte has either its highest occupied molecular orbital (HOMO) or the lowest unoccupied molecular orbital (LUMO) between HOMO and LUMO energy gap of the fluorophore which acts as either a photo-excited electron acceptor or donor, respectively. In the first case, the excited fluorophore of acceptor will have its half-filled HOMO accepting an electron transferred from the HOMO level of the other unit (Figure 1.3a). The other case, the excited electron in the LUMO of the fluorophore, the donor, will transfer to the LUMO level of the acceptor unit (Figure 1.3b). The electron transfer process is a non-radiative process which results in quenching of the fluorescence. So, the fluorescent sensor in turn-off and turn-on mode can be designed based on promoting or inhibiting of the PET process.

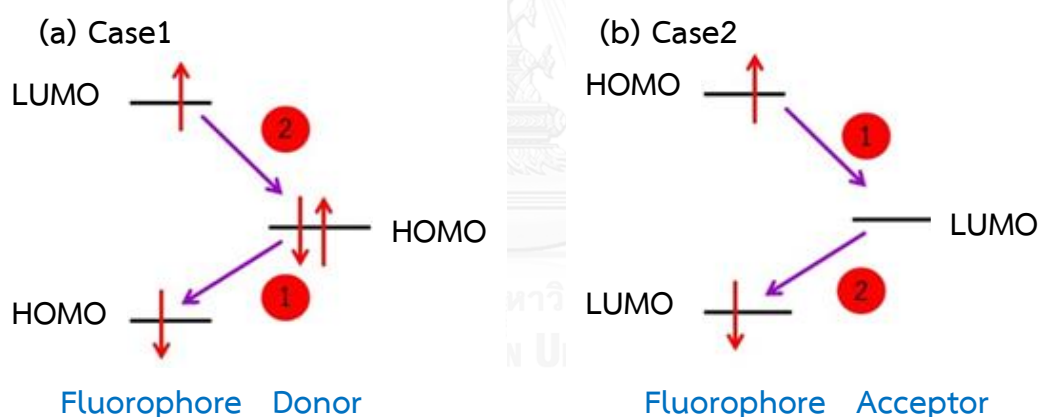


**Figure 1.3** Schematic simplification of PET process [12].

### 1.2.2.2 Internal charge transfer (ICT)

The locally excited (LE) state is the initial most stable excited state of  $S_1$ . In some cases, a molecule in LE state may undergoes another geometrical relaxation along with restructuring of electron density, specifically when the molecule contains both electron withdrawing and donating groups connected *via*  $\pi$ -conjugated system. The relaxation process produces a new lower energy excited state called internal charge transfer (ICT) state having significantly different geometry and dipole moment from the LE state (Figure 1.4). Then The ICT state relaxes to the ground state either by non-radiative or radiative decay. Depending on the energy band gap, this relaxation may give light within or outside the visible light spectrum [13-15]. If detectable, this emission from the ICT state is at a longer wavelength and enhanced by polar solvent as the ICT excited state more populated by the solvent stabilization. Due to multi-step process, ICT emission usually has lower fluorescence quantum yield compared with LE state. The fluorescent sensor can be designed based on the degree of the ICT process to be turn-off or turn-on or wavelength shift mode.

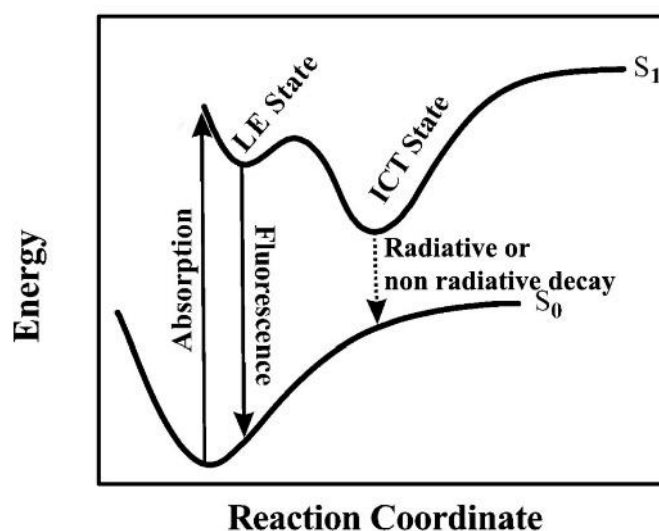


**Figure 1.4** Potential energy surfaces of the ground state ( $S_0$ ) is excited to  $S_1$  then relaxed to LE, and ICT state [16].

### 1.2.2.3 Förster resonance energy transfer (FRET)

Förster resonance energy transfer (FRET) is a dynamic quenching mechanism that the process can occur when emission spectrum of the energy donor (D) overlaps with the absorption spectrum (A) of the acceptor (Figure 1.5) [17, 18]. FRET drops quickly with the distance of donor and acceptor and increase with the spectral overlap between the donor emission and acceptor absorption, and the relative orientation of the donor and acceptor dipole moment. The idea of an oscillating dipole is supported this theory that can get an energy exchange with a second dipole which has a similar resonance frequency. So, resonance energy transfer is similar behavior of coupled oscillators. Measurements of FRET efficiency can be used as a research tool in biology and chemistry, both *in vitro* and *in vivo* to determine the distance between two fluorophores [19]. The sensing application in the term of turn-off and wavelength shift mode can be designed based on FRET process.

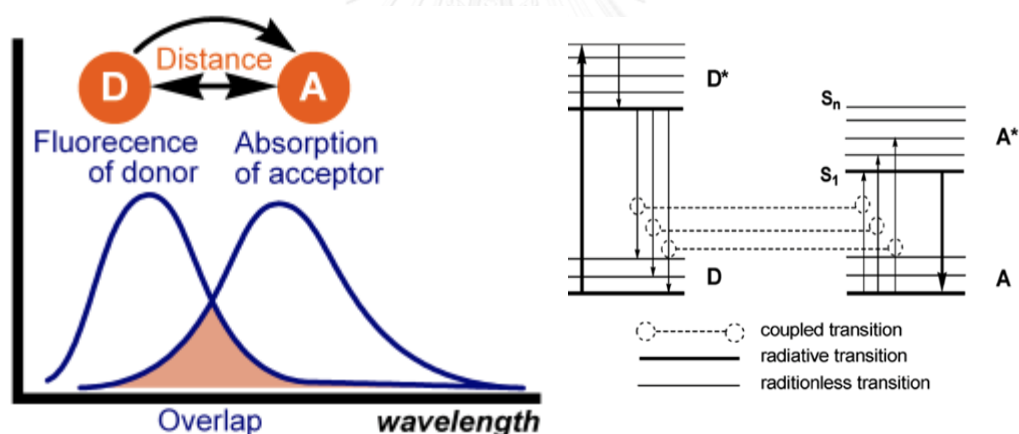
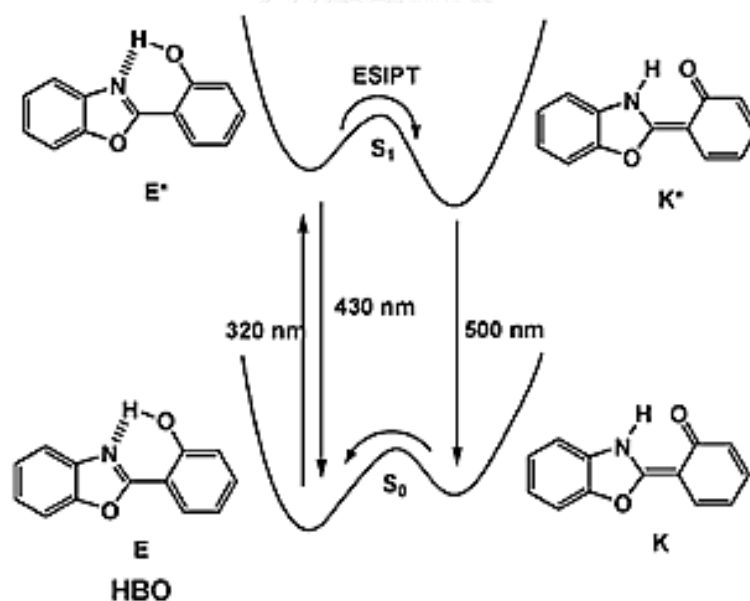


Figure 1.5 Förster resonance energy transfer (FRET) [20].



#### 1.2.2.4 Excited state intramolecular proton transfer ESIPT

The ESIPT process commonly associates with the transfer of a proton from a hydroxyl (or amino) group to a carbonyl oxygen (or imine nitrogen) with a six- or five-membered ring hydrogen bonding configuration intermediate [21]. The 2-(20-hydroxyphenyl)-benzoxazole (HBO) used as an example of the ESIPT photophysical process in Figure 1.6 After irradiation, the excited HBO in enol form ( $E^*$ ) is converted to the excited keto form ( $K^*$ ) in the sub picosecond time scale resulting in significantly red-shift emission compared with the absorption and unusually large Stoke shift. A large Stoke shift is beneficial in fluorescence sensing to avoid the self-absorption or the inner filter effect. The fluorescent sensor that designed with a large wavelength shift can be achieved with ESIPT process.



**Figure 1.6** Principal photophysics of ESIPT illustrated with 2-(20-hydroxyphenyl)-benzoxazole (HBO) [22].

### 1.3 Quinoline-Based Fluorescence Sensors

Quinolines are one of the most interesting classes of heterocyclic compounds forming fluorescent complex with metal ions. The prime example is tris-(8-hydroxy quinoline) aluminium  $AlQ_3$  which is highly fluorescent in both solution and solid states that it has been used as a standard green emissive material for organic light-emitting diodes (OLEDs) [23-28]. Quinoline and its derivatives, mainly 8-hydroxyquinoline and 8-aminoquinoline, are important fluorescence sensor for detecting metal ions [29]. Derivatives of 8-aminoquinoline with an aryl sulfonamide [30] (Figure 1.7) are the first and most widely applied fluorescent chemosensors for  $Zn^{2+}$  in biological samples. They are highly selective sensors for  $Zn^{2+}$  in the presence of high concentrations of  $Ca^{2+}$  and  $Mg^{2+}$ , which is very important for *in vivo* application. However, their poor water solubility has limited their applications [31].

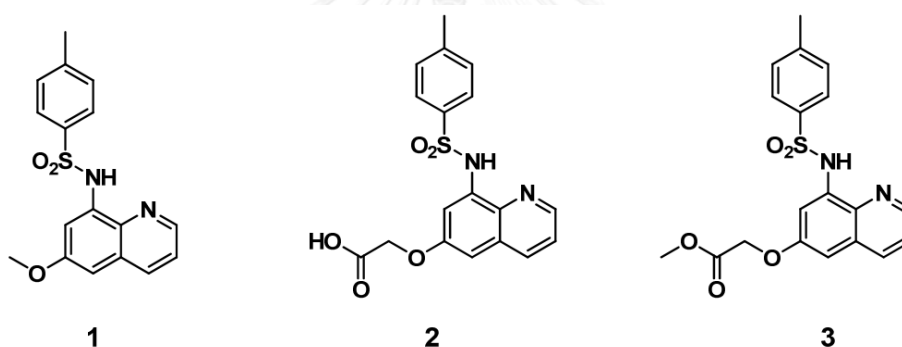


**Figure 1.7** Derivatives of 8-aminoquinoline with an aryl sulfonamide [29].

In 2008, Zhang et al. [32] reported a water-soluble and ratiometric chemosensor **AQZ**, based on 8-aminoquinoline for  $Zn^{2+}$  ion, which showed 8-fold increase in fluorescence quantum yield (Figure 1.8) and a 75 nm red-shift of the emission peak from 440 to 515 nm. The association constant ( $K_a$ ) was determined as  $= 6.7 \times 10^6$  in methanol/water 1:9 (v/v). **AQZ** was applied for sensing of  $Zn^{2+}$  in yeast cells.

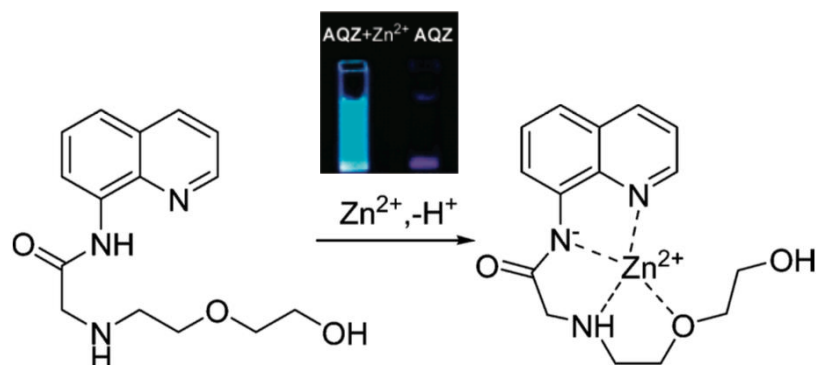


**Figure 1.8** Proposed of  $\text{AQZ-Zn}^{2+}$  complexation resulting in fluorescence enhancement [32].

In 2011, Xiaobo et al. [33] designed and synthesized a pair of carboxamido quinoline pendants onto *trans*-1,2-diaminocyclohexane scaffold via *N*-alkylation, multifunctionalized (**ACAQ** in Figure 1.9). In 50% methanol/aqueous buffer pH 7.4 solution, **ACAQ** displayed a selective ratiometric fluorescence changes with a shift from 410 to 490 nm upon excitation at 316 nm in response to the complexation with  $\text{Zn}^{2+}$ . The enhancement ratio of  $I_{490}/I_{410}$  recorded of 12-fold. The limit of detection (LOD) of **ACAQ** with  $\text{Zn}^{2+}$  was 28.3 nM. The  $K_a$  determined in methanol/water 50:50 (v/v) was  $1.8 \times 10^6$ . Two stoichiometric complexes were observed by  $^1\text{H}$  NMR spectroscopy at different **ACAQ**: $\text{Zn}^{2+}$  ratios. **ACAQ** was applied for  $\text{Zn}^{2+}$  sensing in HK-1 cells.

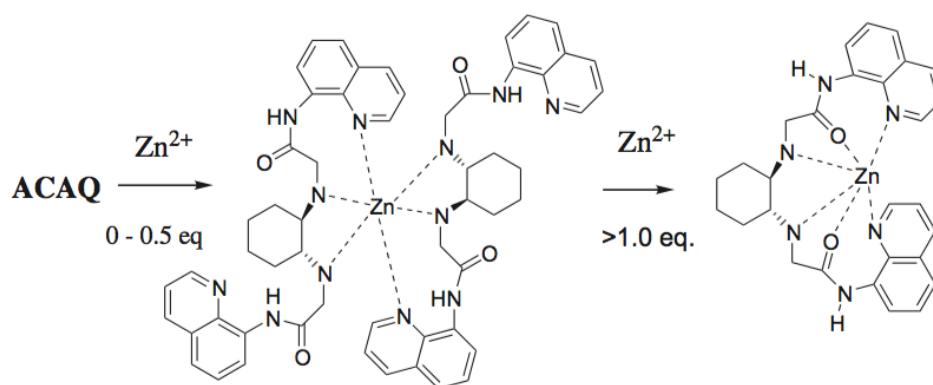


**Figure 1.9** Proposed two complexes observed by  $^1\text{H}$  NMR spectroscopy at different **ACAQ**: $\text{Zn}^{2+}$  ratios [33].

In the same year, Parul et al. [34] designed and synthesized *N*-(quinolin-8-yl)-2-[3-(triethoxysilyl)propylamino]acetamide on ordered mesoporous silica material, MCM-41, for Zn<sup>2+</sup> fluorescent sensing application (Figure 1.10). The **QTEPA-modified MCM-41** showed 3-fold fluorescence emission enhancement and about a 55 nm red shift. The association constant  $K_a$  value was determined to be  $5.7 \times 10^3 \text{ M}^{-1}$  in aqueous buffer solution with the limit of detection (LOD) of 0.1  $\mu\text{M}$ .

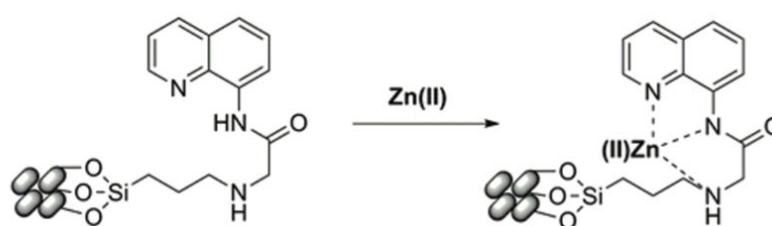


**Figure 1.10** Proposed binding of **QTEPA-modified MCM-41** and Zn<sup>2+</sup> [34].

In 2012, Zhang et al. [35] synthesized a series of carboxamidoquinoline based fluorescent sensors, the **AQZ** family (Figure 1.11a). The substituents and their positions on the quinoline ring were varied for tuning its fluorescence sensing properties. All synthesized **AQZ** derivatives showed high fluorescence enhancement sensitivity for Zn<sup>2+</sup> in aqueous buffer solution. The derivatives containing morpholine (**AQZ4MP** and **AQZ2MP**) also showed very high selectivity (Figure 1.11b). The apparent dissociation constants ( $K_d$ ) of the Zn<sup>2+</sup> complexes were  $10^{-5}$ – $10^{-6}$  M.

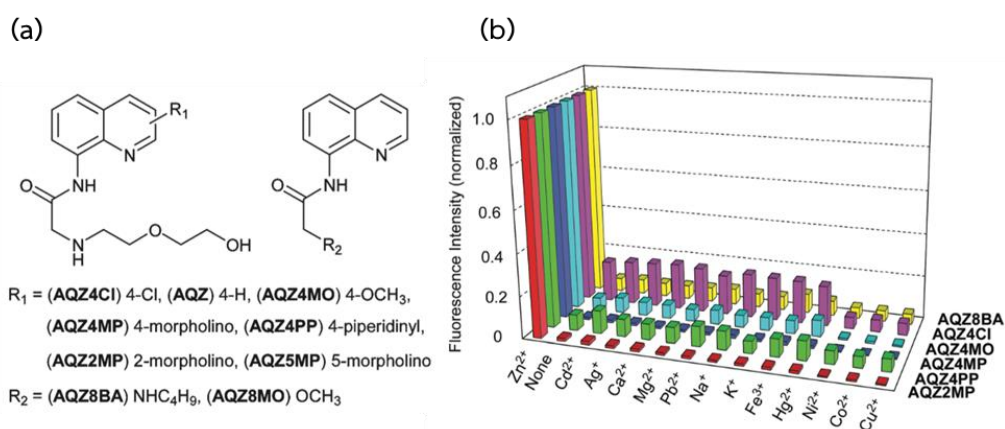


**Figure 1.11** (a) Structure of AQZ derivatives and (b) normalize selectivity graph of AQZ family with various metal ions [35].

In 2013, Zhengping et al. [36] developed (*N*-Quinolin-8-yl-2-[(quinolin-8-ylcarbamoylmethyl)-amino]-acetamide, **NQA**) as a novel fluorescent sensor for  $\text{Zn}^{2+}$ . **NQA** showed selectivity for  $\text{Zn}^{2+}$  in the presence of other metal ions in aqueous solution (Figure 1.12) with the  $K_a$  of  $8.69 \times 10^5 \text{ M}^{-1}$  and the LOD of 0.2 nM. Furthermore, the fluorescent changes of **NQA** upon the addition of cations ( $\text{Cu}^{2+}$  and  $\text{Zn}^{2+}$ ) are utilized to construct an Inhibit logic gate at the molecular level, using  $\text{Cu}^{2+}$  and  $\text{Zn}^{2+}$  as chemical inputs and the fluorescence intensity as output.

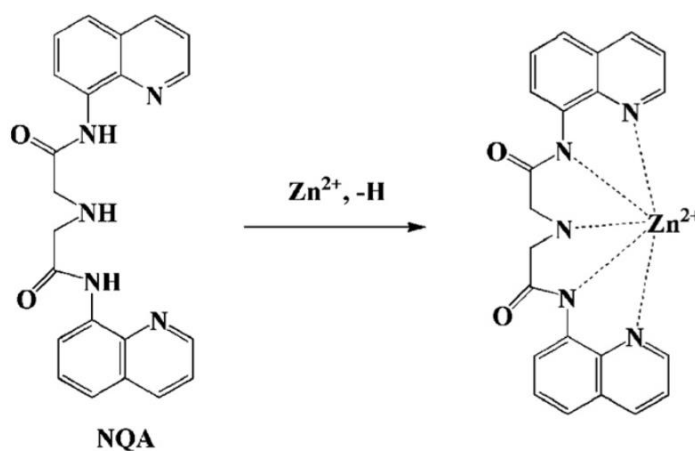


**Figure 1.12** Proposed binding between **NQA** and  $\text{Zn}^{2+}$  resulting in fluorescence enhancement [36].

In the same year, Yang et al. [37] synthesized a quinolone based acetamidoquinoline bearing picolyamine (**R-1**) for the dual detection of  $\text{Zn}^{2+}$  and  $\text{Cd}^{2+}$  in aqueous solution. Upon binding to both metal ions, fluorescence enhancement at 497 nm, corresponding to the 77 nm red-shift, was observed. The binding constants between sensor and metal ions were calculated to be  $1.64 \times 10^5 \text{ M}^{-1}$  for  $\text{Zn}^{2+}$  and  $6.30 \times 10^4 \text{ M}^{-1}$  for  $\text{Cd}^{2+}$ . The detection limits were calculated to be 3.2  $\mu\text{M}$  for  $\text{Zn}^{2+}$  and 170  $\mu\text{M}$  for  $\text{Cd}^{2+}$ , respectively. Addition of excess cysteine, the fluorescence of **R-1**/ $\text{Cd}^{2+}$  complex reduced. However, the fluorescence of **R-1**/ $\text{Zn}^{2+}$  complex unchanged with the addition of cysteine. Thus, by using **R-1** and cysteine,  $\text{Zn}^{2+}$  and  $\text{Cd}^{2+}$  could be readily distinguished (**Figure 1.13**).

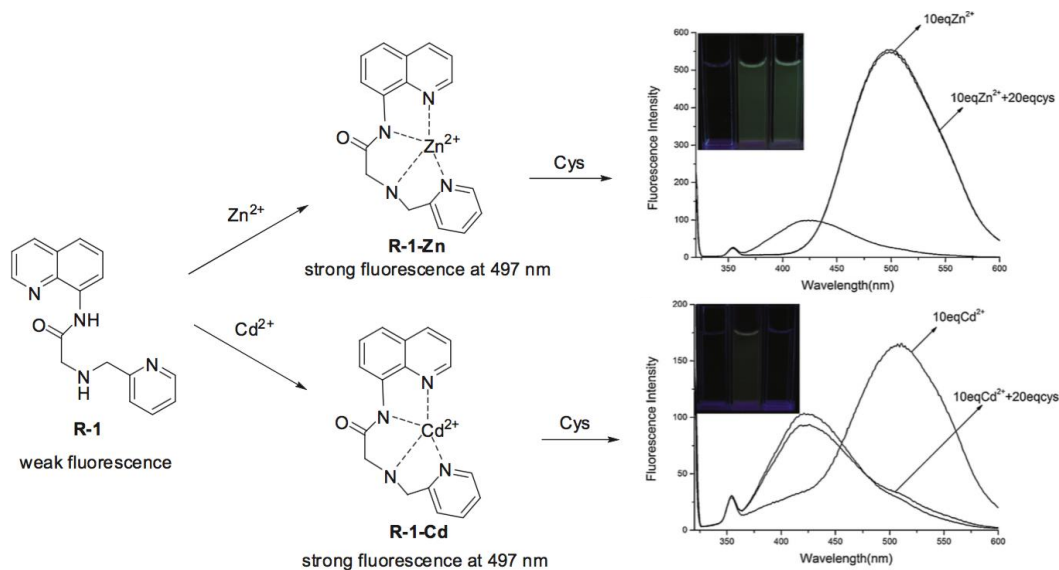


**Figure 1.13** Proposed complexation of  $\text{Zn}^{2+}$  and  $\text{Cd}^{2+}$  with **R-1** and cysteine [37].

In the same year, Shyamaprosad et al. [38] designed and synthesized a new sensor, **TAQ** as see in Figure 1.14. **TAQ** showed good water solubility and high selectivity for  $\text{Zn}^{2+}$  sensing; about a 15-fold increase in fluorescence quantum yield and a 100 nm red-shift of fluorescence emission upon binding  $\text{Zn}^{2+}$  in aqueous HEPES buffer solution are observed. The  $K_a$  value between **TAQ** and  $\text{Zn}^{2+}$  was  $4 \times 10^4 \text{ M}^{-1}$  and the LOD was  $3.2 \mu\text{M}$ . The  $\text{Zn}^{2+}$ -**TAQ** complex can also be used in killing human lung cancer cells (A549).

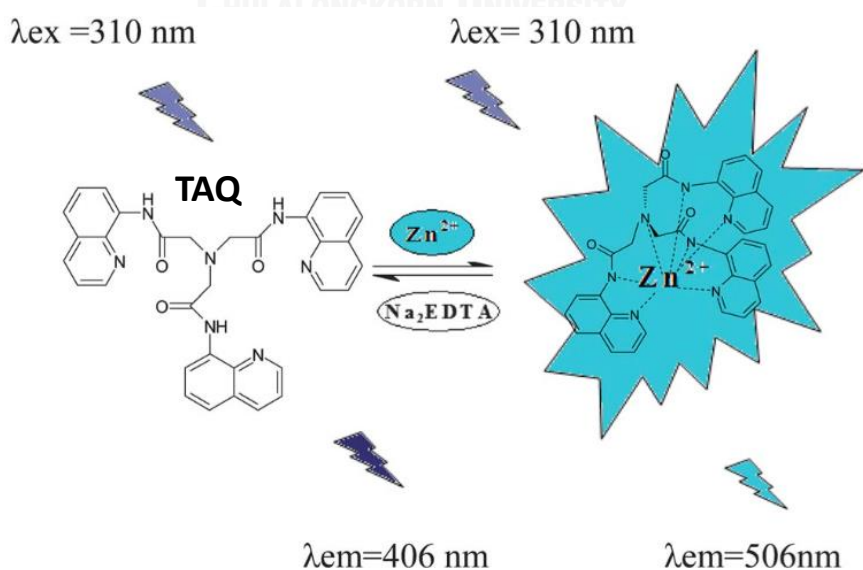


**Figure 1.14** Probable host-guest binding between **TAQ** and  $\text{Zn}^{2+}$  [38].

#### 1.4 Objectives of this research

The objectives of this work is to synthesize and evaluate a series of amide derivatives of 8-aminoquinoline having different amino acid pendants i.e. glycine,  $\beta$ -alanine and glycylglycine (

Figure 1.15) as turn-on fluorescent sensors for  $Zn^{2+}$ . The variation of amino acid pendants is incorporated to investigate essential binding *N*-atoms and their positions in these type quinoline ligands. The sensing study is aimed to optimize the sensing applications in aqueous media, fluorescence imaging, naked eye detection and multiple metal ion detection.

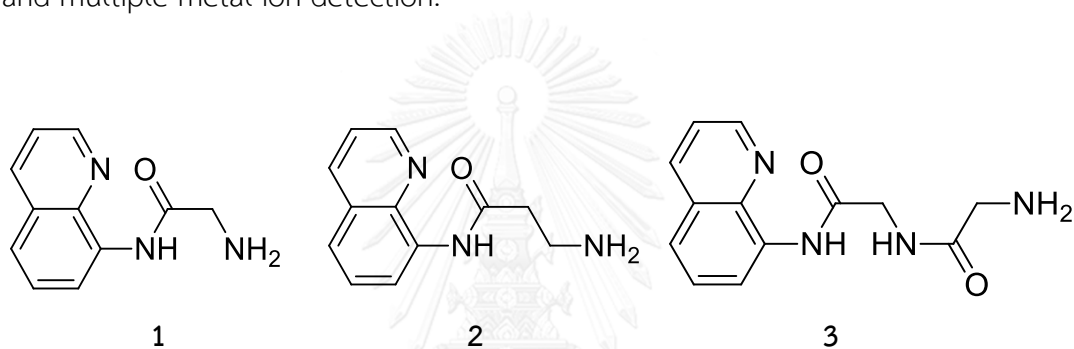


Figure 1.15 Target molecules 1, 2, 3.

## CHAPTER II

### EXPERIMENT

#### 2.1 Reagents and materials

8-Aminoquinoline, Boc-Glycine, Boc- $\beta$ -Alanine, triethanolamine (TEA) and 4-dimethylaminopyridine (DMAP) were purchased from Merck® (Germany). *N*-(3-dimethylaminopropyl)-*N*-ethylcarbodiimide hydrochloride (EDC·HCl) 98%, di-*tert*-butyl dicarbonate (Boc<sub>2</sub>O), ammonium chloride (NH<sub>4</sub>Cl), trifluoroacetic acid (TFA) and sodium bicarbonate (NaHCO<sub>3</sub>) were purchased from Sigma Aldrich (USA). Glycylglycine was purchased from TCI Tokyo Chemical Industry (Japan). In anhydrous reactions, solvent such as dichloromethane was dried before use and stored over molecular sieves. All column chromatography were operated using Merck silica gel 60 (70-230 mesh). Thin layer chromatography (TLC) was performed on silica gel plates (Merck F<sub>245</sub>). Visualization was performed with a 254 nm ultraviolet lamp. Solvents used for extraction and chromatography such as dichloromethane, hexane and ethyl acetate were commercial grade and distilled before use. Milli-Q water was used in all aqueous experiments unless specified otherwise.

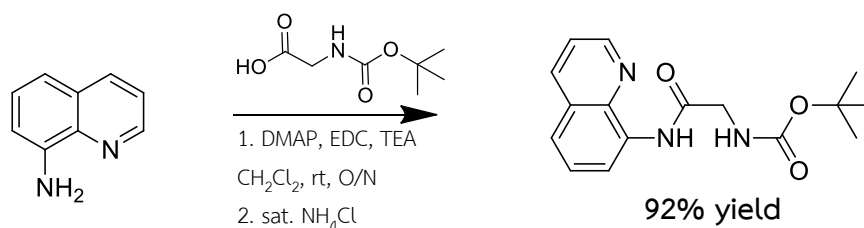
#### 2.2 Analytical instruments

<sup>1</sup>H-NMR and <sup>13</sup>C-NMR spectra were acquired from sample solution in CDCl<sub>3</sub>, CD<sub>3</sub>OD and (CD<sub>3</sub>)<sub>2</sub>SO on Varian Mercury and Bruker AVANCE NMR spectrometers at 400 MHz and 100 MHz, respectively. Mass spectra were recorded on electrospray ionization (ESI) Micro mass Quattro Micro API. The absorption and emission spectra were acquired from solution of the fluorophore in quartz cuvette with 1 cm light path. Absorption spectra were measured by using Varian Cary 50 UV-vis spectrophotometer. Fluorescence spectra were recorded on a Varian Cary Eclipse spectrofluorometer. Fourier transform infrared spectra were acquired on Nicolet 6700 FT-IR spectrometer equipped with a mercury-cadmium telluride (MCT) detector (Nicolet, USA).



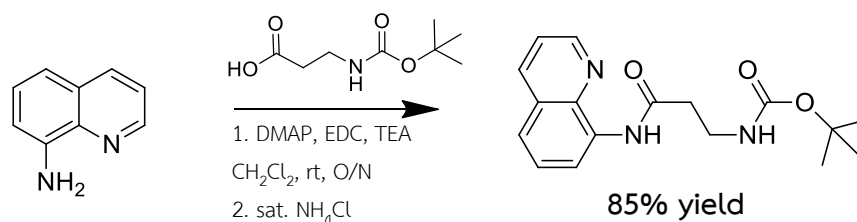
## 2.3 Synthesis of fluorophores

### 2.3.1 Synthesis of compound 4: *tert*-butyl-2-oxo-2-[(quinolin-8-yl)amino]ethyl carbamate



8-Aminoquinoline (200 mg, 1.39 mmol), DMAP (8.47 mg, 0.07 mmol) and triethylamine (0.19 ml, 0.14 mmol) were dissolved in dry dichloromethane (20 mL). Boc-Glycine (729 mg, 4.16 mmol) was added to the mixture and chilled to 0 °C followed by the addition of EDC (798 mg, 4.16 mmol). The reaction mixture was stirred at 0 °C for 2 hours and stirred overnight at room temperature. The reaction mixture was extracted with NH<sub>4</sub>Cl. The combined organic layer was dried over MgSO<sub>4</sub>, filtered and concentrated under vacuum. The crude product was purified on a silica gel column chromatography using 40% ethyl acetate in hexane as an eluent to afford compound 4 as a white solid (385 mg, 92%). <sup>1</sup>H NMR (400 MHz, CDCl<sub>3</sub>) δ 10.27 (s, 1H), 8.80 (d, *J* = 3.0 Hz, 1H), 8.74 (br dd, *J* = 5.5, 2.7 Hz, 1H), 8.20 (d, *J* = 8.2 Hz, 1H), 7.57 – 7.51 (m, 2H), 7.48 (dd, *J* = 8.2, 4.0 Hz, 1H), 5.39 (s, 1H), 4.14 (d, *J* = 4.0 Hz, 2H), 1.51 (s, 9H). MS (ESI): *m/z* calculated for [C<sub>16</sub>H<sub>20</sub>N<sub>3</sub>O<sub>3</sub>]<sup>+</sup> is 302.15; found 302.17 [M + H]<sup>+</sup>.

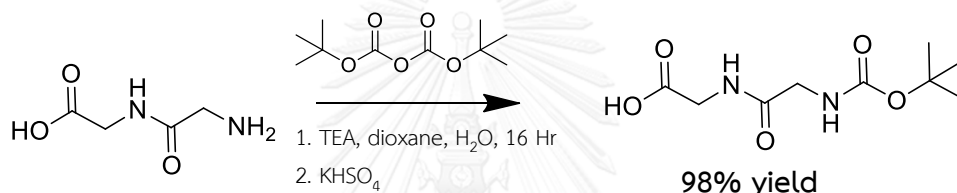
### 2.3.2 Synthesis of compound 5: *tert*-butyl-3-oxo-3-[(quinolin-8-yl)amino]propyl carbamate



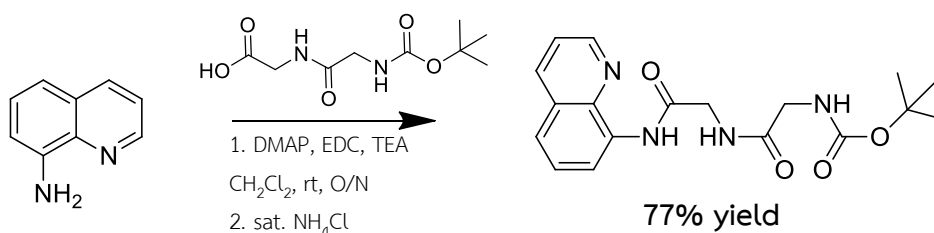
Using a similar procedure in the synthesis of compound **4** but replacing Boc-Glycine with Boc- $\beta$ -Alanine, compound **5** was obtained as a yellow solid (373 mg, 85%).  $^1\text{H}$  NMR (400 MHz,  $\text{CDCl}_3$ )  $\delta$  9.86 (s, 1H), 8.81 (dd,  $J = 4.2, 1.5$  Hz, 1H), 8.74 (dd,  $J = 6.7, 2.0$  Hz, 1H), 8.19 (d,  $J = 7.9$  Hz, 1H), 7.58 – 7.51 (m, 2H), 7.48 (dd,  $J = 8.2, 4.2$  Hz, 1H), 5.28 (br s, 1H), 3.57 (br q,  $J = 5.8$  Hz, 2H), 2.81 (t,  $J = 5.8$  Hz, 2H), 1.43 (s, 9H). MS (ESI):  $m/z$  calculated for  $[\text{C}_{17}\text{H}_{22}\text{N}_3\text{O}_3]^+$  is 316.17; found 316.20  $[\text{M} + \text{H}]^+$ .

### 2.3.3 Synthesis of compound **6**: *tert*-butyl-2-oxo-2-(2-oxo-2-[(quinolin-8-yl)amino]ethylamino)ethylcarbamate

#### 2.3.3.1 Preparation of Boc-Glycylglycine

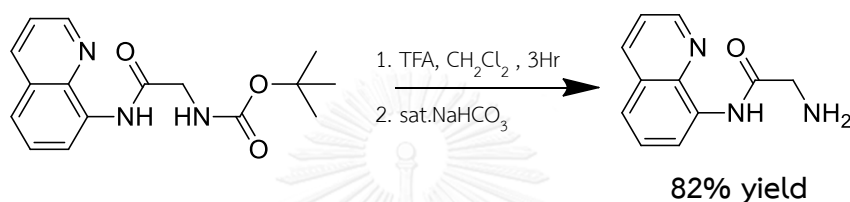


TEA (1.58 mL, 11.35 mmol) and Boc<sub>2</sub>O (1.98 g, 9.08 mmol) were added dropwise to a solution of glycylglycine (1.00 g, 7.57 mmol) in a mixture of dioxane (20 mL) and H<sub>2</sub>O (5 mL) at 0°C. The mixture was stirred at room temperature for 16 hours. Then the reaction mixture was diluted with H<sub>2</sub>O (50 mL), acidified to pH 3 by an addition of solid KHSO<sub>4</sub> and extracted with ethyl acetate (5 times  $\times$  50 mL). After that the combined organic phases were dried over Na<sub>2</sub>SO<sub>4</sub> and all solvents were removed under high vacuum to give a white solid (1.72 g, 98% yield).  $^1\text{H}$  NMR (400 MHz,  $(\text{CD}_3)_2\text{SO}$ )  $\delta$  12.58 (s, 1H), 8.06 (t,  $J = 5.8$  Hz, 1H), 7.01 (t,  $J = 6.1$  Hz, 1H), 3.75 (d,  $J = 5.8$  Hz, 2H), 3.56 (d,  $J = 6.1$  Hz, 2H), 1.38 (s, 9H).

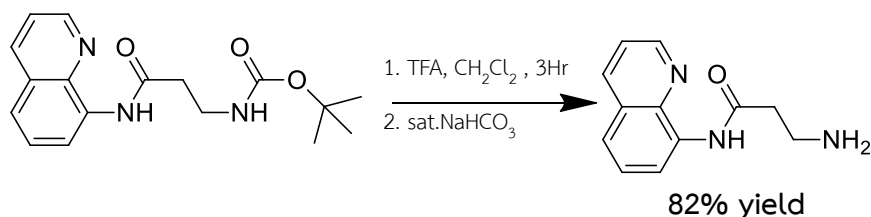


Using a similar procedure in the synthesis of compound **4** but replacing Boc-Glycine with Boc-Glycylglycine, compound **6** was obtained as a yellow solid (383 mg, 77%).  $^1\text{H}$  NMR (400 MHz,  $\text{CDCl}_3$ )  $\delta$  10.07 (br s, 1H), 8.81 (br dd,  $J = 4.3, 1.2$  Hz, 1H), 8.67 (br t,  $J = 4.5$  Hz, 1H), 8.16 (d,  $J = 8.2$  Hz, 1H), 7.55 – 7.49 (m, 2H), 7.46 (dd,  $J = 8.2, 4.3$  Hz, 1H), 7.11 (s, 1H), 5.32 (br s, 1H), 4.31 (d,  $J = 5.2$  Hz, 2H), 3.97 (br d,  $J = 5.6$  Hz, 2H), 1.45 (s, 9H). MS (ESI):  $m/z$  calculated for  $[\text{C}_{18}\text{H}_{23}\text{N}_4\text{O}_4]^+$  is 359.22; found 316.20  $[\text{M} + \text{H}]^+$ .

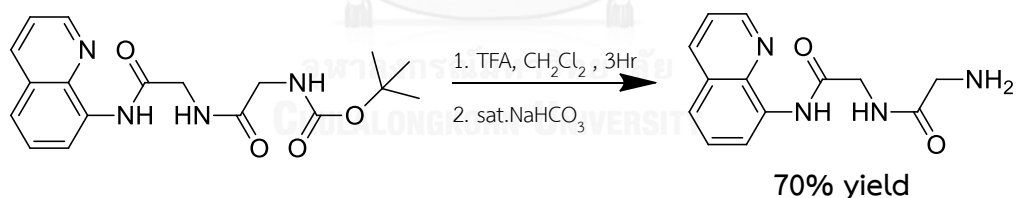
#### 2.3.4 Synthesis of compound **1**: 2-amino-*N*-(quinolin-8-yl)acetamide



The deprotection of the *N*-tert-Boc group of compound **4** (200 mg, 0.66 mmol) was achieved by using TFA (1.0 mL, 13.3 mmol) in dichloromethane (10 mL). The stirring was continued at room temperature for 3 hours. Solvent and excess TFA were removed under high vacuum and then the reaction mixture was neutralized by saturated  $\text{NaHCO}_3$  solution followed by an addition of dichloromethane (10 mL). The organic layer was separated and dried over  $\text{MgSO}_4$ , filtered and concentrated under high vacuum. Compound **1** was obtained as a yellow solid (110 mg, 82%).  $^1\text{H}$  NMR (400 MHz,  $\text{CD}_3\text{OD}$ )  $\delta$  8.90 (dd,  $J = 4.2, 1.6$  Hz, 1H), 8.66 (dd,  $J = 7.6, 0.9$  Hz, 1H), 8.33 (dd,  $J = 8.3, 1.6$  Hz, 1H), 7.68 (dd,  $J = 8.3, 0.9$  Hz, 1H), 7.57 (dd,  $J = 8.3, 4.2$  Hz, 1H), 7.57 (br t,  $J = 7.9$  Hz, 1H), 4.11 (s, 2H).  $^1\text{H}$  NMR (400 MHz,  $(\text{CD}_3)_2\text{SO}$ )  $\delta$  11.64 (s, 1H), 8.93 (dd,  $J = 4.1, 1.6$  Hz, 1H), 8.75 (dd,  $J = 7.5, 1.2$  Hz, 1H), 8.40 (dd,  $J = 8.3, 1.6$  Hz, 1H), 7.68 – 7.54 (m, 3H), 3.40 (s, 2H), 2.42 (s, 2H).  $^{13}\text{C}$  NMR (100 MHz,  $\text{CD}_3\text{OD}$ )  $\delta$  174.3, 150.0, 140.3, 137.5, 135.3, 129.6, 127.9, 123.4, 123.0, 117.9, 46.5. IR(ATR)  $\nu_{\text{max}}$  3382, 3363, 3291, 1650  $\text{cm}^{-1}$ . MS (ESI):  $m/z$  calculated for  $[\text{C}_{11}\text{H}_{11}\text{N}_3\text{O}]^+$  is 201.09; found 202.10  $[\text{M} + \text{H}]^+$ .

2.3.5 Synthesis of compound **2**: 3-amino-*N*-(quinolin-8-yl)propanamide

Using a similar procedure in the synthesis of compound **1** but replacing compound **4** with compound **5**, compound **2** was obtained as a yellow solid (112 mg, 82% yield).  $^1\text{H}$  NMR (400 MHz,  $\text{CD}_3\text{OD}$ )  $\delta$  8.89 (dd,  $J = 4.2, 1.5$  Hz, 1H), 8.64 (d,  $J = 7.6$  Hz, 1H), 8.33 (dd,  $J = 8.2, 1.5$  Hz, 1H), 7.66 (d,  $J = 8.2$  Hz, 1H), 7.57 (dd,  $J = 8.2, 4.2$  Hz, 1H), 7.56 (br t,  $J = 7.9$  Hz, 1H), 3.35 (t,  $J = 6.2$  Hz, 2H), 3.05 (t,  $J = 6.2$  Hz, 2H).  $^{13}\text{C}$  NMR (100 MHz,  $\text{CD}_3\text{OD}$ )  $\delta$  170.6, 150.1, 140.2, 137.8, 135.3, 129.7, 127.9, 124.0, 123.1, 119.1, 36.9, 34.3. IR(ATR)  $\nu_{\text{max}}$  3335, 3165 1667  $\text{cm}^{-1}$ . MS (ESI):  $m/z$  calculated for  $[\text{C}_{12}\text{H}_{14}\text{N}_3\text{O}]^+$  is 216.11; found: 216.12  $[\text{M} + \text{H}]^+$ .

2.3.6 Synthesis of compound **3**: 2-amino-*N*-2-oxo-2-[(quinolin-8-yl)amino]ethyl acetamide

Using a similar procedure in the synthesis of compound **1** but replacing compound **4** with compound **6**, compound **3** was obtained as a yellow solid (101 mg, 70% yield).  $^1\text{H}$  NMR (400 MHz,  $\text{CD}_3\text{OD}$ )  $\delta$  8.89 (dd,  $J = 4.3, 1.7$  Hz, 1H), 8.62 (dd,  $J = 7.6, 1.1$  Hz, 1H), 8.33 (dd,  $J = 8.4, 1.7$  Hz, 1H), 7.66 (dd,  $J = 8.1, 1.1$  Hz, 1H), 7.60 – 7.53 (m, 2H), 4.30 (s, 2H), 3.86 (s, 2H).  $^{13}\text{C}$  NMR (100 MHz,  $\text{CD}_3\text{OD}$ )  $\delta$  169.4, 168.2, 150.2, 140.1, 137.8, 135.1, 129.7, 128.0, 123.9, 123.2, 118.5, 44.6, 41.61. IR(ATR)  $\nu_{\text{max}}$  3326, 285, 1711 1670  $\text{cm}^{-1}$ . MS (ESI):  $m/z$  calculated for  $[\text{C}_{13}\text{H}_{14}\text{N}_4\text{O}_2]^+$  is 258.11; found 259.16  $[\text{M} + \text{H}]^+$ .

## 2.4 Photophysical property study

### 2.4.1 UV-Visible spectroscopy

The stock solutions of **1**, **2** and **3** (10 mM) in methanol were prepared. The absorption spectra of all fluorophores were recorded from 250 nm to 600 nm at ambient temperature.

#### 2.4.1.1. Molar Absorption Coefficients ( $\epsilon$ )

Molar Absorption Coefficients ( $\epsilon$ ) of all fluorophores were estimated from UV absorption spectra of analytical for 8-aminoquinoline derivatives at various concentrations in Tris-HCl aqueous buffer pH 7.4 solution containing methanol (1% v/v). The intensities at maximum absorption wavelength ( $\lambda_{\max}$ ) of each compound were plotted against the concentrations. Each plot should be a straight line goes through origin. Molar Absorption Coefficients ( $\epsilon$ ) can be obtained from the slopes of these plots according to the following equation:

$$A = \epsilon bC$$

\*b is the cell path length.

### 2.4.2 Fluorescence spectroscopy

The stock solutions of **1**, **2** and **3** were dilute to 10  $\mu$ M in Tris-HCl aqueous buffer pH 7.4 solution containing methanol (1% v/v). The emission spectra of fluorophores were recorded from 300 nm to 700 nm at ambient temperature using an excitation wavelength at 300 nm.

### 2.4.3 Fluorophore quantum yields

The fluorescence quantum yields of **1**, **2**, **3** and complex between **1** and  $\text{Zn}^{2+}$  were performed in Tris-HCl aqueous buffer pH 7.4 solution containing methanol (1% v/v). Each sample used quinine sulphate ( $\Phi_{\text{ST}} = 0.54$ :  $\lambda_{\text{ex}} 336$  nm) in 0.5 M  $\text{H}_2\text{SO}_4$  or fluorescein ( $\Phi_{\text{ST}} = 0.95$ :  $\lambda_{\text{ex}} 496$  nm) in 0.1 M NaOH as a reference [39-42].

The UV-Vis absorption spectra of ten analytical samples and ten reference samples at varied concentrations were recorded. The maximum absorbance of all samples should never exceed 0.1. The fluorescence emission spectra of the same solution using appropriate excitation wavelengths selected were recorded based on the absorption maximum wavelength ( $\lambda_{\text{max}}$ ) of each compound. Graphs of integrated fluorescence intensities were plotted against the absorbance at the respective excitation wavelengths. Each plot should be a straight line with 0 interception and gradient  $m$ .

In addition, the fluorescence quantum yield ( $\Phi_x$ ) was obtained from plotting of integrated fluorescence intensity vs absorbance represented into the following equation:

$$\Phi_x = \Phi_{\text{ST}} \left( \frac{\text{Grad}_x}{\text{Grad}_{\text{ST}}} \right) \left( \frac{\eta_x^2}{\eta_{\text{ST}}^2} \right)$$

The subscript  $\Phi_{\text{ST}}$  denote the fluorescence quantum yield of a standard reference  $\Phi_x$  is the fluorescence quantum yield of sample and  $\eta$  is the refractive index of the solvent.

## 2.5 Fluorescent sensor study

### 2.5.1 Selectivity study

The 10 mM stock solutions of the cation tested were prepared by dissolving their salts LiCl, NaOAc, KCl,  $\text{Mg}(\text{NO}_3)_2$ ,  $\text{Ca}(\text{OAc})_2$ ,  $\text{Ba}(\text{NO}_3)_2$ ,  $\text{Al}(\text{NO}_3)_3$ ,  $\text{Cr}(\text{NO}_3)_3$ ,  $\text{FeSO}_4$ ,  $\text{Fe}(\text{NO}_3)_3$ ,  $\text{Co}(\text{NO}_3)_2$ ,  $\text{Ni}(\text{NO}_3)_2$ ,  $\text{Cu}(\text{OAc})_2$ ,  $\text{Zn}(\text{OAc})_2$ ,  $\text{AgNO}_3$ ,  $\text{Cd}(\text{OAc})_2$ ,  $\text{HgCl}_2$  and  $\text{Pb}(\text{OAc})_2$  in Milli-Q water. The cation stock solution (10  $\mu\text{L}$ ) was added to the fluorophore stock solution in methanol (1 mM, 10  $\mu\text{L}$ ). The volume of the mixture was adjusted by Tris-HCl buffer solution or ethanol to 1 mL to afford the final concentration of 10  $\mu\text{M}$  for the fluorophore and 100  $\mu\text{M}$  for the cation. All final aqueous solutions used for fluorescence measurement contain  $\sim 1\%$  methanol. The emission spectra were recorded starting from 10 nm longer than the excitation wavelength to 700 nm.

### 2.5.2 Fluorescence titration

The stock solution of the sensing compound in methanol (10 mM, 10  $\mu$ L) was diluted with Tris-HCl buffer solution (900  $\mu$ L) in a 1 mL quartz cuvette. Designated volumes (0-100  $\mu$ L) of the Zn(OAc)<sub>2</sub> stock solution (10 mM) in Milli-Q water was added into the sensor solution. The final volumes were adjusted to 1 mL by adding Tris-HCl buffer solution. The final concentration of each fluorophore is 10  $\mu$ M in Tris-HCl aqueous buffer pH 7.4 solution containing methanol (1% v/v). The emission spectra were recorded from 300 nm to 700 nm at ambient temperature using an excitation wavelength at 300 nm.

### 2.5.3 The association constant ( $K_a$ )

The association constant ( $K_a$ ) could be determined from the slope of the straight line of the plot of  $1/(I - I_0)$  against  $1/[Zn^{2+n}]^n$  as shown in Figure 3.10  $K_a$  was calculated following the equation stated below.

$$K_a = \frac{\text{intercept}}{\text{slope}}$$

### 2.5.4 Competition with other metal ions

The mixture of each compound  $1/Zn^{2+}$ /other metal ions in concentration of 10/100/100  $\mu$ M with ratio 1/10/10 were used to investigate the interference of other metal ions to  $Zn^{2+}$  binding with sensor.

### 2.5.5 Limit of detection for turn-on sensing

In fluorescent sensing, limit of detection (LOD) is the lowest concentration of analyte in a sample that is required to produce a signal greater than three times the standard deviation of the blank sample. However the value is not necessarily quantitated as an exact value. For turn-on sensing, the limit of detection can be calculated according to the equation:

$$LOD = [(I_0 + 3SD)/I_0 - \text{Intercept}]/K$$

The variables were similar to those in turn-on sensing. Except  $K$  is the slope of the straight line of the plot of  $I/I_0$  against the concentration of an analyte  $[A]$ . Example of the calibration curve is shown in Figure 2.1

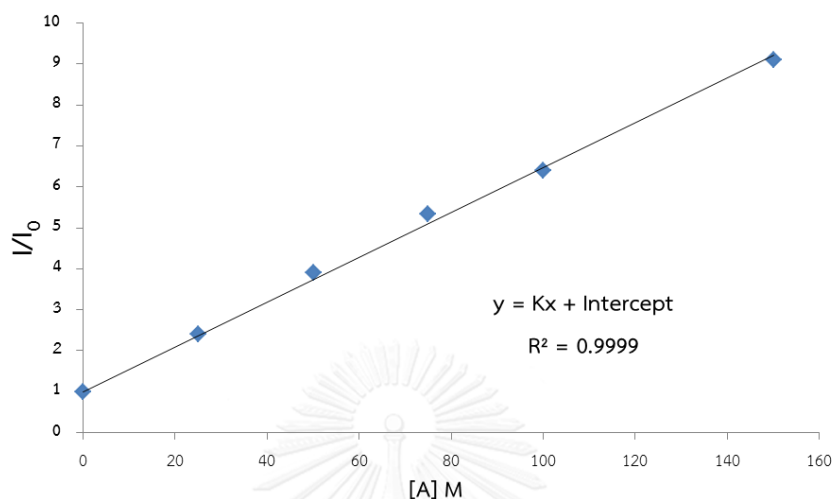


**Figure 2.1** the calibration curve for turn-on sensing.

## 2.6 NMR titration

A solution of **1** (10.0 mg, 0.05 mmol) in  $(CD_3)_2SO$  (0.4 mL) and a solution of  $Zn(OAc)_2$  (0.1 mmol) in  $(CD_3)_2SO$  (0.2 mL) were prepared. For  $^1H$  NMR titration of, the calculated volume of  $Zn(OAc)_2$  solution, at designated equivalent, was added to the solution of **1**. After thorough mixing,  $^1H$  NMR spectra were recorded.

## 2.7 Fluorescence images of $Zn^{2+}$ and $Cd^{2+}$ in plant samples

A sprout (5 mm) closest to the root of 4-day old Chinese cabbage (*Brassica rapa*.) seedling was cut longitudinal-section into two half. The samples were incubated with  $Zn(OAc)_2$  aqueous solution (100  $\mu M$ ) for 40 minutes, and then placed in ethanol for 40 minutes to remove chlorophyll. For comparison, one sample was left in distilled water and the other sample was left in fresh ethanol for 10 minutes. These two samples were placed side by side (5 mm apart) on a microscope slide (25  $\times$  75 mm<sup>2</sup>) and separately closed with two cover slides (22  $\times$  22 mm<sup>2</sup>). The prepared sample slide was mounted on a confocal laser scanning fluorescence microscope (Nikon, Eclipse-C1 Ti series). The fluorescence image was acquired by using the



excitation and detection wavelengths of 488 and 525 nm, respectively. A solution of **1** in methanol (100  $\mu\text{M}$ , 10  $\mu\text{L}$ ) was allowed to be drawn into each sample via the cover slide edge and the fluorescence image was then acquired again. For detecting of  $\text{Cd}^{2+}$ , the similar procedure was performed but the samples were incubated in  $\text{Cd}(\text{OAc})_2$  aqueous solution (100  $\mu\text{M}$ ) instead of the  $\text{Zn}(\text{OAc})_2$  solution.

## 2.8 Naked eye detection of $\text{Zn}^{2+}$ and $\text{Cd}^{2+}$ on paper-based sensors

A microwell plate style array of circular hydrophilic detection area with 3.0 mm diameter and 1.0 cm center-to-center distance (Figure 3.21) was created on a filter paper sheet (Whatman No. 1,  $21 \times 29.7 \text{ cm}^2$ ) by a wax-printing technique (Xerox Phaser 8860) and a common graphic software to create hydrophobic pattern of black wax ink. The printing pattern was heated at  $200^\circ\text{C}$  for 120 s on a hot plate to define the hydrophobic barriers and hydrophilic detection area [43]. For selectivity test, various metal ions (0.1 mM, 1.0  $\mu\text{L}$ ) were pipetted into the detection circles. After air drying, the solution of **1** in methanol (1.0 mM, 1.0  $\mu\text{L}$ ) was added on top of the metal ion area and allowed for air dry. The fluorescence images of the samples were photographically recorded by a digital camera under black light illumination.

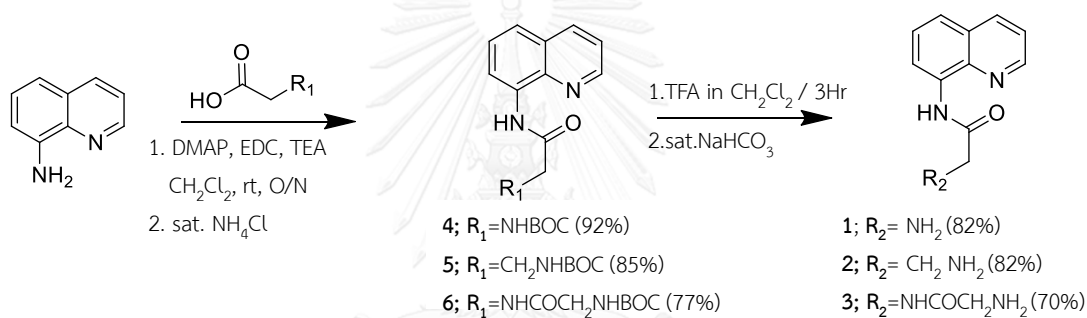
The simultaneous detection of  $\text{Zn}^{2+}$  and  $\text{Cd}^{2+}$ , was performed with chromatographic separation on filter paper strip (Whatman No. 1,  $9.5 \times 3.0 \text{ cm}^2$ ) with multi-channelled hydrophilic/hydrophobic pattern (Figure 3.22) created on a filter paper by the wax-printing technique. Each hydrophilic channel was 1.0 mm wide and 9.5 cm long having a circular reservoir (3.0 mm diameter) at 2.0 cm from the bottom of the filter paper. The channels were 5.0 mm separated from each other with the hydrophobic wax barrier generated by the heating technique described above. Each of  $\text{Zn}(\text{OAc})_2$  and  $\text{Cd}(\text{OAc})_2$  aqueous solution (1 mM, 1  $\mu\text{L}$ ) was separately pipetted onto the surface of the reservoir area. For the third spot, both solutions were spotted on top of each other. Then, the strip was placed in a closed chamber containing  $\text{CH}_3\text{NH}_2$  4% (v/v) in Milli-Q water as the mobile phase. After the development and an air dry, the methanol solution of **1** (1 mM) was sprayed on the developed strip for visualization. The fluorescence images of the samples were photographically recorded by a digital camera under black light illumination.

## CHAPTER III

### RESULTS AND DISCUSSION

#### 3.1 Synthesis and characterization of 1, 2 and 3

The synthesis of ligands **1-3** were achieved according to Scheme 3.1. The coupling of 8-aminoquinoline with an *N*-BOC protected amino acid (glycine,  $\beta$ -alanine and glycyglycine) in the presence of TEA, DMAP and EDC gave BOC-protected precursors (**4-6**). Upon the Boc deprotection, compounds **1-3** were obtained in satisfactory yields. The structures and purity of compounds **1-3** were confirmed by  $^1\text{H}$  NMR,  $^{13}\text{C}$  NMR, IR, and MS.



**Scheme 3.1** Synthesis of 8-aminoquinoline ligands modified with amino acids.

For the NMR characterization,  $^1\text{H}$  NMR spectrum of fluorophores **1-3** is shown in Figure 3.1. All fluorophores **1-3** showed the quinoline proton signals around 7.5-9.0 ppm, the (C-H) peaks for compound **1** at 4.11 ppm, for compound **2** at 3.35, 3.05 ppm and for compound **3** at 4.26, 3.66.

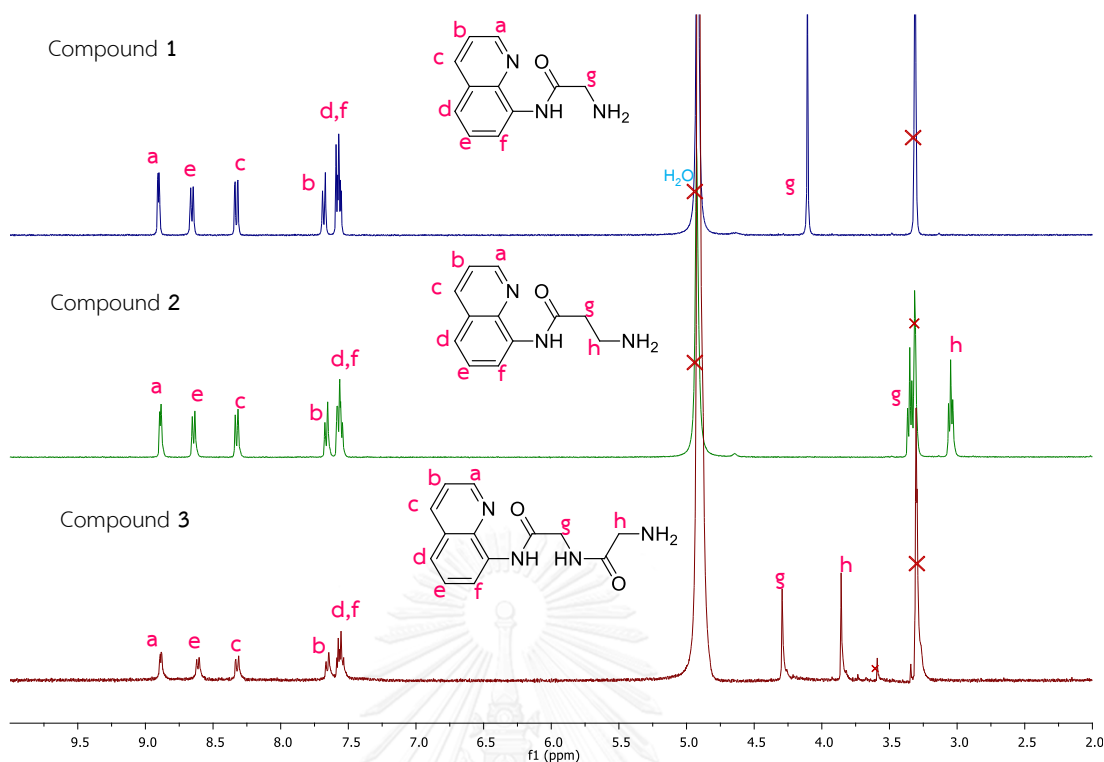
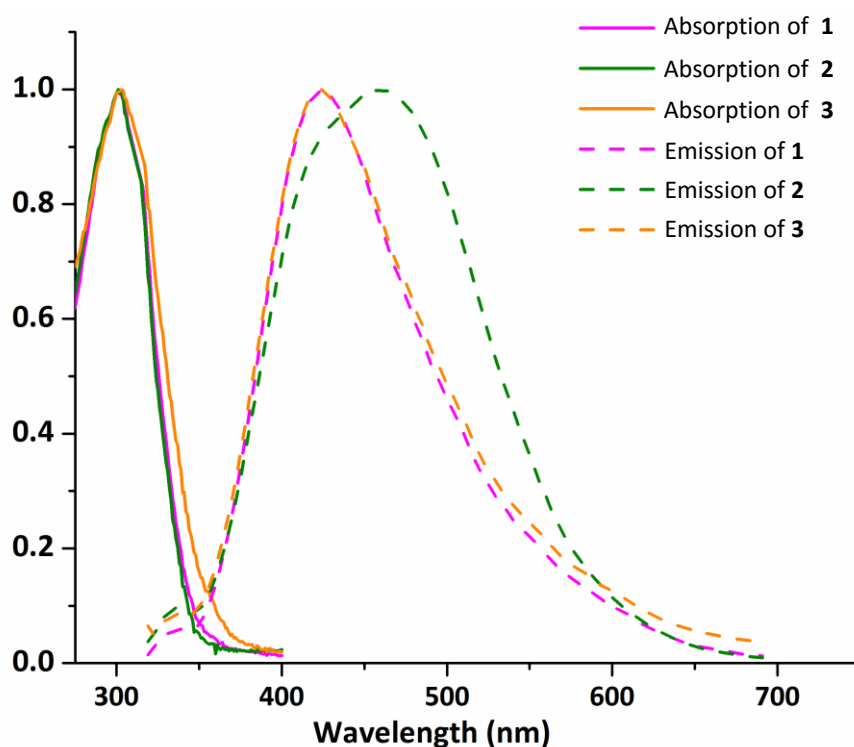


Figure 3.1  $^1\text{H}$  NMR spectra of compound 1-3.

### 3.2. Photophysical properties of 1-3

The normalized electronic absorption and emission spectra of **1–3** in aqueous solutions are shown in Figure 3.2 and their photophysical data are summarized in Table 3.1. The UV-vis absorption spectrum of each fluorophore showed a broad absorption band with  $\lambda_{\text{max}}$  around 300 nm related with the  $\pi\text{--}\pi^*$  electronic transition. The similar  $\lambda_{\text{max}}$  values of these compounds indicate their comparable HOMO and LUMO energy levels. The emission spectra of **2** appeared at lower energy representing a larger Stokes shifts in comparison with that of **1** and **3**. This larger Stokes shift of **2** suggested the greater difference in the most stable geometry between the ground and excited states that likely associates with the change in six-membered ring intramolecular hydrogen bonding between the amide O and  $\beta$ -amino N-H. Like most other 8-aminoquinoline derivatives, **1–3** possessed very low fluorescence quantum efficiency ( $< 0.5\%$ ) due to photoinduced electron transfer (PET) [44].



**Figure 3.2** Normalized absorption (solid line) and emission (dash line) spectra of the fluorophores **1**, **2** and **3** in Tris-HCl aqueous buffer solution pH7.4 containing 1% methanol, v/v. The  $\lambda_{\text{max}}$  of each fluorophore was used as the excitation wavelength in the corresponding emission spectrum.

**Table 3.1** Photophysical data of **1**, **2** and **3** in Tris-HCl aqueous buffer pH 7.4 solution containing methanol (1% v/v)

Compound	Absorption		Emission	
	$\lambda_{\text{max}}$ (nm)	$\log \epsilon$	$\lambda_{\text{em}}$ (nm)	$\Phi$
<b>1</b>	301	3.58	425	<0.005
<b>2</b>	301	3.47	458	<0.005
<b>3</b>	301	3.50	425	<0.005

### 3.3 Metal ions sensing study

The fluorescence enhancement ratios ( $I/I_0$ ) of **1**, **2** and **3** determined from the fluorescence intensity in the presence ( $I$ ) and absence ( $I_0$ ) of various metal ions are shown in Figure 3.3. In aqueous buffer solution, **1** displayed strong fluorescence enhancement selectively in the presence of  $Zn^{2+}$  while the fluorescence of **2** and **3** were insignificantly affected by any metal ions under the same condition (Figure 3.3a derived from spectra in Figure 3.4). For a similar sensing study in ethanol, **1** however showed fluorescence enhancement for both  $Zn^{2+}$  and  $Cd^{2+}$  (Figure 3.3 derived from the spectra in Figure 3.5) whereas **2** and **3** still gave insignificant response to the metal ions tested. The results suggested that the amino group at  $\alpha$ -position of the amino acid pendant was essential for metal ion binding. The shift of amino group to  $\beta$ -position such as in **2** or the modification of the  $\alpha$ -amino group to the amide group such as in **3** may adversely affect the binding of the ligands to the metal ions. The additional amino group from the second glycine unit in **3** also could not improve the sensitivity. Interestingly, many ligands based on 8-aminoquinoline reported for high sensitivity and selectivity toward  $Zn^{2+}$  have a core structure similar to **1** [45-50]. The fluorescence quantum efficiency enhancement of **1** by  $Zn^{2+}$  in aqueous buffer solution was found to be as high as 24-fold ( $= 0.0809/0.0034$ ). This is one of the highest values for all of the  $Zn^{2+}$  sensors based on 8-aminoquinoline derivatives reported to date (Error! Reference source not found.). Ligand **1**, which has a very simple structure, turns out to be one of the most sensitive ligand for  $Zn^{2+}$ . Its binding properties and sensing applications, especially in aqueous solution, is thus worth for detail investigation.

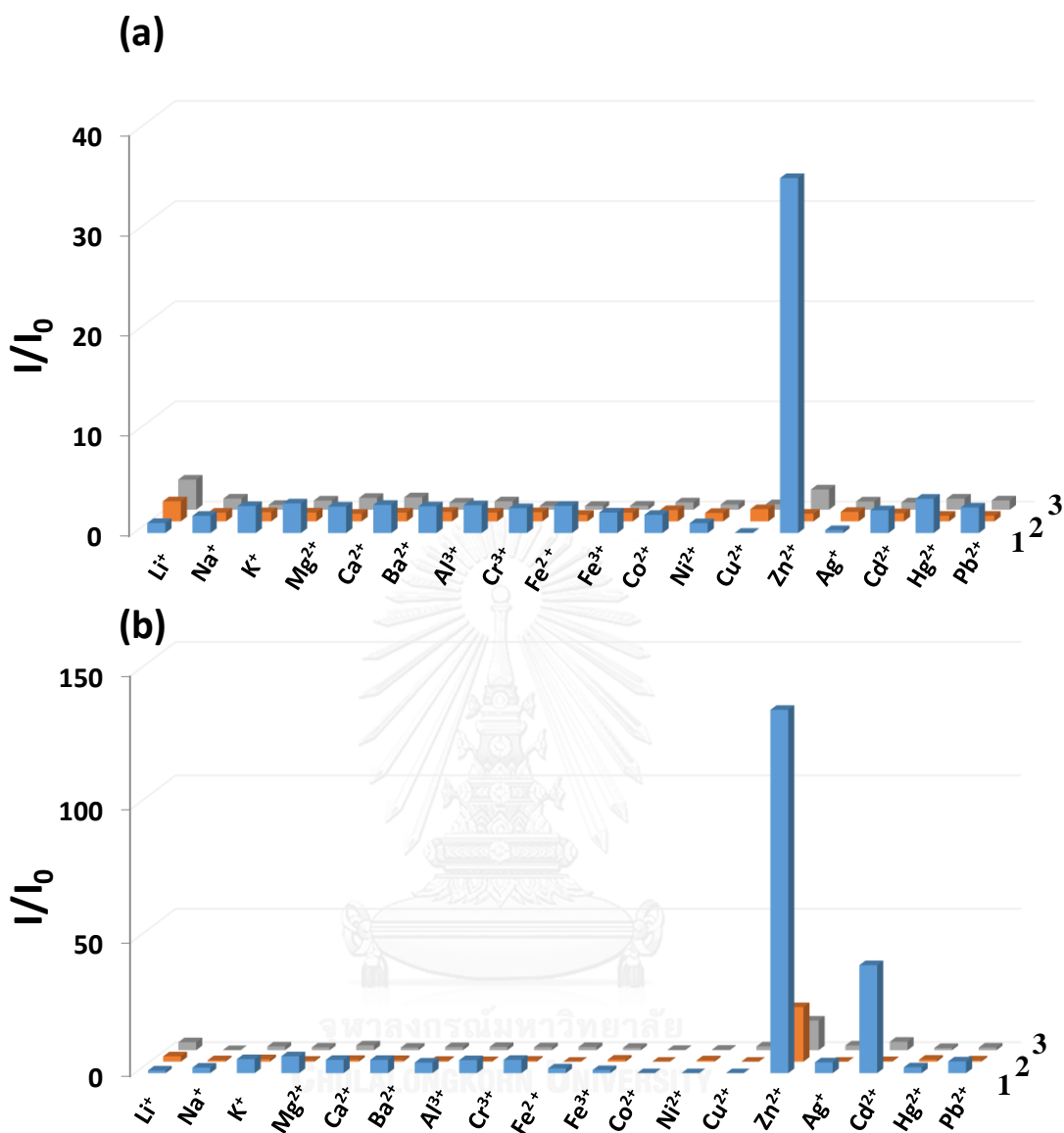


**Figure 3.3** Fluorescence enhancement ratios of ligands (10  $\mu\text{M}$ ) in (a) Tris-HCl aqueous buffer pH 7.4 solution containing methanol (1% v/v) upon addition of various metal ions (100  $\mu\text{M}$ );  $\lambda_{\text{ex}} = 300 \text{ nm}$  ( $\lambda_{\text{em}} = 502, 510$  and  $502$  for **1, 2** and **3**, respectively) (b) ethanol;  $\lambda_{\text{ex}} = 310 \text{ nm}$  ( $\lambda_{\text{em}} = 502, 510$  and  $502$  for **1, 2** and **3**, respectively)

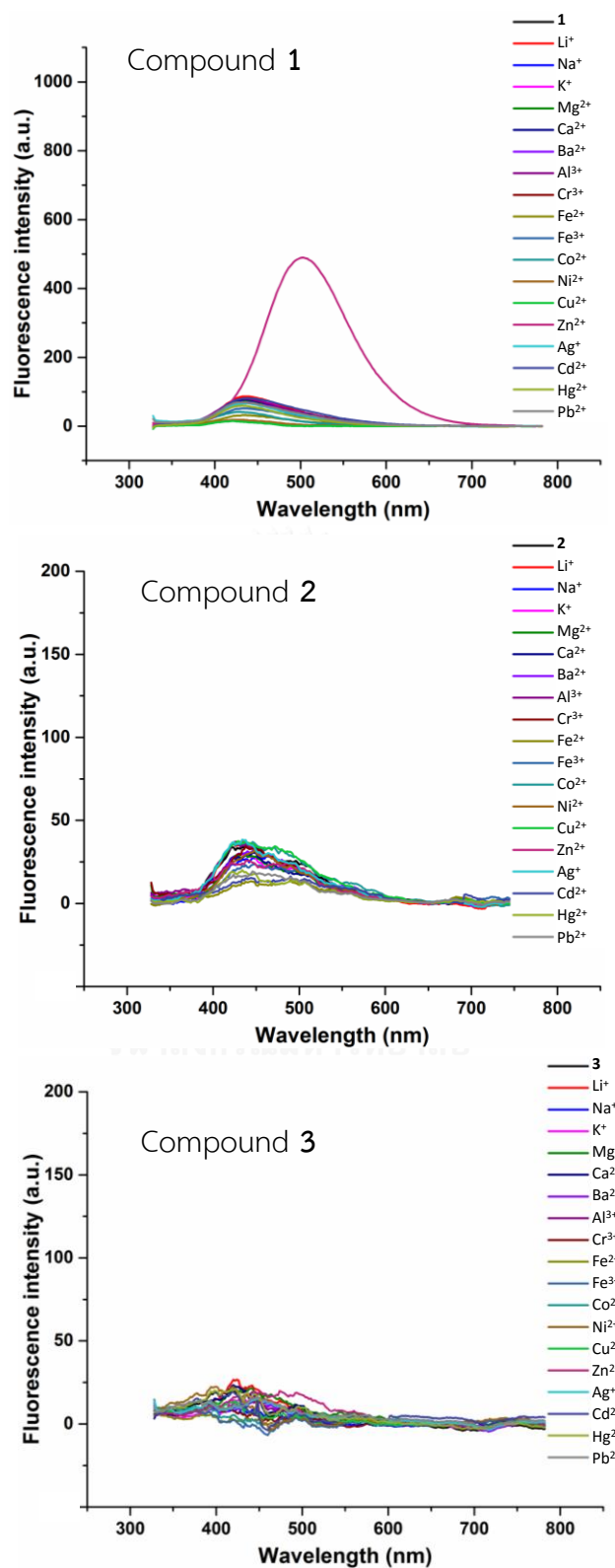


**Figure 3.4** Fluorescence spectra of ligands (10  $\mu$ M) in Tris-HCl aqueous buffer pH 7.4 solution containing methanol (1% v/v) upon addition of various metal ions (100  $\mu$ M);  $\lambda_{\text{ex}} = 300$  nm

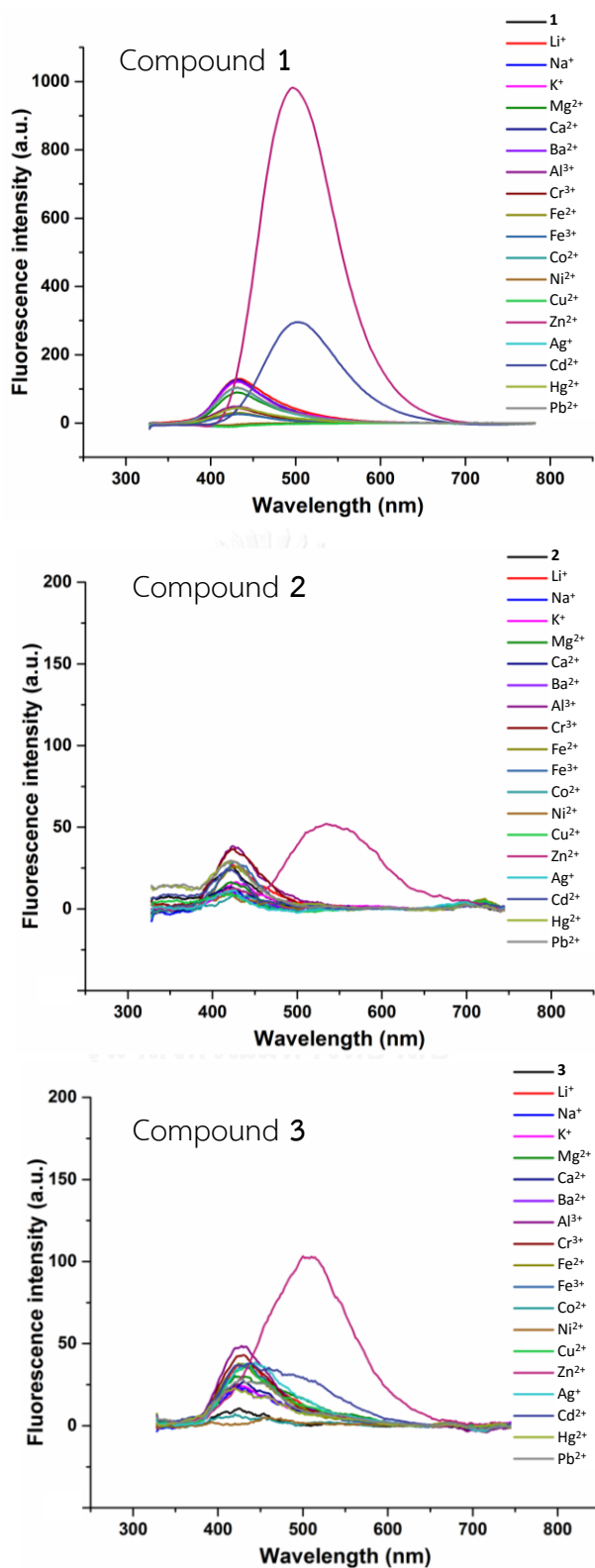
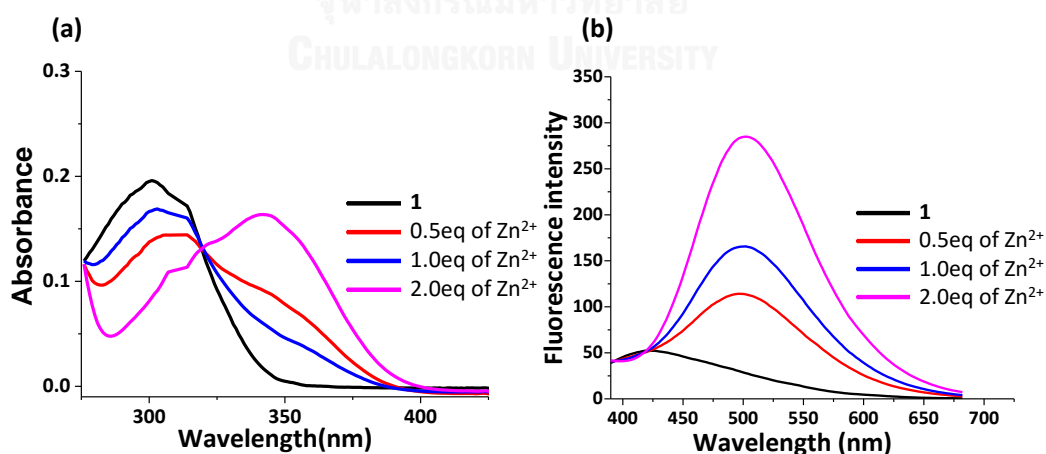


Figure 3.5 Fluorescence spectra of ligands (10  $\mu\text{M}$ ) in ethanol upon addition of various metal ions (100  $\mu\text{M}$ );  $\lambda_{\text{ex}} = 310 \text{ nm}$ .



### 3.4 Metal binding properties of **1**

The binding property of **1** with  $\text{Zn}^{2+}$  in aqueous solution was first investigated by UV-vis absorption titration in Tris-HCl aqueous buffer solution at room temperature. The absorption peak of **1** at 300 nm decreased while a new peak at 344 nm increased with increasing concentration of  $\text{Zn}^{2+}$  (Figure 3.6a). The large bathochromic shift of the absorption band upon the addition of  $\text{Zn}^{2+}$  indicated greater electron delocalization in accordance to the deprotonation of the amide proton upon binding with  $\text{Zn}^{2+}$ . This deprotonation likely increases the binding ability of ligand **1** with the positively charged  $\text{Zn}^{2+}$  (Figure 3.7). The addition of  $\text{Zn}^{2+}$  also resulted in enhancement and shift of fluorescence signal of **1** from a very weak emission band at 420 nm to strong emission at 504 nm, a considerable red-shift (Figure 3.6b). The strong chelation enhanced fluorescence (CHEF) signal was probably the result of the suppression of the PET from the amino group to quinoline ring, ESIPET between the amidic proton and N atom in quinoline ring and geometrical relaxation, posed upon the complexation with  $\text{Zn}^{2+}$ . This bathochromic shift of the fluorescence peak was also accompanied by larger Stokes shift (from 120 nm to 160 nm) that implied a greater involvement of the ICT process in the excited state of the complex.



**Figure 3.6** (a) UV-vis absorption spectra of **1** (100  $\mu\text{M}$ ) upon the addition of varied concentrations of  $\text{Zn}^{2+}$  and (b) fluorescence spectra of **1** (10  $\mu\text{M}$ ) before and after addition of  $\text{Zn}^{2+}$  (100  $\mu\text{M}$ ) ( $\lambda_{\text{ex}} = 300\text{nm}$ ) in Tris-HCl aqueous buffer pH 7.4 solution containing methanol (1% v/v).

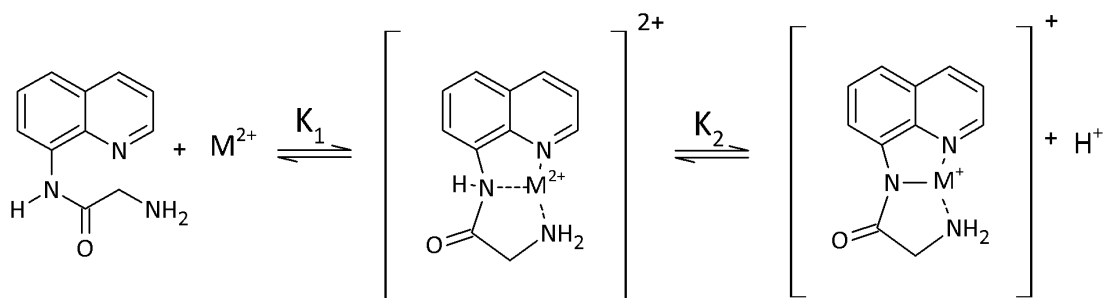


**Figure 3.7** Proposed mechanism of complex between **1** and a metal ion.

The fluorescence responses of **1** toward  $Zn^{2+}$  and  $Cd^{2+}$  in aqueous media at various pHs were investigated. The results gave more insight understanding about the binding properties of the ligands with both metal ions. For  $Zn^{2+}$ , the fluorescence turn on signal was observed starting from pH 6 and reached the maximum at pH 7.4 (Figure 3.8). The fluorescence intensity was then gradually dropped as the pH increased beyond 7.4 probably due to the formation of  $Zn(OH)_2$  precipitate. For  $Cd^{2+}$ , the fluorescence turn on signal was observed at higher pH (pH 8) and the fluorescence intensity increased more gradually in comparison with that was observed for  $Zn^{2+}$ . The complexation between **1** and the metal ion is probably involved the ligand association to the metal ion followed by deprotonation of the initially formed  $[M \cdot \mathbf{1}]^{2+}$  complex to give the final  $[M \cdot (\mathbf{1-H})]^+$  complex as proposed in Figure 3.7. The fact that the fluorescence turns fluorescence enhancement of **1** by both  $Zn^{2+}$  and  $Cd^{2+}$  in ethanol (Figure 3.3). It is important to point out here that the association and deprotonation processes may occur either in a step-wise, as proposed, or concerted fashions.

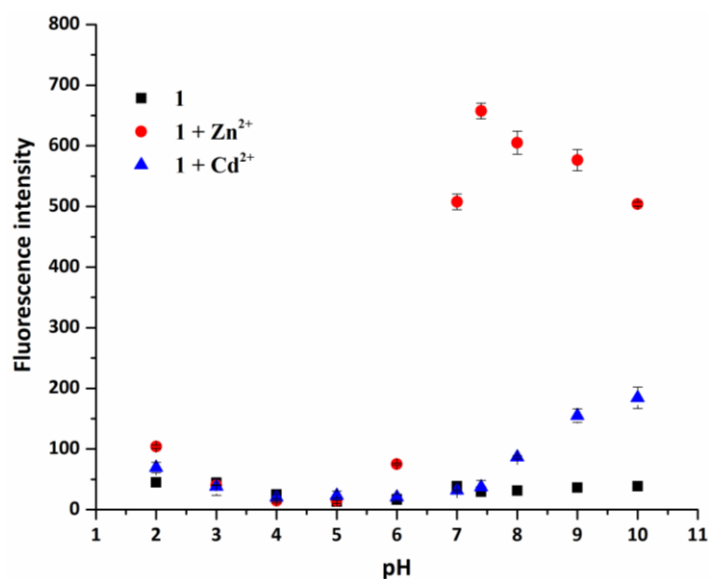


**Figure 3.8** Fluorescence intensity ( $\lambda_{\text{ex}} = 300 \text{ nm}$ ;  $\lambda_{\text{em}} = 504 \text{ nm}$ ) of **1** ( $10 \mu\text{M}$ ) at various pHs in Tris-HCl aqueous buffer pH 7.4 solution containing methanol (1% v/v) in the absence and presence of  $\text{Zn}^{2+}$  and  $\text{Cd}^{2+}$  (10 equivalent).

The Job plots of UV-vis absorption on by  $\text{Cd}^{2+}$  appeared at higher pH and gave significantly lower enhancement ratio suggested its lower  $K_1$  in comparison with  $\text{Zn}^{2+}$ . The lower polarity and acidity of ethanol, in comparison with water, can increase both  $K_1$  and  $K_2$  that is supported by the observation of greater and emission titrations revealed a 1:1 binding ratio of the complexation between **1** and  $\text{Zn}^{2+}$  in the aqueous buffer solution (Figure 3.9). The complexation constant ( $K$ ) of this 1:1 complex was  $8.03 \times 10^5 \text{ M}^{-1}$  as obtained from the Benesi-Hildebrand plot using data from the emission intensity (Figure 3.10). In ethanol solution, the complexation constant increased to  $1.20 \times 10^6 \text{ M}^{-1}$  (Table 3.2) which supported the binding mechanism described above. The complexation constants of **1** with  $\text{Cd}^{2+}$  were also determined in aqueous and ethanol solutions and found to be lower than those of  $\text{Zn}^{2+}$  that somewhat explained the lower fluorescence responses described earlier. The complexation constant of **1** with  $\text{Zn}^{2+}$  is relatively high comparing with other ligands with similar 8-aminoquinoline core (Error! Reference source not found.). The result confirms that only three N atoms, as in ligand **1**, are essential for the  $\text{Zn}^{2+}$  binding.

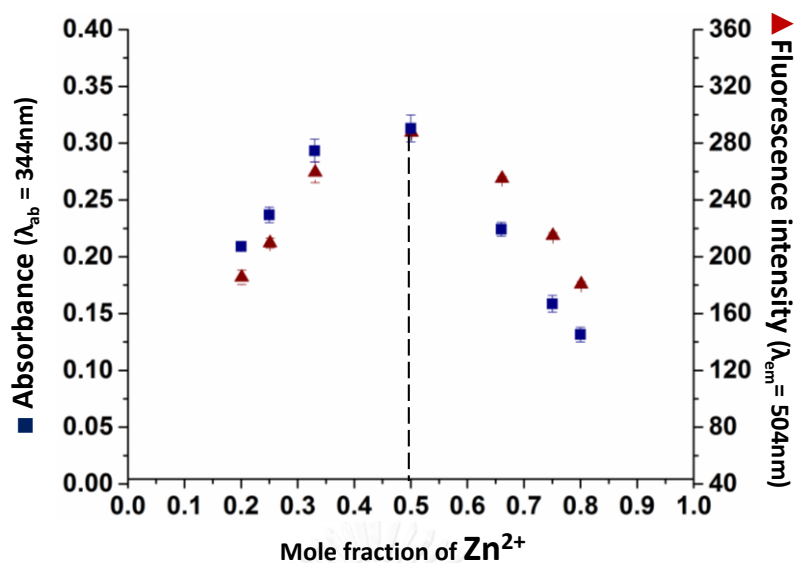


**Figure 3.9** Job plots of UV-vis absorption (at 344 nm) and emission (at 504 nm) titration between compound **1** and Zn<sup>2+</sup> in Tris-HCl aqueous buffer pH 7.4 solution containing methanol (1% v/v) ([1]+[Zn<sup>2+</sup>] = 10 μM), (■ = absorption, ▲ = emission).

**Table 3.2** Association constants of **1** with Zn<sup>2+</sup> and Cd<sup>2+</sup> in aqueous and ethanol solutions

Metal ion	Solvent	Concentration of <b>1</b> (μM) <sup>b</sup>	K <sub>a</sub> (M <sup>-1</sup> )
Zn <sup>2+</sup>	Tris-HCl buffer pH 7.4	10	8.03 × 10 <sup>5</sup>
	Ethanol	5	1.20 × 10 <sup>6</sup>
Cd <sup>2+</sup>	Tris-HCl buffer pH 8.0 <sup>a</sup>	50	2.38 × 10 <sup>5</sup>
	Ethanol	5	4.61 × 10 <sup>5</sup>

<sup>a</sup> Slightly higher pH was used for Cd<sup>2+</sup> because the fluorescence response was too low at pH 7.4.

<sup>b</sup> Different concentrations of **1** were used to obtain high linear correlation coefficient (R<sup>2</sup>) for Benesi-Hildebrand plots under similar instrumentation set up.

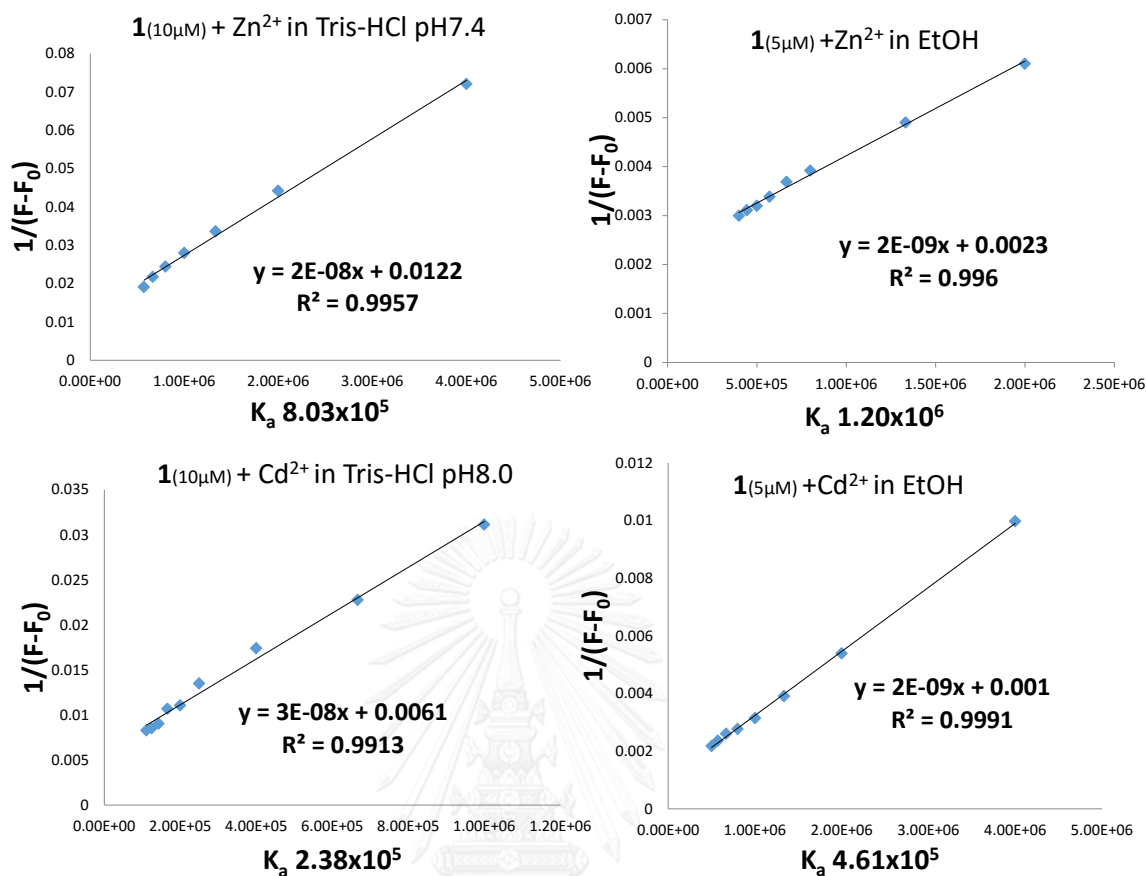


**Figure 3.10** Benesi-Hildebrand plot for determination of  $K_a$  of **1** with  $Zn^{2+}$  and  $Cd^{2+}$  in aqueous and ethanol solutions.

Mass spectrum of **1** with 0.5 equivalents of  $Zn^{2+}$  showed important peaks at  $m/z = 264.01$  and  $465.10$  corresponding to  $[Zn \cdot (1-H)]^+$  and  $[Zn \cdot (1-H)_2 + H]^+$ , respectively, that revealed the co-existence of both 1:1 and 2:1 complexes under this condition (Figure 3.11). However, with 1.0 equivalent of  $Zn^{2+}$ , the peak of 2:1 complex at  $m/z = 465.10$  disappeared while the peak of 1:1 complex at  $m/z = 264.01$  remained (Figure 3.12). The results confirmed the deprotonation of **1** upon the coordination with  $Zn^{2+}$  and implied that the binding of the second ligand to  $Zn^{2+}$  is much weaker than the first one.

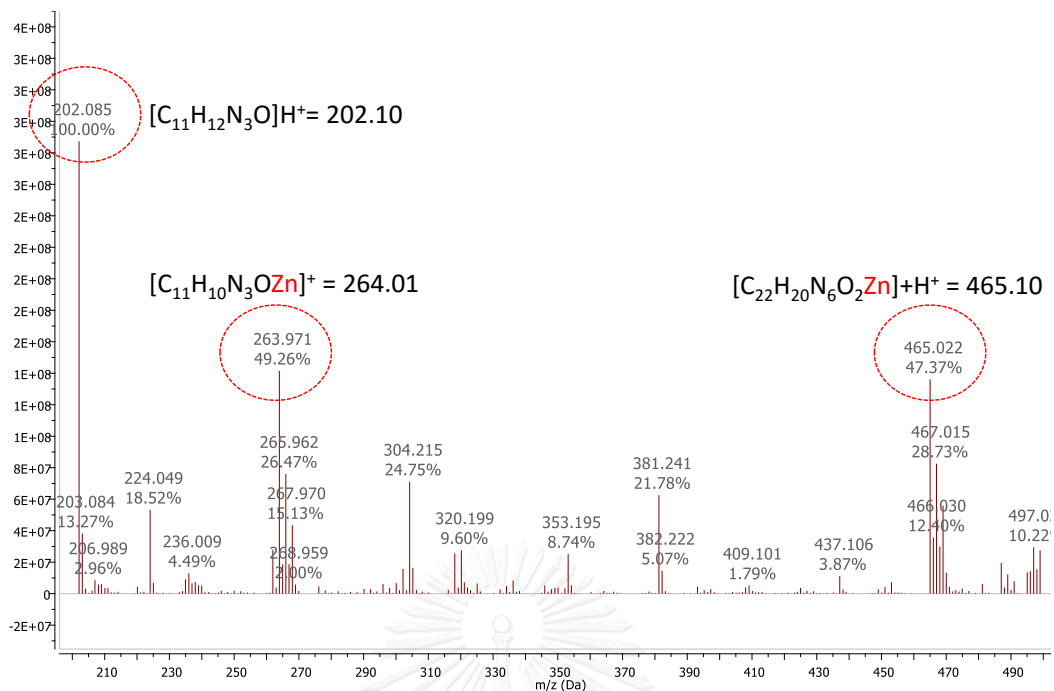


**Figure 3.11** Positive-ion electrospray mass spectrum of **1** (10  $\mu\text{M}$ ) upon addition of 0.5 equivalent of  $\text{Zn}^{2+}$  in methanol.

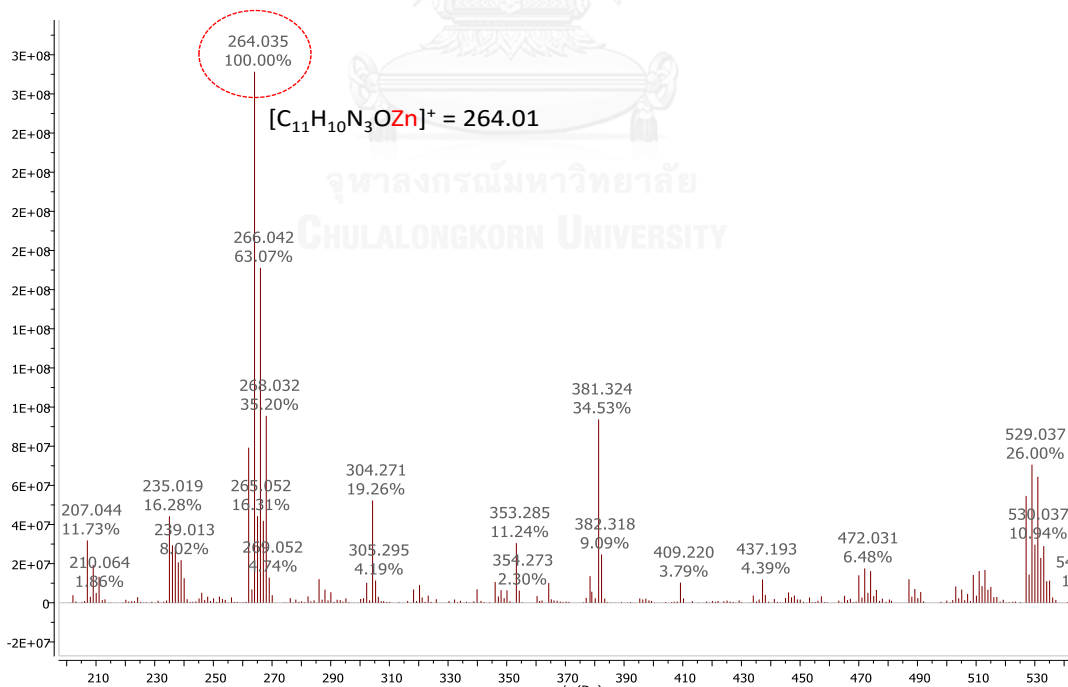


**Figure 3.12** Positive-ion electrospray mass spectrum of **1** (10  $\mu\text{M}$ ) upon addition of 1.0 equivalent of  $\text{Zn}^{2+}$  in methanol.

The evidence of 2:1 and 1:1 complexes between **1** and  $\text{Zn}^{2+}$  were also observed in  $^1\text{H}$  NMR titration in  $(\text{CD}_3)_2\text{SO}$ . The proton chemical shifts of **1** and its complexes were assigned based on  $J$  coupling constants in  $^1\text{H}$  NMR spectrum and COSY correlation in comparison with 8-aminoquinoline (Figure 3.13, Figure 3.14 and Figure 3.15) The  $^1\text{H}$  NMR spectrum of **1** displayed a secondary amide peak at 11.64 ppm and three signals of aromatic protons  $\text{H}_a$ ,  $\text{H}_f$  and  $\text{H}_c$  at 8.93, 8.75, and 8.40 ppm (Figure 3.16). Upon the addition of 0.25 equivalent of  $\text{Zn}^{2+}$  to the solution of **1**, a new set of proton signals appeared. Notably, three doublet signals at 9.21, 8.23 and 8.09 ppm assigned to  $\text{H}_{f'}$ ,  $\text{H}_{c'}$  and  $\text{H}_{a'}$  of the 2:1 complex. At this low equivalent of  $\text{Zn}^{2+}$ , there remained  $\text{H}_a$ ,  $\text{H}_f$  and  $\text{H}_c$  signals of the free ligand. The aromatic signals of both free ligand and 2:1 complex totally disappeared when the addition of  $\text{Zn}^{2+}$  was over 1.0 equivalent. At this high equivalent of  $\text{Zn}^{2+}$ , another set of aromatic signals appeared at 8.92, 8.71 and 8.45 ppm which assigned as  $\text{H}_{f''}$ ,  $\text{H}_{a''}$  and  $\text{H}_{c''}$  of the 1:1 complex. The other aromatic signals ( $\text{H}_d$ ,  $\text{H}_b$  and  $\text{H}_e$ ) in the range of 7.7–7.5 ppm were also significantly shifted upon the complexation. The spectra at 0.50 and 0.75 equivalent of  $\text{Zn}^{2+}$  suggested the conditions where all three species i.e. free ligand, 2:1 complex and 1:1 complex were coexisted. Whereas the spectra at 0.25 and 1.50 equivalent of  $\text{Zn}^{2+}$  were the conditions where there was only either the 2:1 complex or 1:1 complex, respectively. Moreover, the absence of secondary amide signal of the 1:1 complex also confirmed that the amide group of **1** was deprotonated upon binding with  $\text{Zn}^{2+}$ .

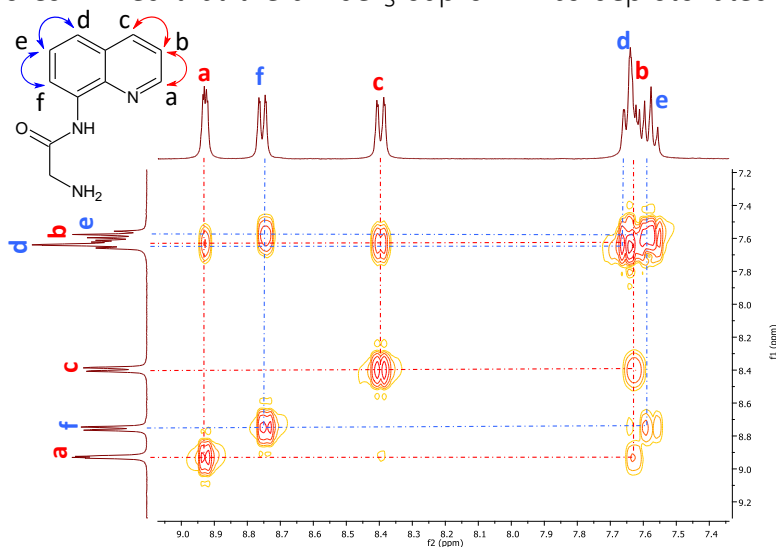


Figure 3.13 COSY correlation spectra of compound **1** in  $(\text{CD}_3)_2\text{SO}$ .

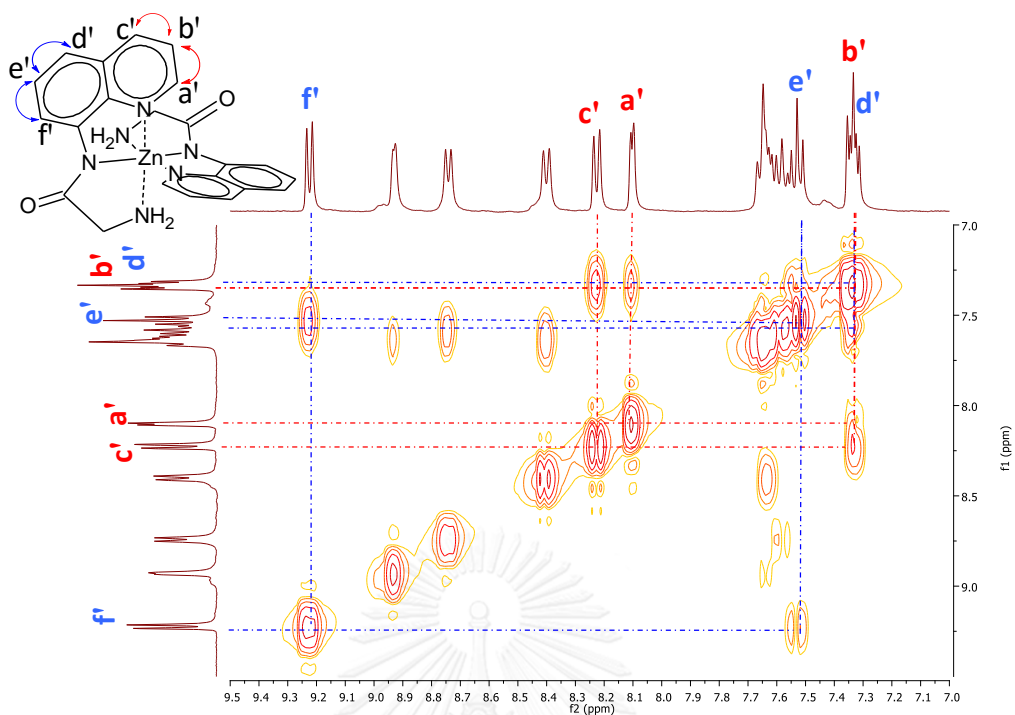


Figure 3.14 COSY correlation spectra of compound **1** in the presence of 0.25 equivalent of  $\text{Zn}^{2+}$  in  $(\text{CD}_3)_2\text{SO}$ .

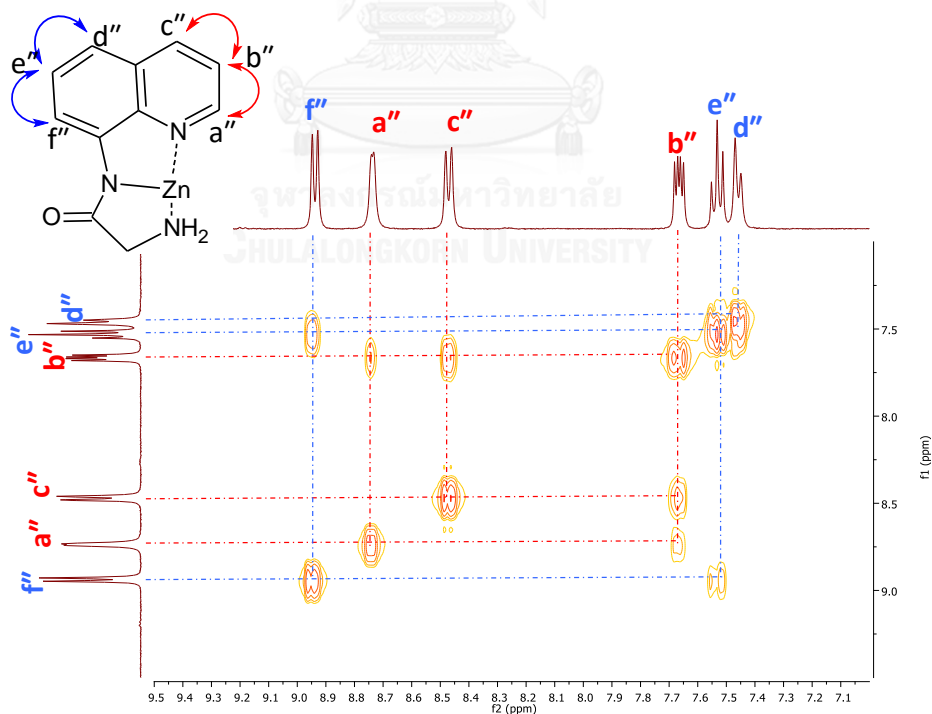
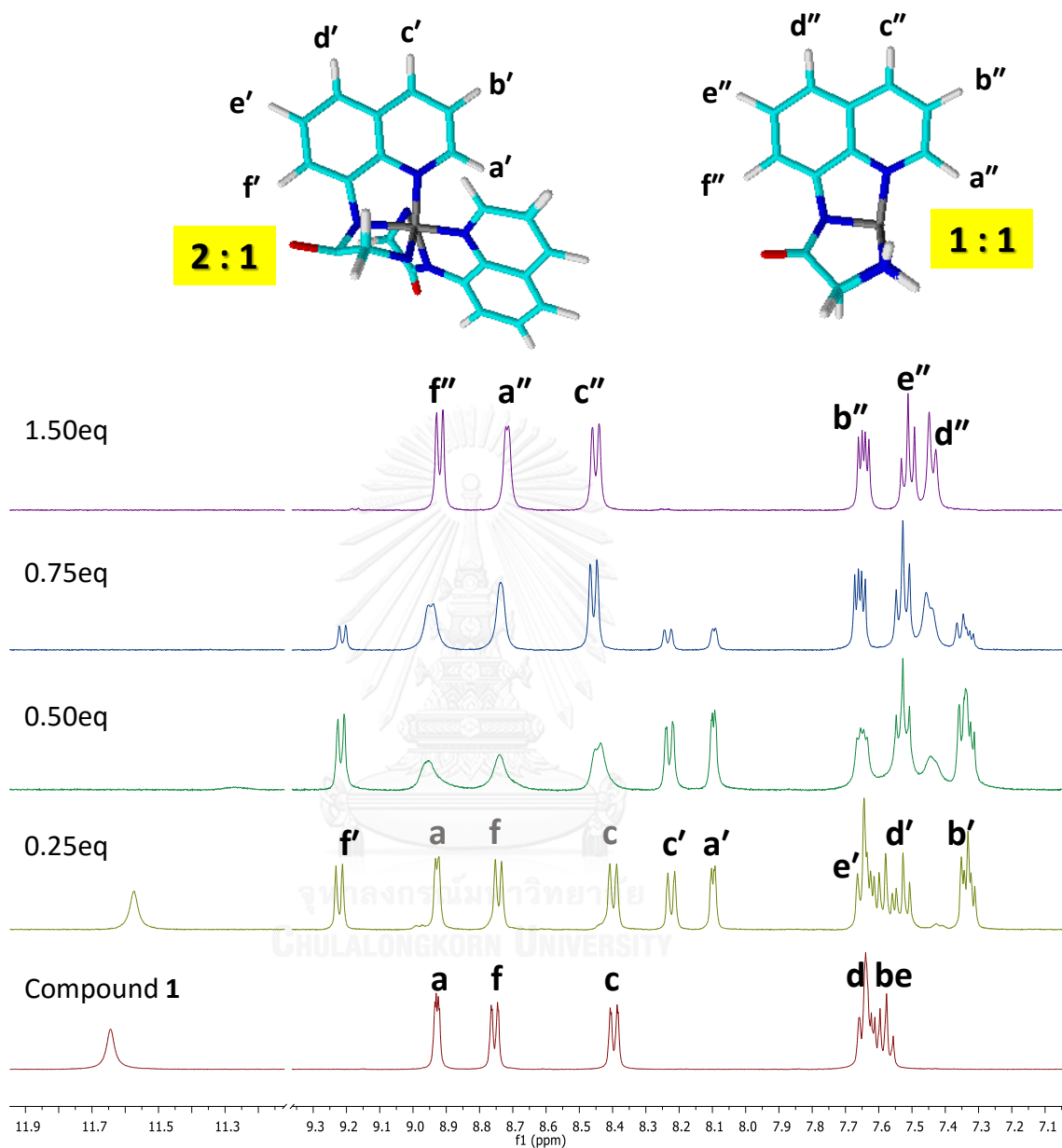


Figure 3.15 COSY correlation spectra of compound **1** in the presence of 1.5 equivalent of  $\text{Zn}^{2+}$  in  $(\text{CD}_3)_2\text{SO}$ .





**Figure 3.16** (a) Proposed structures of complexes between  $Zn^{2+}$  and **1** optimized by CHARMM and (b) partial  $^1H$  NMR spectra (400 MHz) of **1** (0.15 M) in  $(CD_3)_2SO$  in the presence of various equivalents of  $Zn^{2+}$ .

The interference test showed that most cations tested, except  $\text{Co}^{2+}$ ,  $\text{Ni}^{2+}$  and  $\text{Cu}^{2+}$ , did not interfere the fluorescence response of **1** to  $\text{Zn}^{2+}$  (Figure 3.17). These three interfering ions quenched the emission of **1**- $\text{Zn}^{2+}$  complex, probably due to the competitive binding of form non-fluorescent high spin metal complexes. The fluorescence turn-on signal of **1** can thus be a strong positive prove for the presence of  $\text{Zn}^{2+}$  in aqueous solution but a lack of turn-on signal can be fault negative due to the quenching effect of  $\text{Co}^{2+}$ ,  $\text{Ni}^{2+}$  and  $\text{Cu}^{2+}$ . Since these metal ions are not common in water and biological samples, their interference should be lesser concern.

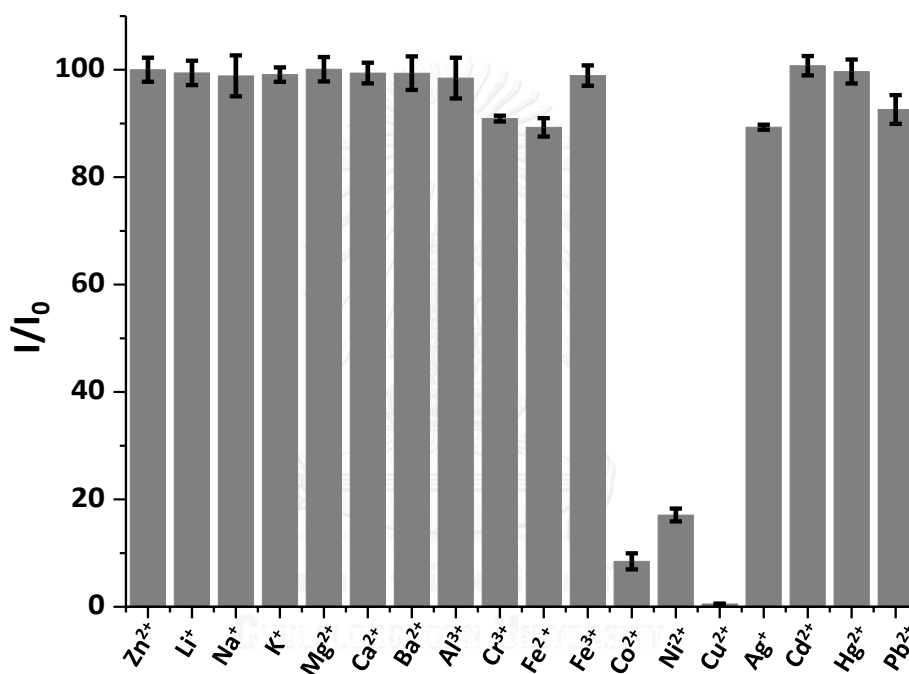


**Figure 3.17** Fluorescence responses of **1** (10  $\mu\text{M}$ ) to the addition of solution of  $\text{Zn}^{2+}$  (10 equivalent) mixed with various metal ions (10 equivalent) in Tris-HCl aqueous buffer pH 7.4 solution containing methanol (1% v/v); ( $\lambda_{\text{ex}} = 300 \text{ nm}$  and  $\lambda_{\text{em}} = 504 \text{ nm}$ ).

For quantitative analysis, the fluorescence signals of the solutions of **1** was measured in the presence of  $\text{Zn}(\text{OAc})_2$  at various concentrations and the results are shown in Figure 3.18

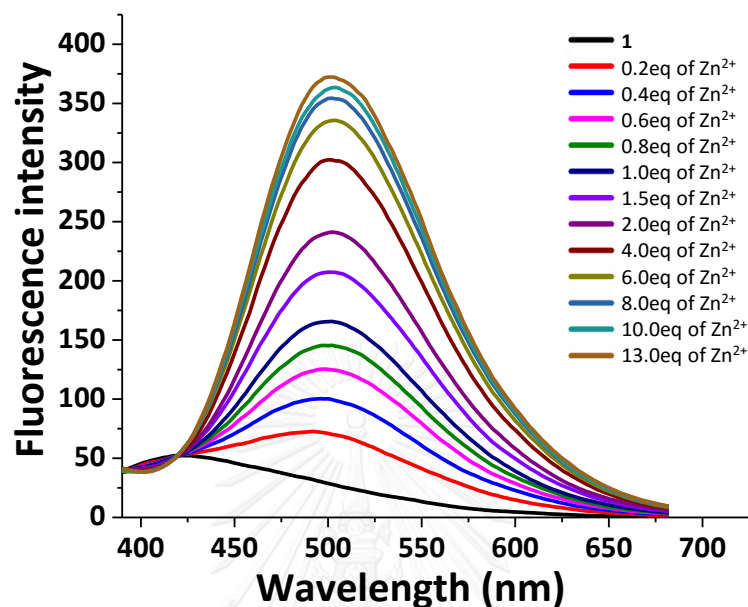


**Figure 3.18** Fluorescence spectra ( $\lambda_{\text{ex}} = 300 \text{ nm}$ ) of **1** ( $10 \mu\text{M}$ ) in Tris-HCl aqueous buffer pH 7.4 solution containing methanol (1% v/v) in the presence of  $\text{Zn}^{2+}$  at various concentrations.

The fluorescence intensity ratio ( $I/I_0$ ) increased almost linearly in the low concentration range (0–10  $\mu\text{M}$ ) of  $\text{Zn}^{2+}$  and reached saturation around 100  $\mu\text{M}$  (10 equivalent) of  $\text{Zn}^{2+}$  (Figure 3.19). A plot of ( $I/I_0$ ) at the low concentration range gave a linear calibration line ( $R^2 = 0.9918$ ) for quantitative determination of  $\text{Zn}^{2+}$  with a detection limit of 1.6  $\mu\text{M}$  (Fig. 7b inset;  $\text{LOD} = 3\text{SD}/\text{slope}$ ).

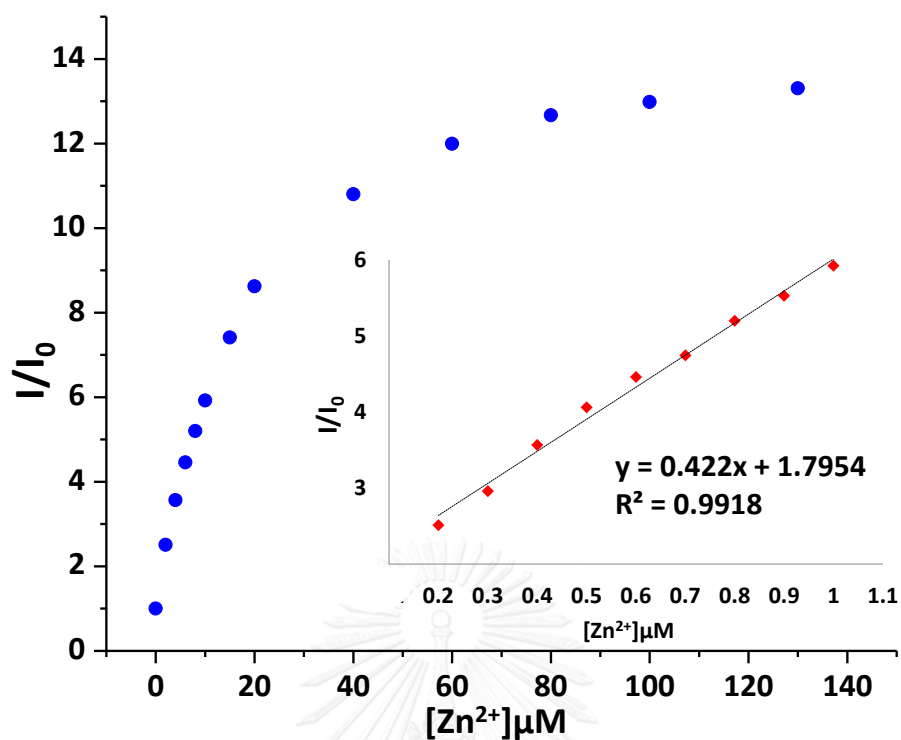


**Figure 3.19** Fluorescence intensity ratio as a function of  $Zn^{2+}$  concentration; inset: linear calibration line for quantitative determination of  $Zn^{2+}$  concentration.

Plants serve as a major entry point for  $Zn^{2+}$  into the food chain.[51] Therefore, a quick and simple method for detection of  $Zn^{2+}$  in plants can be useful in the fields of biology and food nutrition. Although several fluorescent probes have been used for detection of  $Zn^{2+}$  in mammal cells, [52-55] a fluorescent imaging of  $Zn^{2+}$  in plants has not been demonstrated. We therefore would like to apply **1** for detection of  $Zn^{2+}$  and  $Cd^{2+}$  in plant tissue. Chinese cabbage (*Brassica rapa*.) sprout was chosen as a model sample for fluorescence imaging. The longitudinal-section of root tissue samples were treated separately with  $Zn^{2+}$  and  $Cd^{2+}$  solution (100  $\mu M$ ) and finally washed with either Milli-Q water or ethanol just prior to the imaging under a microscope. For the samples washed with Milli-Q water, only the one treated with  $Zn^{2+}$  showed green fluorescence after the addition of **1** (Figure 3.20a). However, the strong fluorescence was apparent in both  $Zn^{2+}$  and  $Cd^{2+}$  treated samples washed with ethanol (Figure 3.20b). The results indicated that probe **1** may be used for detection of  $Zn^{2+}$  or  $Cd^{2+}$ , depending on the sample preparation, in plant tissue.

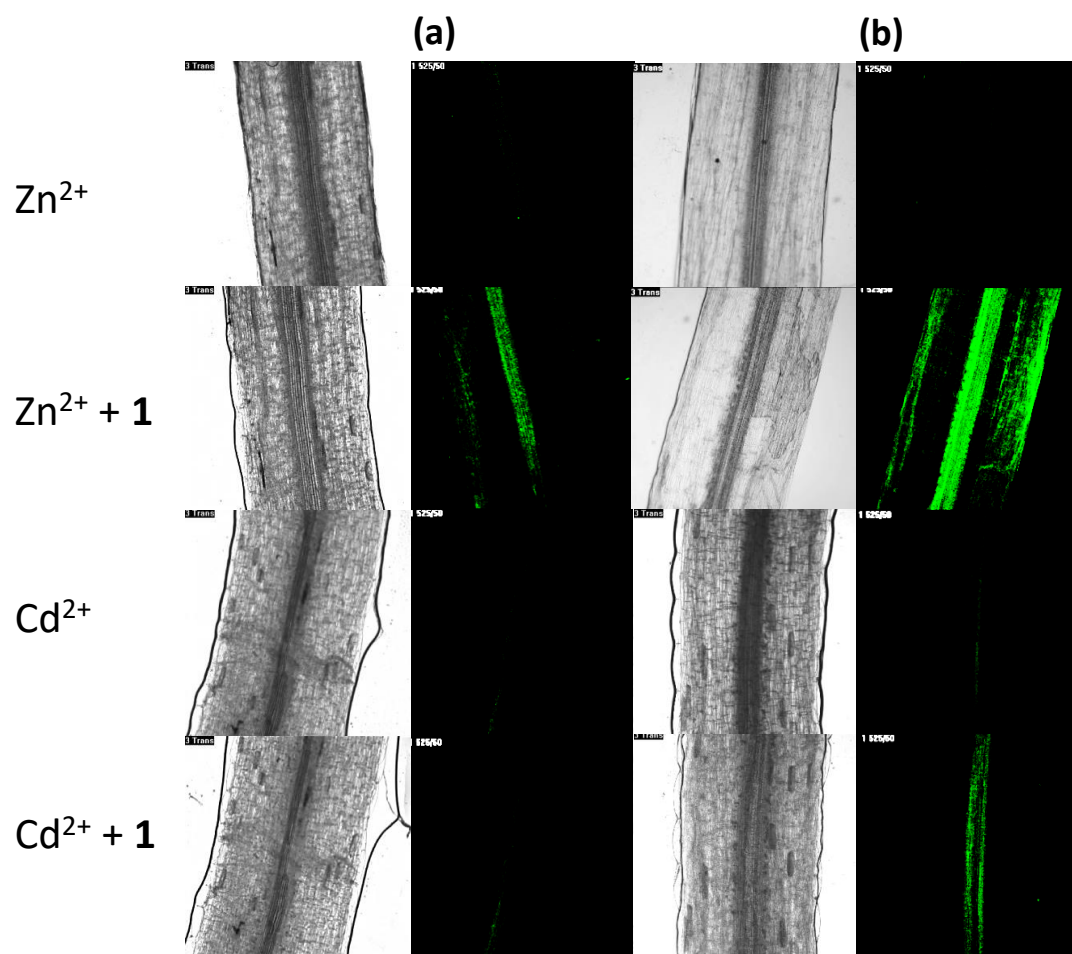


**Figure 3.20** Fluorescence images of Chinese cabbage (*Brassica rapa*.) sprout tissue samples treated with  $Zn^{2+}$  (100  $\mu$ M) and  $Cd^{2+}$  (100 $\mu$ M), (a) washed with Milli-Q water and (b) washed with ethanol, before and after addition of  $\mathbf{1}$  (100  $\mu$ M, 10  $\mu$ L).

Another interesting application of fluorescent sensing probe is to apply it as a litmus-type paper indicator for detection of specific metal ions. To develop the application of **1** for naked eye detection of metal ions on filter paper, the selectivity of **1** was tested by visual observation and recorded by a digital camera under black light illumination. Unlike in aqueous solution, both  $\text{Zn}^{2+}$  and  $\text{Cd}^{2+}$  gave bright green-blue emission in the detection areas on filter paper substrate. The other metal ions tested gave negative result (Figure 3.21).

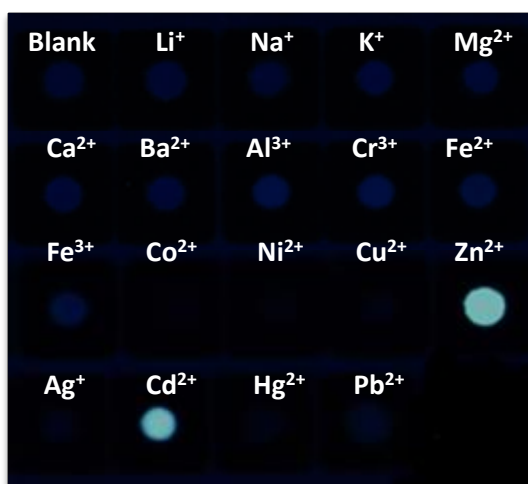


**Figure 3.21** Photographic image of metal ion (0.1 mM) detection by **1** (1 mM) on wax patterned filter paper tested by simple drop and dry. The sample was illuminated by black light (wavelength  $365 \pm 50$  nm).

Therefore, **1** may be useful for specific and simultaneous detection of  $\text{Zn}^{2+}$  and  $\text{Cd}^{2+}$  provided that both ions can be separated from each other. We therefore investigated a chromatographic separation of these ions on a filter paper strip. With multiple attempts using various eluent systems, we found that an aqueous solution containing 4% (v/v)  $\text{CH}_3\text{NH}_2$  gave the most satisfactory results. After elution, spraying the solution of **1** on the test zone of the filter paper revealed two well separated fluorescent streaks corresponding to  $\text{Zn}^{2+}$  and  $\text{Cd}^{2+}$  ions (Figure 3.22). The results clearly demonstrate that **1** can be visualization agent for selective detection of  $\text{Zn}^{2+}$  and  $\text{Cd}^{2+}$  that allows simultaneous detection of both metal ions with a simple paper chromatographic technique.

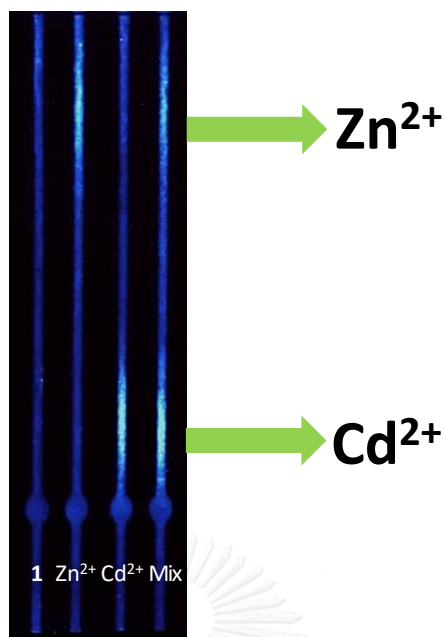


**Figure 3.22** Photographic image for dual detection of  $Zn^{2+}$  and  $Cd^{2+}$  (1 nmol) by **1** (1 mM) using paper chromatography for separation after elution with  $CH_3NH_2$  4% (v/v). The sample was irradiated by black light (wavelength  $365 \pm 50$  nm).

## CHAPTER IV

### CONCLUSION

Three amide derivatives (**1**, **2**, and **3**) of 8-aminoquinoline were synthesized. In ethanol, the derivative containing glycine pendant (**1**) gave selective turn-on fluorescence responses to both  $\text{Zn}^{2+}$  and  $\text{Cd}^{2+}$ . In Tris-HCl aqueous buffer pH 7.4 solution, the fluorescence signal of **1** responded only to  $\text{Zn}^{2+}$ . The fluorescence enhancement associates with the strong complexation between the ligand and metal ions that involves the deprotonation of the amide group within **1**. Upon complexation, several non-radiative decay pathways such as PET, ESIPT and geometrical relaxation are probably suppressed. Compound **1** can be readily applied for fluorescent imaging to locate  $\text{Zn}^{2+}$  and  $\text{Cd}^{2+}$  in plant as well as simultaneous detection of  $\text{Zn}^{2+}$  and  $\text{Cd}^{2+}$  in paper chromatography. Most importantly, ligand **1** has a very simple structure but yet is a very effective turn-on fluorescent sensor for  $\text{Zn}^{2+}$  and  $\text{Cd}^{2+}$ .



## REFERENCES

- [1] Pawlizak, S. Fluorescence Microscopy [Online]. 2009. Available from: <https://www.unileipzig.de/~pwm/web/?section=introduction&page=fluorescence>
- [2] Gunnlaugsson, T., et al. Fluorescent Photoinduced Electron Transfer (PET) Sensors for Anions; From Design to Potential Application. Journal of Fluorescence 15(3) (2005): 287-299.
- [3] Callan, J.F., de Silva, A.P., and Magri, D.C. Luminescent Sensors and Switches in the Early 21st century. Tetrahedron 61(36) (2005): 8551-8588.
- [4] de Silva, A.P., et al. Signaling Recognition Events with Fluorescent Sensors and Switches. Chemical Reviews 97(5) (1997): 1515-1566.
- [5] Martínez-Máñez, R. and Sancenón, F. Fluorogenic and Chromogenic Chemosensors and Reagents for Anions. Chemical Reviews 103(11) (2003): 4419-4476.
- [6] Valeur, B. and Leray, I. Design Principles of Fluorescent Molecular Sensors for Cation Recognition. Coordination Chemistry Reviews 205(1) (2000): 3-40.
- [7] Xu, Z., Yoon, J., and Spring, D.R. Fluorescent Chemosensors for Zn<sup>2+</sup>. Chemical Society Reviews 39(6) (2010): 1996-2006.
- [8] Sapsford, K.E., Berti, L., and Medintz, I.L. Materials for Fluorescence Resonance Energy Transfer Analysis: Beyond Traditional Donor–Acceptor Combinations. Angewandte Chemie International Edition 45(28) (2006): 4562-4589.
- [9] Carlson, H.J. and Campbell, R.E. Genetically Encoded FRET-Based Biosensors for Multiparameter Fluorescence Imaging. Current Opinion in Biotechnology 20(1) (2009): 19-27.
- [10] Wu, J., Liu, W., Ge, J., Zhang, H., and Wang, P. New Sensing Mechanisms for Design of Fluorescent Chemosensors Emerging in Recent Years. Chemical Society Reviews 40(7) (2011): 3483-3495.
- [11] Peng, X., Wu, Y., Fan, J., Tian, M., and Han, K. Colorimetric and Ratiometric Fluorescence Sensing of Fluoride: Tuning Selectivity in Proton Transfer. The Journal of Organic Chemistry 70(25) (2005): 10524-10531.

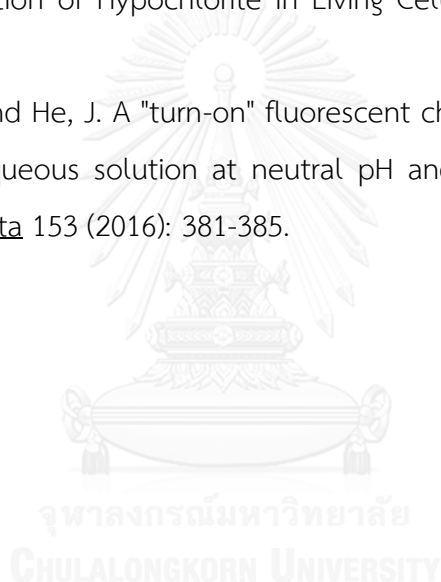
- [12] de Silva, A.P., Moody, T.S., and Wright, G.D. Fluorescent PET (Photoinduced Electron Transfer) sensors as potent analytical tools. *Analyst* 134(12) (2009): 2385-2393.
- [13] Druzhinin, S.I., Mayer, P., Stalke, D., von Bülow, R., Noltemeyer, M., and Zachariasse, K.A. Intramolecular Charge Transfer with 1-tert-Butyl-6-cyano-1,2,3,4-tetrahydroquinoline (NTC6) and Other Aminobenzonitriles. A Comparison of Experimental Vapor Phase Spectra and Crystal Structures with Calculations. *Journal of the American Chemical Society* 132(22) (2010): 7730-7744.
- [14] Galievsky, V.A., et al. Ultrafast Intramolecular Charge Transfer with N-(4-Cyanophenyl)carbazole. Evidence for a LE Precursor and Dual LE + ICT Fluorescence. *The Journal of Physical Chemistry A* 114(48) (2010): 12622-12638.
- [15] Chung, S.-K., Tseng, Y.-R., Chen, C.-Y., and Sun, S.-S. A Selective Colorimetric Hg<sup>2+</sup> Probe Featuring a Styryl Dithiaazacrown Containing Platinum(II) Terpyridine Complex through Modulation of the Relative Strength of ICT and MLCT Transitions. *Inorganic Chemistry* 50(7) (2011): 2711-2713.
- [16] Ghosh, S., Banik, D., Roy, A., Kundu, N., Kuchlyan, J., and Sarkar, N. Spectroscopic investigation of the binding interactions of a membrane potential molecule in various supramolecular confined environments: contrasting behavior of surfactant molecules in relocation or release of the probe between nanocarriers and DNA surface. *Physical Chemistry Chemical Physics* 16(45) (2014): 25024-25038.
- [17] Baudin, B.H. *Electron and Energy Transfer in Supramolecular Complexes Designed for Artificial Photosynthesis*. Sweden: Akademityck AB, 2001.
- [18] Kim, J.S. and Quang, D.T. Calixarene-Derived Fluorescent Probes. *Chemical Reviews* 107(9) (2007): 3780-3799.
- [19] Zheng, J. Spectroscopy-Based Quantitative Fluorescence Resonance Energy Transfer Analysis. in Stockand, J.D. and Shapiro, M.S. (eds.), *Ion Channels: Methods and Protocols* pp. 65-77. Totowa, NJ: Humana Press, 2006.

- [20] Freeman, R. and Willner, I. Optical molecular sensing with semiconductor quantum dots (QDs). Chemical Society Reviews 41(10) (2012): 4067-4085.
- [21] Henary, M.M. and Fahrni, C.J. Excited State Intramolecular Proton Transfer and Metal Ion Complexation of 2-(2'-Hydroxyphenyl)benzazoles in Aqueous Solution. The Journal of Physical Chemistry A 106(21) (2002): 5210-5220.
- [22] Zhang, L., Duan, D., Cui, X., Sun, J., and Fang, J. A selective and sensitive fluorescence probe for imaging endogenous zinc in living cells. Tetrahedron 69(1) (2013): 15-21.
- [23] Choong, V.E., Park, Y., Gao, Y., Mason, M.G., and Tang, C.W. Photoluminescence quenching of Alq<sub>3</sub> by metal deposition: A surface analytical investigation. Journal of Vacuum Science and Technology A: Vacuum, Surfaces and Films 16(3) (1998): 1838-1841.
- [24] Higginson, K.A., Zhang, X.-M., and Papadimitrakopoulos, F. Thermal and Morphological Effects on the Hydrolytic Stability of Aluminum Tris(8-hydroxyquinoline) (Alq<sub>3</sub>). Chemistry of Materials 10(4) (1998): 1017-1020.
- [25] Pohl, R. and Anzenbacher, P. Emission Color Tuning in AlQ<sub>3</sub> Complexes with Extended Conjugated Chromophores. Organic Letters 5(16) (2003): 2769-2772.
- [26] Pohl, R., Montes, V.A., Shinar, J., and Anzenbacher, P. Red-Green-Blue Emission from Tris(5-aryl-8-quinolinolate)Al(III) Complexes. The Journal of Organic Chemistry 69(5) (2004): 1723-1725.
- [27] Lee, C.B., Uddin, A., Hu, X., and Andersson, T.G. Study of Alq<sub>3</sub> thermal evaporation rate effects on the OLED. Materials Science and Engineering: B 112(1) (2004): 14-18.
- [28] Bhagat, S.A., Borghate, S.V., Kalyani, N.T., and Dhoble, S.J. Novel Na<sup>+</sup> doped Alq<sub>3</sub> hybrid materials for organic light-emitting diode (OLED) devices and flat panel displays. Luminescence 30(3) (2015): 251-256.
- [29] Xiangming Meng, Wang, S., and Zhu, M. Quinoline-Based Fluorescence Sensors. Molecular Photochemistry - Various Aspects. InTech, 2012.
- [30] Fahrni, C.J. and O'Halloran, T.V. Aqueous Coordination Chemistry of Quinoline-Based Fluorescence Probes for the Biological Chemistry of Zinc. Journal of the American Chemical Society 121(49) (1999): 11448-11458.

- [31] Zalewski, P.D., et al. Flux of intracellular labile zinc during apoptosis (gene-directed cell death) revealed by a specific chemical probe, Zinquin. Chemistry & Biology 1(3) (1994): 153-161.
- [32] Zhang, Y., Guo, X., Si, W., Jia, L., and Qian, X. Ratiometric and Water-Soluble Fluorescent Zinc Sensor of Carboxamidoquinoline with an Alkoxyethylamino Chain as Receptor. Organic Letters 10(3) (2008): 473-476.
- [33] Zhou, X., et al. Ratiometric fluorescent Zn<sup>2+</sup> chemosensor constructed by appending a pair of carboxamidoquinoline on 1,2-diaminocyclohexane scaffold. Tetrahedron 67(19) (2011): 3412-3419.
- [34] Pal, P., Rastogi, S.K., Gibson, C.M., Aston, D.E., Branen, A.L., and Bitterwolf, T.E. Fluorescence Sensing of Zinc(II) Using Ordered Mesoporous Silica Material (MCM-41) Functionalized with N-(Quinolin-8-yl)-2-[3-(triethoxysilyl)propyl amino]acetamide. ACS Applied Materials & Interfaces 3(2) (2011): 279-286.
- [35] Zhang, Y., et al. Substituent-dependent fluorescent sensors for zinc ions based on carboxamidoquinoline. Dalton Transactions 41(38) (2012): 11776-11782.
- [36] Dong, Z., Guo, Y., Tian, X., and Ma, J. Quinoline group based fluorescent sensor for detecting zinc ions in aqueous media and its logic gate behaviour. Journal of Luminescence 134 (2013): 635-639.
- [37] Ma, Y., Wang, F., Kambam, S., and Chen, X. A quinoline-based fluorescent chemosensor for distinguishing cadmium from zinc ions using cysteine as an auxiliary reagent. Sensors and Actuators B: Chemical 188 (2013): 1116-1122.
- [38] Goswami, S., et al. Ratiometric and absolute water-soluble fluorescent tripod zinc sensor and its application in killing human lung cancer cells. Analyst 138(16) (2013): 4593-4598.
- [39] Brouwer Albert, M. Standards for Photoluminescence Quantum Yield Measurements in Solution (IUPAC Technical Report). in *Pure and Applied Chemistry*. 2011. 2213.
- [40] Du, H., Fuh, R.-C.A., Li, J., Corkan, L.A., and Lindsey, J.S. PhotochemCAD $\ddagger$ : A Computer-Aided Design and Research Tool in Photochemistry. Photochemistry and Photobiology 68(2) (1998): 141-142.

- [41] Fery-Forgues, S. and Lavabre, D. Are Fluorescence Quantum Yields So Tricky to Measure? A Demonstration Using Familiar Stationery Products. Journal of Chemical Education 76(9) (1999): 1260.
- [42] Fang, J.-K., et al. Synthesis and spectroscopic study of phenylene–(poly)ethynylenes substituted by amino or amino/cyano groups at terminal(s): electronic effect of cyano group on charge-transfer excitation of acetylenic **TT** systems. Tetrahedron 66(29) (2010): 5479-5485.
- [43] Taudte, R.V., Beavis, A., Wilson-Wilde, L., Roux, C., Doble, P., and Blanes, L. A portable explosive detector based on fluorescence quenching of pyrene deposited on coloured wax-printed [small mu ]PADs. Lab on a Chip 13(21) (2013): 4164-4172.
- [44] Lakowicz, J.R. Introduction to Fluorescence. in Principles of Fluorescence Spectroscopy, pp. 1-26: Springer US, 2006.
- [45] Ma, Y., Wang, F., Kambam, S., and Chen, X. A quinoline-based fluorescent chemosensor for distinguishing cadmium from zinc ions using cysteine as an auxiliary reagent. Sensors and Actuators B: Chemical 188 (2013): 1116-1122.
- [46] Zhang, Y., Guo, X., Si, W., Jia, L., and Qian, X. Ratiometric and Water-Soluble Fluorescent Zinc Sensor of Carboxamidoquinoline with an Alkoxyethylamino Chain as Receptor. Organic Letters 10(3) (2008): 473-476.
- [47] Pal, P., Rastogi, S.K., Gibson, C.M., Aston, D.E., Branen, A.L., and Bitterwolf, T.E. Fluorescence Sensing of Zinc(II) Using Ordered Mesoporous Silica Material (MCM-41) Functionalized with N-(Quinolin-8-yl)-2-[3-(triethoxysilyl)propyl amino]acetamide. ACS Applied Materials & Interfaces 3(2) (2011): 279-286.
- [48] Zhang, Y., et al. Substituent-Dependent Fluorescent Sensors For Zinc Ions Based On Carboxamidoquinoline. Dalton Transactions 41(38) (2012): 11776-11782.
- [49] Dong, Z., Guo, Y., Tian, X., and Ma, J. Quinoline group based fluorescent sensor for detecting zinc ions in aqueous media and its logic gate behaviour. Journal of Luminescence 134 (2013): 635-639.
- [50] Lee, H.G., et al. Zinc selective chemosensors based on the flexible dipicolylamine and quinoline. Inorganica Chimica Acta 394 (2013): 542-551.

- [51] Assunção, A.G.L., Schat, H., and Aarts, M.G.M. Regulation of the adaptation to zinc deficiency in plants. *Plant Signaling & Behavior* 5(12) (2010): 1553-1555.
- [52] Li, P., et al. A highly fluorescent chemosensor for Zn<sup>2+</sup> and the recognition research on distinguishing Zn<sup>2+</sup> from Cd<sup>2+</sup>. *Dalton Transactions* 43(2) (2014): 706-713.
- [53] Ding, W.H., Cao, W., Zheng, X.J., Ding, W.J., Qiao, J.P., and Jin, L.P. A tetrazole-based fluorescence "turn-on" sensor for Al(iii) and Zn(ii) ions and its application in bioimaging. *Dalton Transactions* 43(17) (2014): 6429-6435.
- [54] Mei, Q., et al. Zinc-Dithizone Complex Engineered Upconverting Nanosensors for the Detection of Hypochlorite in Living Cells. *Small* 11(35) (2015): 4568-4575.
- [55] Li, Y., Li, K., and He, J. A "turn-on" fluorescent chemosensor for the detection of Zn(II) in aqueous solution at neutral pH and its application in live cells imaging. *Talanta* 153 (2016): 381-385.



## APPENDIX

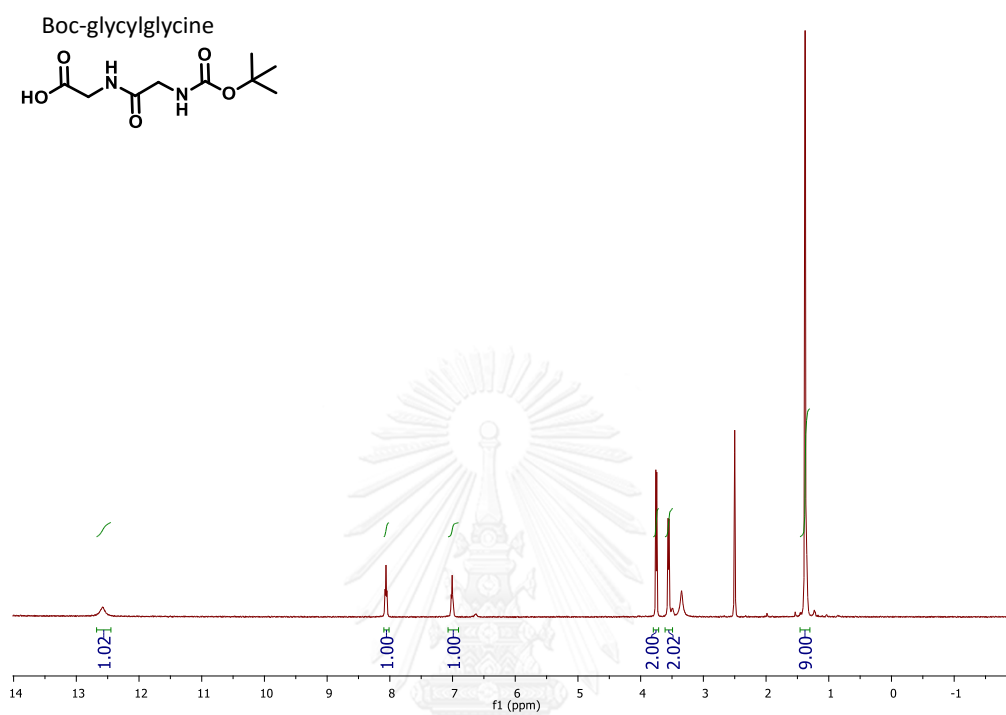
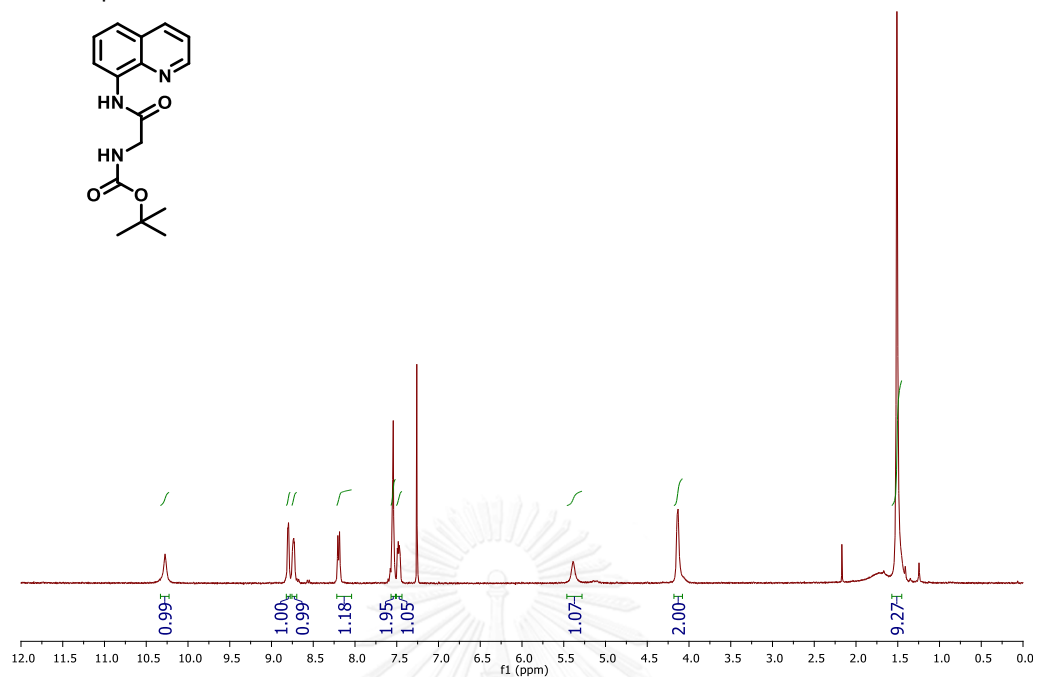
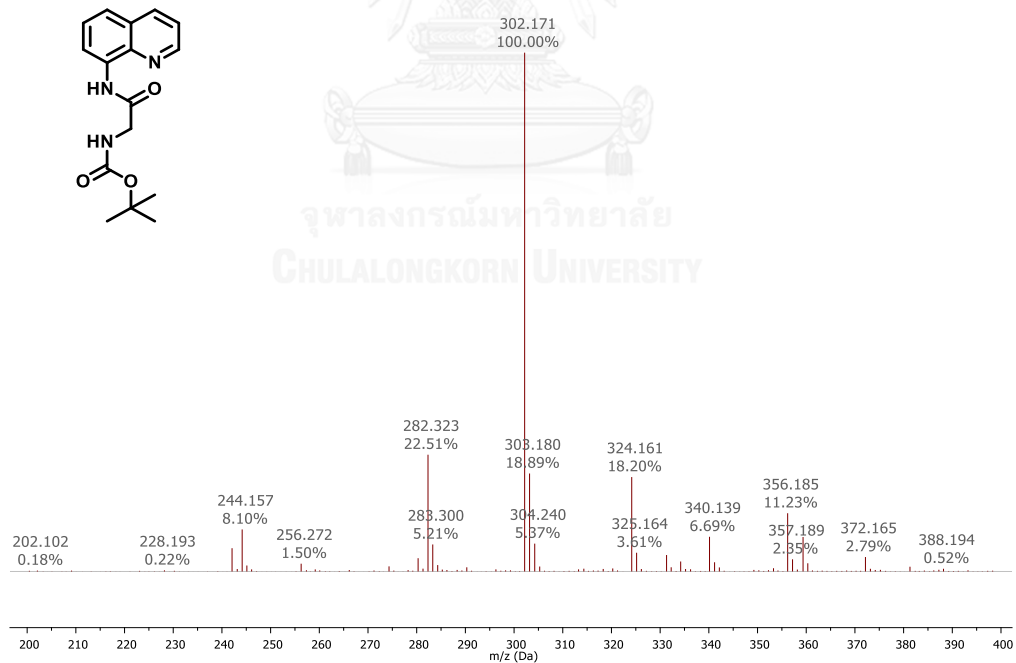


Figure A.1  $^1\text{H-NMR}$  (400 MHz) of Boc-glycylglycine in  $(\text{CD}_3)_2\text{SO}$ .

Compound 4

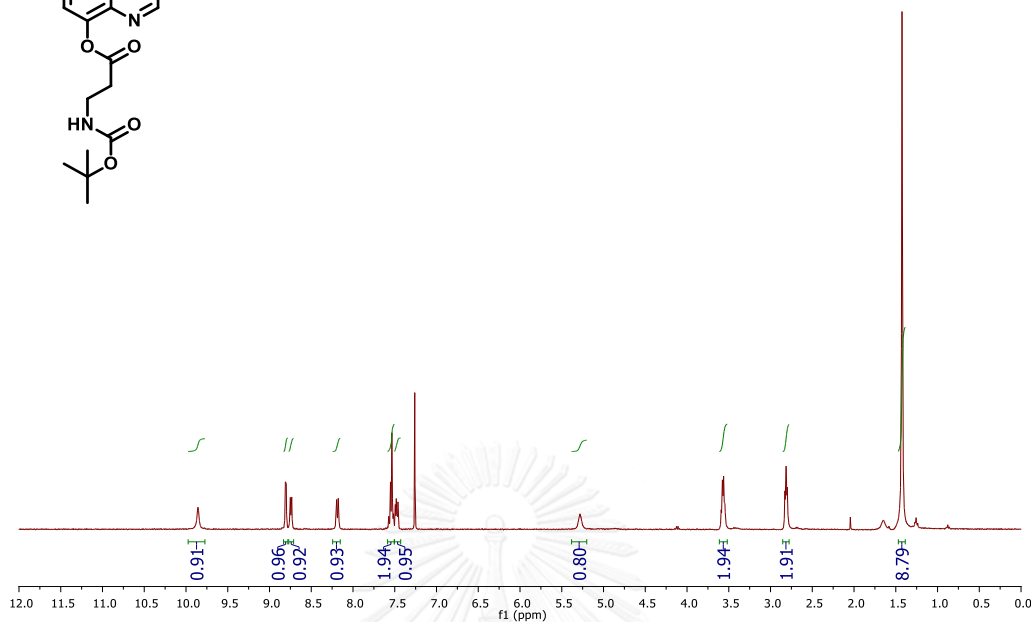
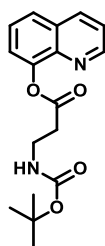
Figure A.2  $^1\text{H-NMR}$  (400 MHz) of **4** in  $\text{CDCl}_3$ .

Compound 4

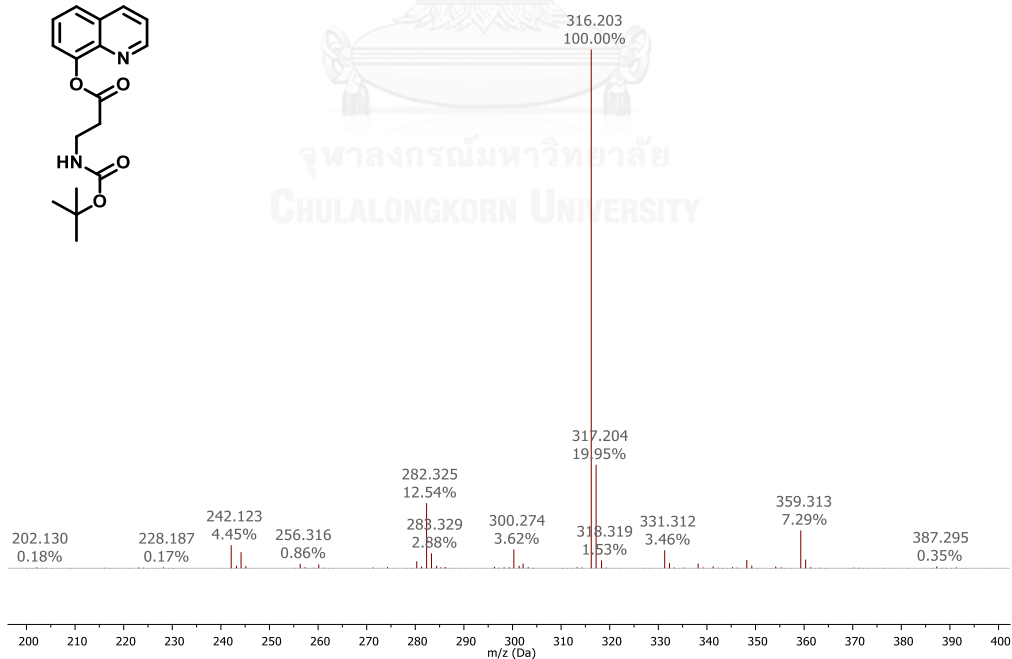
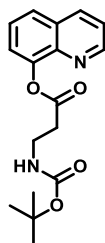
Figure A.3 MS (ESI) of **4** in Methanol.



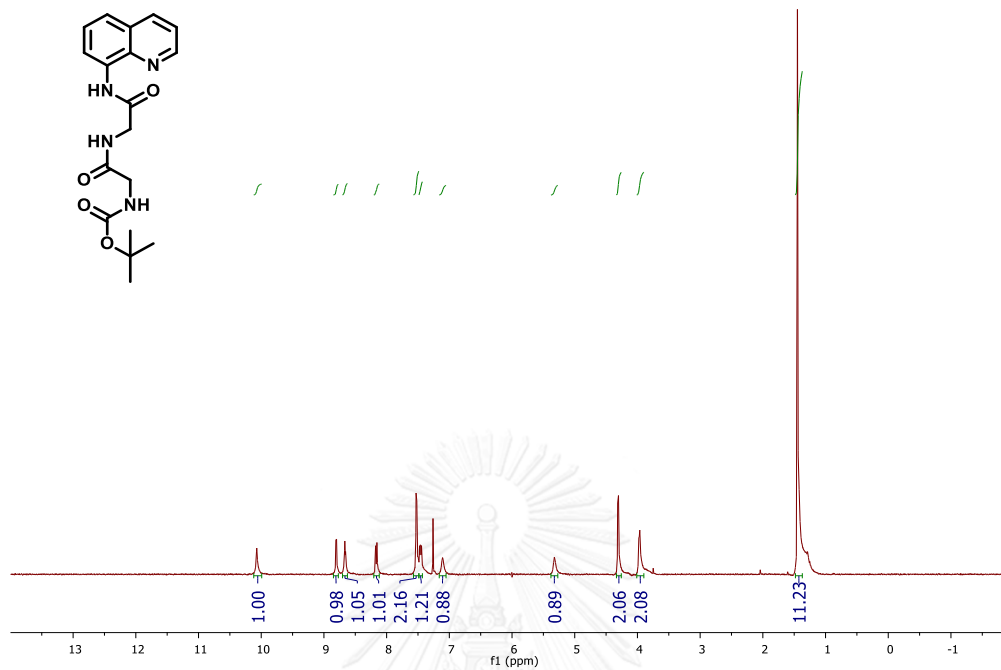
Compound 5

Figure A.4  $^1\text{H-NMR}$  (400 MHz) of **5** in  $\text{CDCl}_3$ .

Compound 5

Figure A.5 MS (ESI) of **5** in Methanol.

Compound 6

Figure A.6  $^1\text{H-NMR}$  (400 MHz) of 6 in  $\text{CDCl}_3$ .

Compound 6

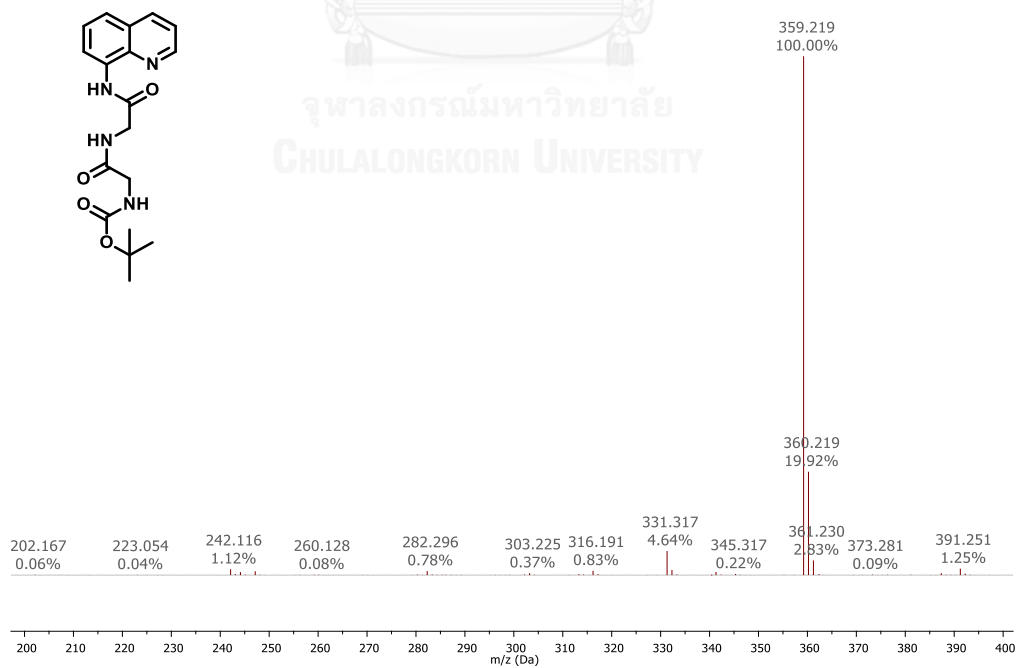
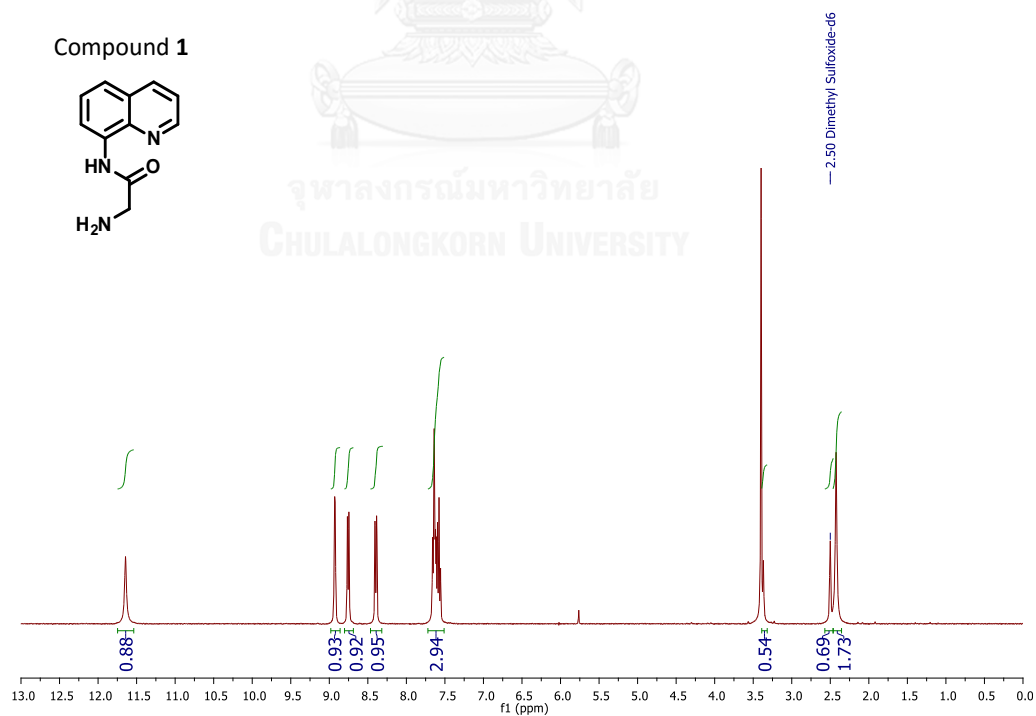
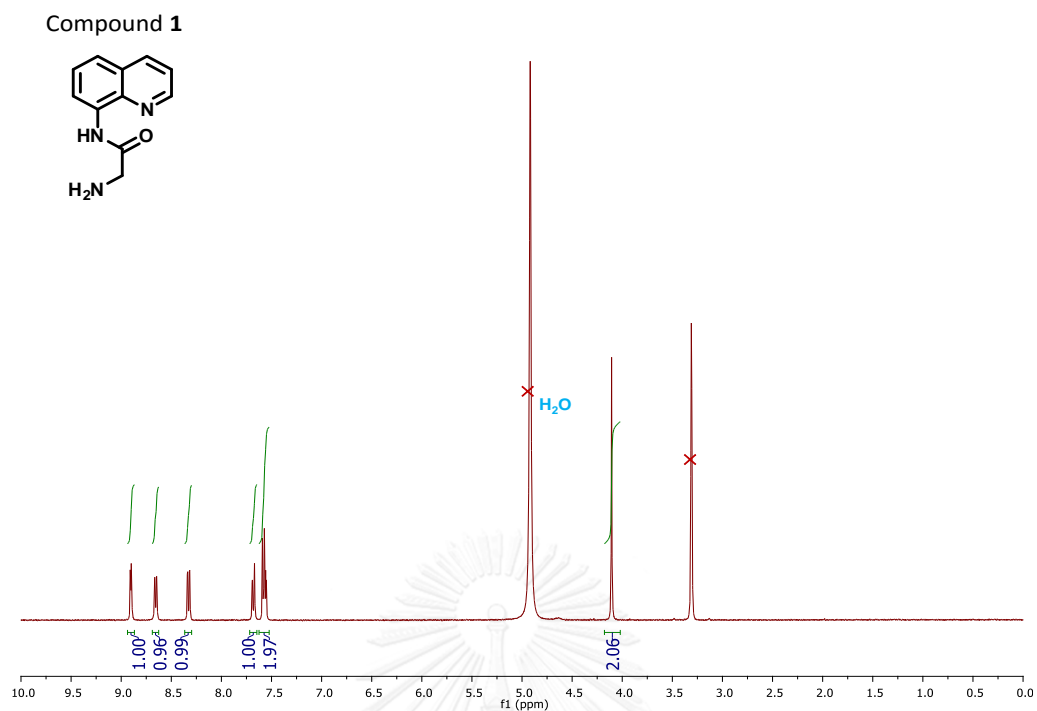


Figure A.7 MS (ESI) of 6 in Methanol.



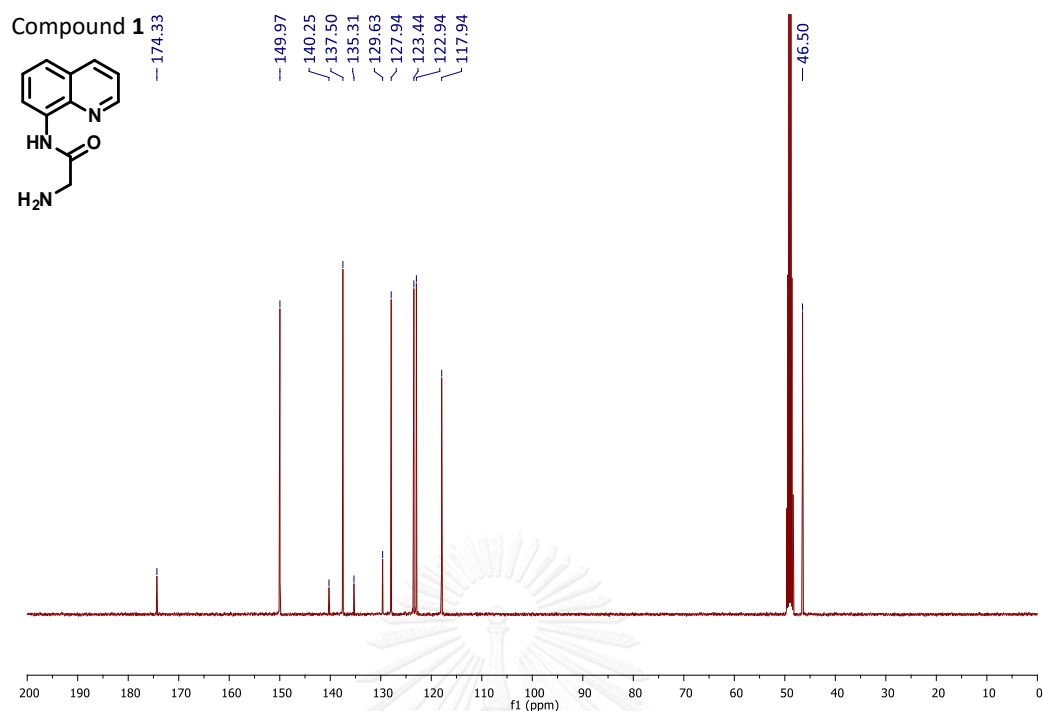


Figure A.10  $^{13}\text{C-NMR}$  (100 MHz) of 1 in  $\text{CD}_3\text{OD}$

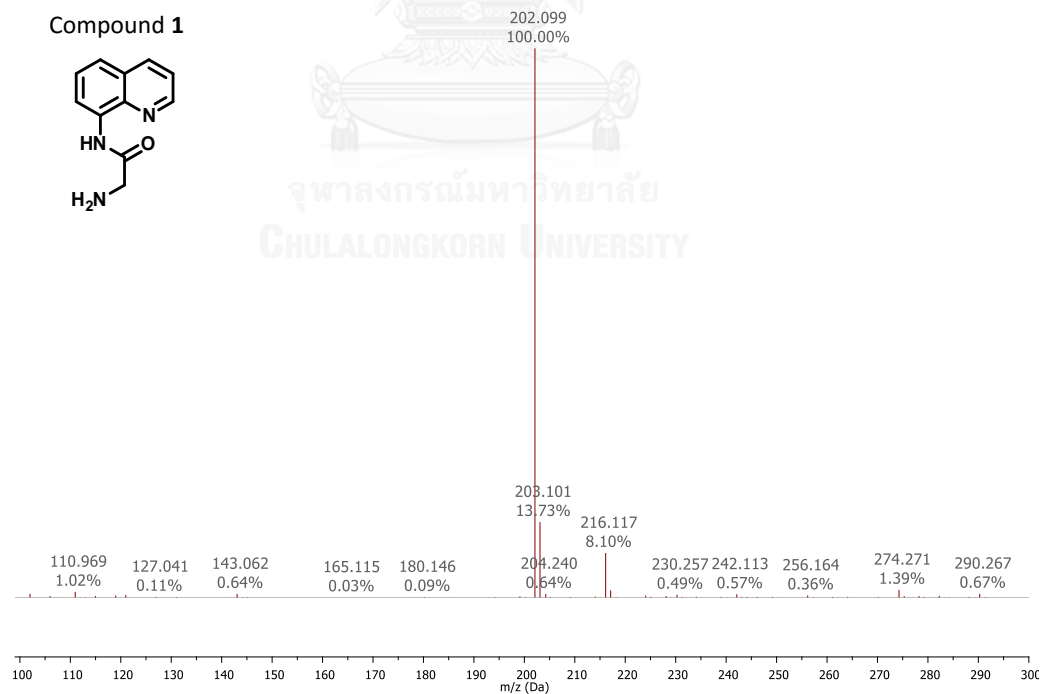


Figure A.11 MS (ESI) of 1 in Methanol.

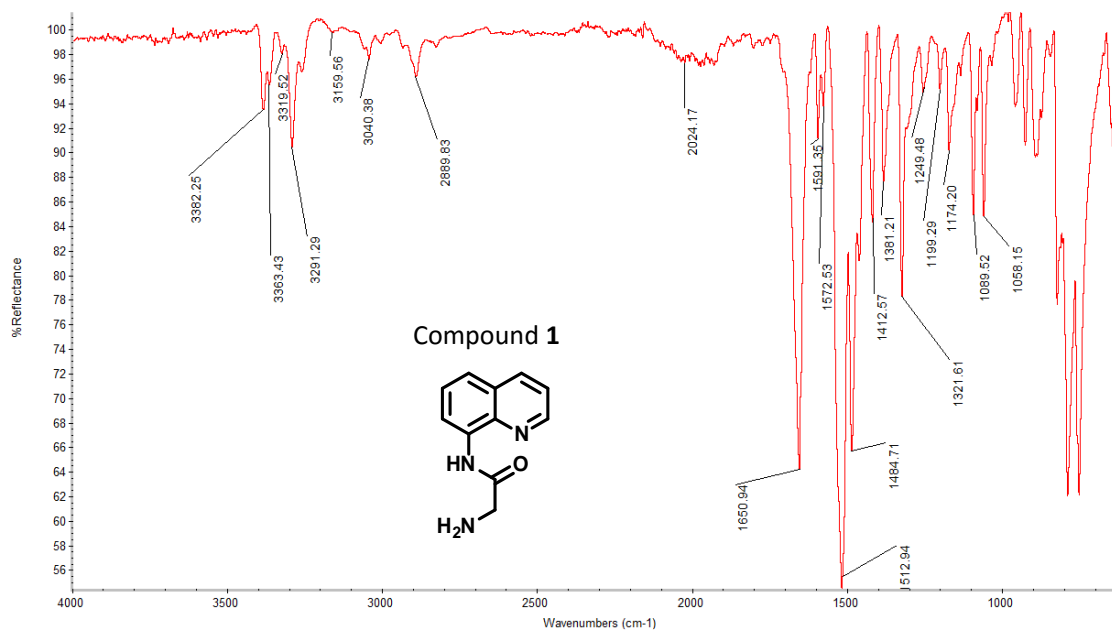
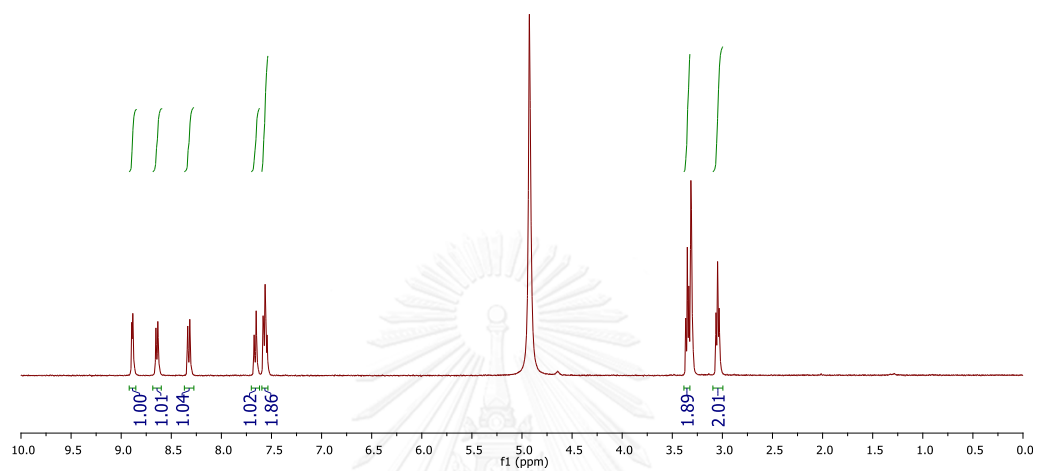
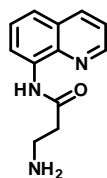


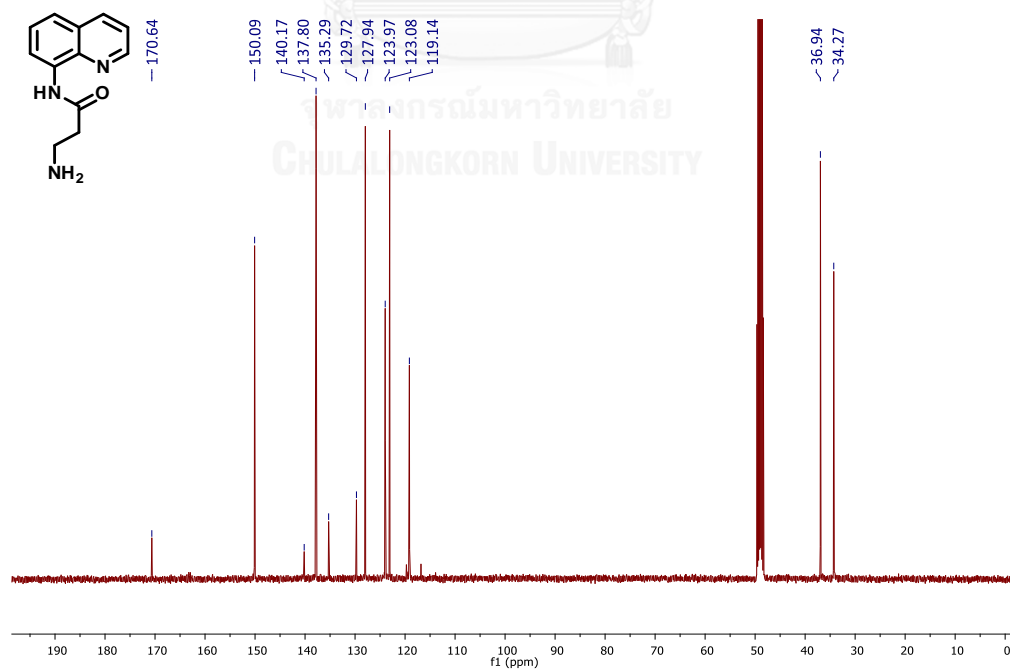
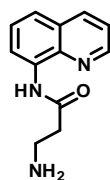
Figure A.12 IR(ATR) of 1.



Compound 2

Figure A.13  $^1\text{H-NMR}$  (400 MHz) of 2 in  $\text{CD}_3\text{OD}$ .

Compound 2

Figure A.14  $^{13}\text{C-NMR}$  (100 MHz) of 2 in  $\text{CD}_3\text{OD}$ .

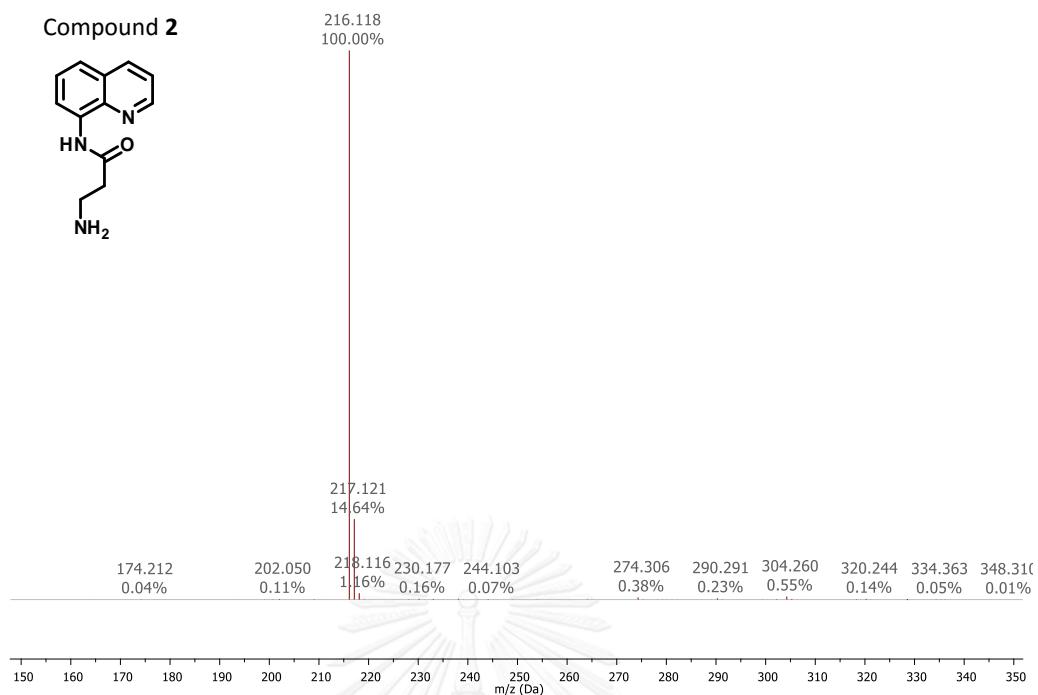


Figure A.15 MS (ESI) of 2 in Methanol.

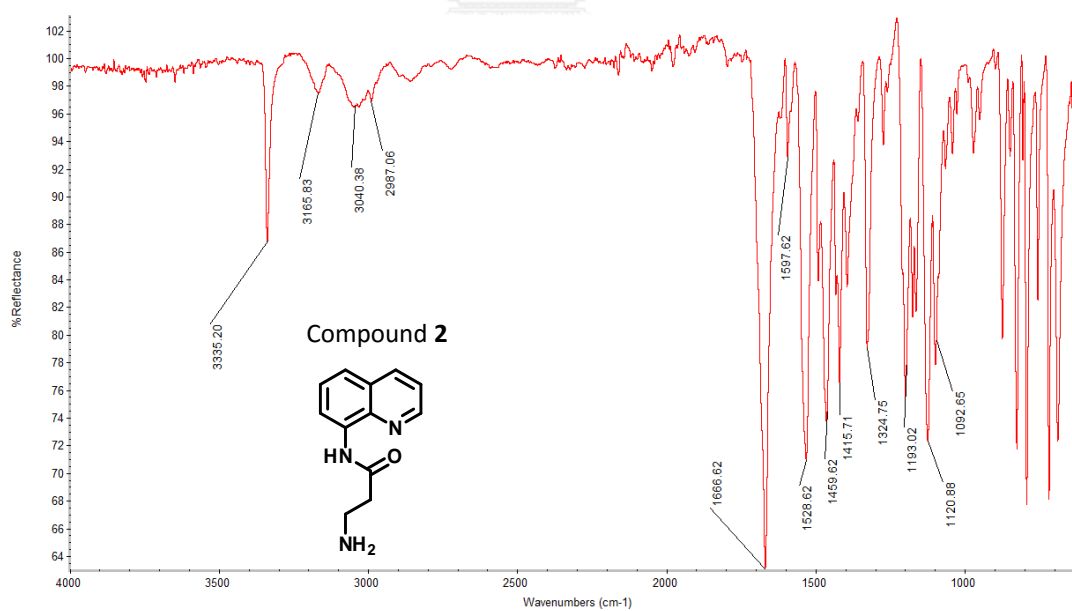
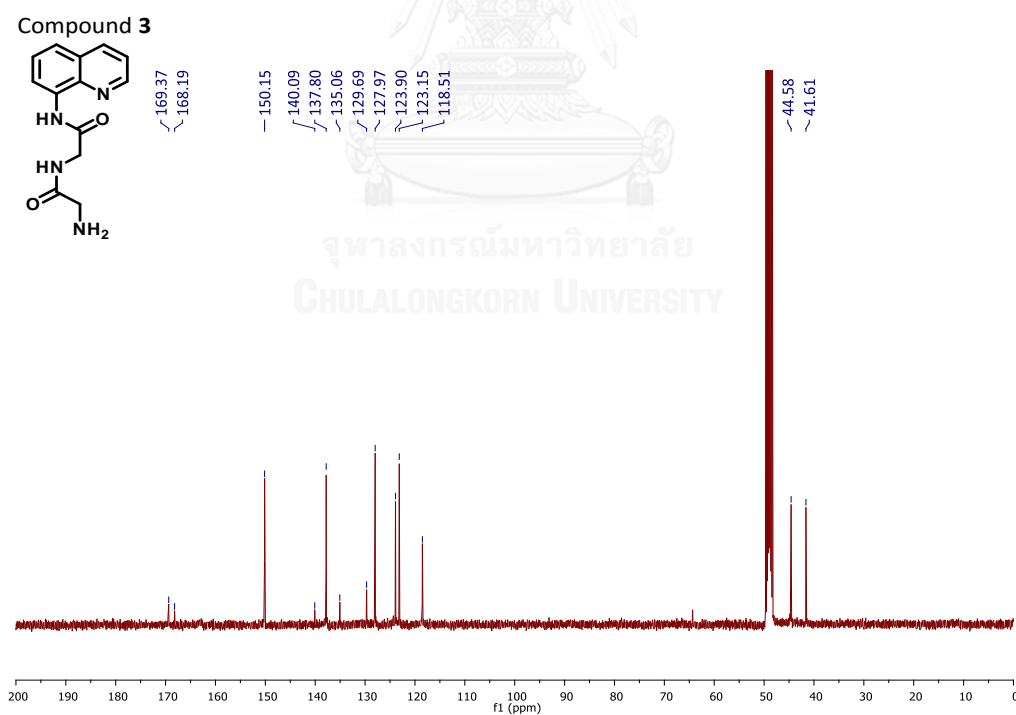
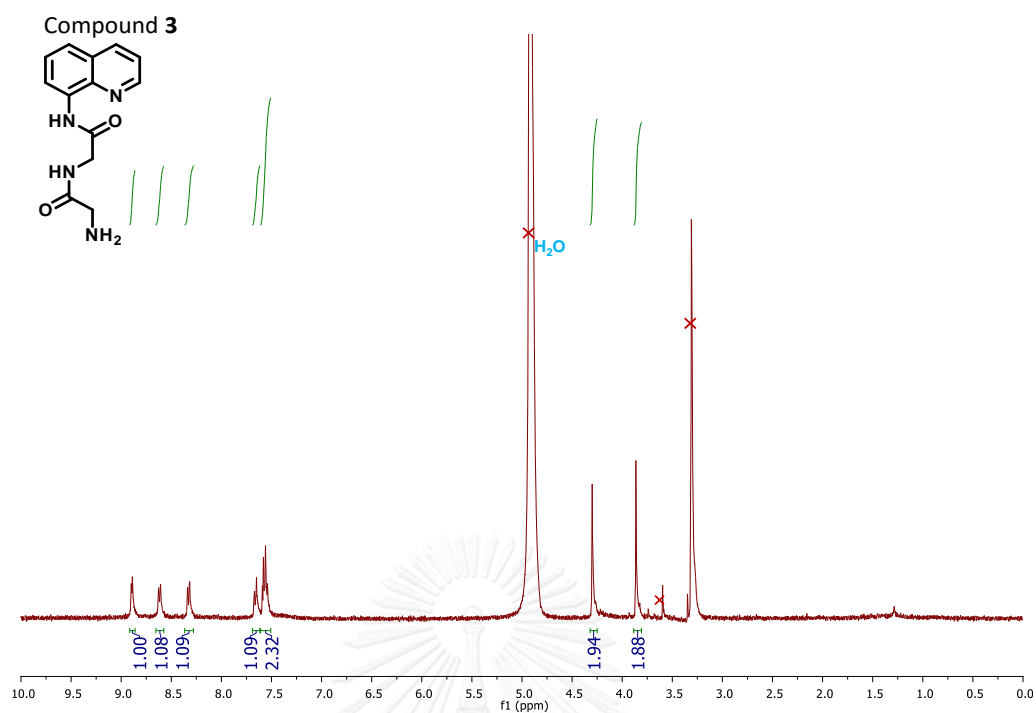


Figure A.16 IR(ATR) of 2.





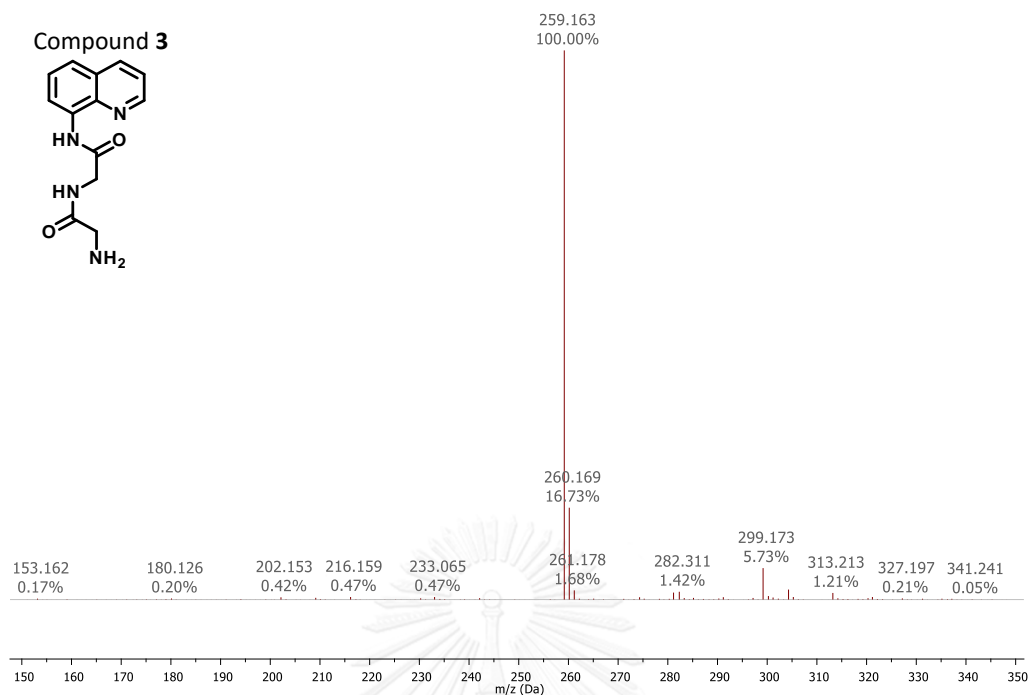


Figure A.19 MS (ESI) of 3 in Methanol

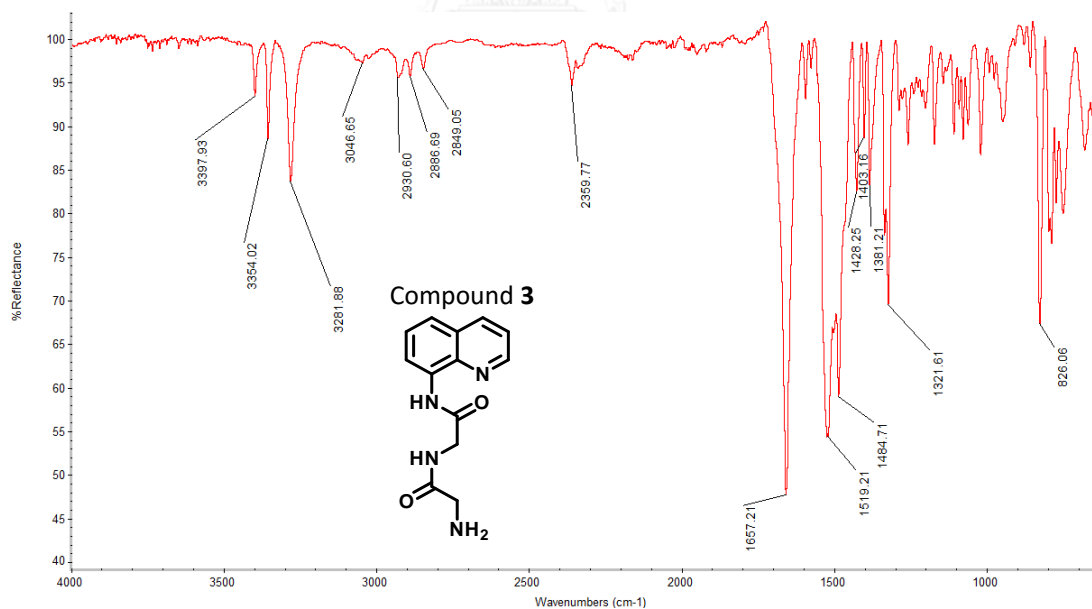
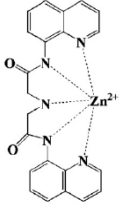
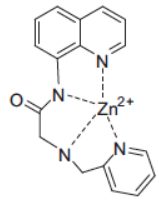
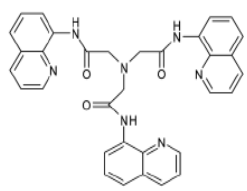
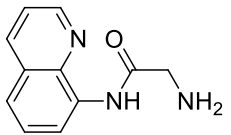


Figure A.20 IR(ATR) of 3.

**Table A.1** The Zn<sup>2+</sup> sensors based on 8-aminoquinoline derivatives reported to date

Reference	Selectivity	Media	K <sub>s</sub> (M <sup>-1</sup> )	LOD (μM)	Φ / Φ <sub>0</sub>	Interferences <sup>a</sup>	Cell study
[32]	Zn <sup>2+</sup>	(MeOH/water ) 1:9, v/v, tris-HCl pH = 7.22	6.7 × 10 <sup>6</sup>	-	7.9 6	Fe <sup>2+</sup> Fe <sup>3+</sup> Co <sup>2+</sup> Ni <sup>2+</sup> Cu <sup>2+</sup> N/ A NI I NI I	yeast cells
[33]	Zn <sup>2+</sup> , Cd <sup>2+</sup>	HEPES, MeOH:water = 5:5 (v/v), pH = 7.4	1.8 × 10 <sup>6</sup>	0.0283	12	Fe <sup>2+</sup> Fe <sup>3+</sup> Co <sup>2+</sup> Ni <sup>2+</sup> Cu <sup>2+</sup> Li <sup>2+</sup> Na <sup>2+</sup> Mg <sup>2+</sup> Ca <sup>2+</sup> N/A NI NI I NI I I I I I	HK-1 cells
[34]	Zn <sup>2+</sup>	Tris-HCl pH 7.22	5.7 × 10 <sup>3</sup>	0.1	3.31	Fe <sup>2+</sup> Fe <sup>3+</sup> Co <sup>2+</sup> Ni <sup>2+</sup> Cu <sup>2+</sup> I N/A I I I	-
[35]	Zn <sup>2+</sup>	MeOH:water 1:9, v/v, tris-HCl pH = 7.22	-	1-10	16.3	Fe <sup>2+</sup> Fe <sup>3+</sup> Co <sup>2+</sup> Ni <sup>2+</sup> Cu <sup>2+</sup> N/A NI I NI I	yeast cells

Compounds	Selectivity	Media	$K_a$ ( $M^{-1}$ )	LOD ( $\mu M$ )	$\Phi / \Phi_0$	Interferences <sup>a</sup>	Cell study
[36]	Zn <sup>2+</sup> , Cd <sup>2+</sup>	Tris-HCl (pH 7.22)	$8.69 \times 10^5$	0.02	-	Fe <sup>2+</sup> N/A Fe <sup>3+</sup> NI Co <sup>2+</sup> I Ni <sup>2+</sup> NI Cu <sup>2+</sup> I	-
							
[37]	Zn <sup>2+</sup> , Cd <sup>2+</sup>	HEPES buffer pH=7.4	$1.64 \times 10^5$	1-10	8.8	Fe <sup>2+</sup> I Fe <sup>3+</sup> I Co <sup>2+</sup> I Ni <sup>2+</sup> I Cu <sup>2+</sup> I	-
							
[38]	Zn <sup>2+</sup>	HEPES buffer pH=7.4	$4 \times 10^4$	3.2	15	Fe <sup>2+</sup> I Fe <sup>3+</sup> N/A Co <sup>2+</sup> NI Ni <sup>2+</sup> N/A Cu <sup>2+</sup> NI	A549 cells
							
<b>This work</b>	Zn <sup>2+</sup>	(MeOH/water ) 1:99, v/v, tris-HCl pH =7.4	$8.03 \times 10^5$	0.15	24	Fe <sup>2+</sup> NI Fe <sup>3+</sup> NI Co <sup>2+</sup> I Ni <sup>2+</sup> I Cu <sup>2+</sup> I	Chinese cabbage
							

a

NI : Non-interfere

I : Interfere

N/A : No data support

## VITA

Ms. Atchareeporn Smata was born on January 11th, 1990 in Bangkok, Thailand. She was graduated with Bachelor Degree of Science, majoring in Chemistry from Chulalongkorn University in 2011. She has been a graduate student in organic chemistry and become a member of Organic Synthesis Research Unit under supervision of Prof. Dr. Mongkol Sukwattanasinitt. She graduated with a Master's degree in Chemistry in academic year 2015. Her present address is 269, Khu Bon Road, Bang Chan, Klongsamwa, Bangkok, Thailand 10510.

